

**SHOX2 IS ESSENTIAL FOR MAINTENANCE OF PHYSIOLOGICAL  
PROPERTIES AND FUNCTIONS OF THALAMIC NEURONS IN  
YOUNG ADULT MOUSE**

AN ABSTRACT

SUBMITTED ON THE SEVENTH DAY OF NOVEMBER 2017

TO THE NEUROSCIENCE PROGRAM


IN PARTIAL FULFILLMENT OF THE REQUIREMENTS

OF THE SCHOOL OF SCIENCE AND ENGINEERING

OF TULANE UNIVERSITY

FOR THE DEGREE OF DOCTOR OF PHILOSOPHY



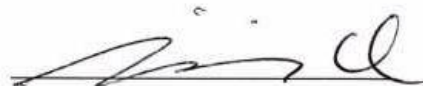
BY



---

DIANKUN YU

APPROVED:

  
LAURA SCHRADER, Ph.D.  
ADVISOR  
JEFFREY TASKER, Ph.D.  
YIPING CHEN, Ph.D.  
ANDREA ZOMBOK, Ph.D.

## Abstract

The lack of Short Stature Homeobox Gene, *SHOX*, caused several symptoms in humans including the short stature, skeletal abnormalities, heart diseases and cognitive problems. To understand the role of *SHOX* and *SHOX2* in humans, the study of homolog gene *Shox2* in mice has been applied. Previous researches have revealed that *Shox2* has important role in bone, palate, heart and hindbrain development. Especially, *Shox2* is critical for the development of heart pacemaker cells. In this dissertation, we studied the role of *Shox2* in the thalamus of young adult mice.

Our results indicated that *Shox2* expression during development in the forebrain is relatively limited in the thalamus. To study the role of *Shox2* in thalamic properties and functions, we conducted tamoxifen inducible knock out (KO) in *Rosa<sup>CreERT/+</sup>*, *Shox2<sup>f/f</sup>* mice. Our behavioral studies showed that *Shox2* KO impairs mice total activity, somatosensory function and learning and memory process, suggesting *Shox2* is critical for thalamus-related behaviors. To investigate the underlying mechanism, we conducted electrophysiological experiment to test physiological properties of thalamic neurons. Our results showed that *Shox2* KO caused changes in intrinsic properties including decreased cell excitability. Besides, our TUNEL staining results revealed *Shox2* inducible KO in midline thalamus of *Gbx2<sup>CreERT/+</sup>*, *Shox2<sup>f/f</sup>* mice caused increased cell death in the midline thalamus. We further investigate whether pacemaking related ion channels are involved in cellular properties impairments caused by *Shox2* KO. The following experiments revealed a decrease in mRNA and protein expression of *Ca<sub>v</sub>3.1*

and T-type calcium current density, and in mRNA and protein expression of HCN2 and HCN4 channels and HCN current. The similar enriched genes related to T-type calcium and HCN channels with heart pacemaker cells and the specific down-regulation of these genes by Shox2 KO suggested the critical role of Shox2 in maintenance of thalamic pacemaking properties and behavioral functions. Our mRNA sequencing results indicated that enriched differently expressed genes (DEGs) in gene ontology (GO) terms of cell death, neuron projection development and response to stimulus between CR and KO samples and thalamus specifically enriched genes are highly regulated by Shox2 KO, suggesting Shox2 is important for thalamic identity and survival.

**SHOX2 IS ESSENTIAL FOR MAINTENANCE OF PHYSIOLOGICAL  
PROPERTIES AND FUNCTIONS OF THALAMIC NEURONS IN  
YOUNG ADULT MOUSE**

A DISSERTATION

SUBMITTED ON THE SEVENTH DAY OF NOVEMBER 2017

TO THE NEUROSCIENCE PROGRAM

IN PARTIAL FULFILLMENT OF THE REQUIREMENTS

OF THE SCHOOL OF SCIENCE AND ENGINEERING

OF TULANE UNIVERSITY

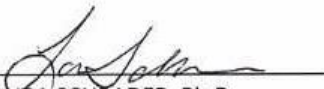
FOR THE DEGREE OF DOCTOR OF PHILOSOPHY

BY

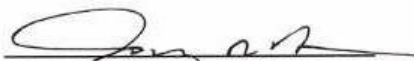



DIANKUN YU

APPROVED:

  
LAURA SCHRADER, Ph.D.

ADVISOR

  
JEFFREY TASKER, Ph.D.  
YIPING CHEN, Ph.D.  
ANDREA ZSOMBOK, Ph.D.

**©Copyright By Diankun Yu  
All Rights Reserved**

## **ACKNOWLEDGEMENT**

First and foremost, I would like to express my deep appreciation and sincere gratitude to my advisor, Dr. Laura A. Schrader. She gave me the best guide and consistent supports not just in my Ph.D. research, but also in my personal life, my family and my future. I really appreciate the freedom she provided, especially in my research, but also in the way to communicate with her and in the way I work with undergraduates. Her positive attitude to any results and strong passion in research prospectus really encouraged me to devote myself into future research.

In addition, I would like to thank my committee members, Dr. Jeffrey Tasker, Dr. Yiping Chen and Dr. Andrea Zsombok. Dr. Tasker introduced me the department when I came to neuroscience program at the first time and offered nice questions and suggestions about my research whenever he had a chance. Dr. Chen generally provided us with Shox2 transgenic mouse strains and development-related knowledge about Shox2. Dr. Zsombok asked nice questions in my committee meeting and gave nice advice on my experimental design.

I would like to thank every member in Schrader's lab. Whenever I have a problem in my research or personal life, everyone tried their best to help. Jeremiah Harter is a

best friend of me and provided me great help in every field. Damek Homiack and Ted Sawyer contributed greatly in my research projects. Matthieu Maroteaux provided nice suggestions and help in my dissertation preparation. Undergraduates Stuart Rowe, Shreya Gunda, Erika Moxley and Master students Keung Tiffie Man Yee and Mary Stanley contributed to my research.

Besides, I would like to thank lab members in Dr. Yiping Chen's lab, especially Cheng Sun, Wenduo Ye and Yingnan Song. They gave me great help in breeding mice, acquiring histology techniques and understanding development-related knowledge.

Finally, I would like to acknowledge my sincerest thanks and deepest love to my wife Chun Cherry Chen, my son Roger Runqing Yu and my daughter Leah Zhiqing Yu. Besides, I would like to thank my parents and my sister for their selfless and ubiquitous love and support over my life. I would like to thank my parents-in-law for their great supports in my career and life, especially they provides great finance and labor help since my wife and I have kids.

## TABLE OF CONTENT

<b>ACKNOWLEDGEMENTS .....</b>	<b>ii</b>
<b>LIST OF FIGURES.....</b>	<b>vii</b>
<b>LIST OF TABLES.....</b>	<b>x</b>
<b>Chapter I: Introduction .....</b>	<b>1</b>
1.1 Introduction of <i>SHOX</i> and <i>SHOX2</i> .....	1
1.2 <i>Shox2</i> has critical roles in the development of bone, palate and joint in mouse .....	3
1.3 <i>Shox2</i> is critical for the development of heart pacemaker nodal-like cells in mouse.....	4
1.4 <i>Shox2</i> has important roles in the nervous system in mice.....	8
1.5 The anatomy and function of the greater thalamus .....	10
1.6 The anatomy and function of the thalamus .....	16
1.7 Electrophysiological properties of thalamus neurons .....	21
1.8 HCN2/4 channels and T-type calcium channels are important currents implicated in pacemaking function.....	25
1.8.1 HCN channels .....	25
1.8.2 T-type Ca <sup>2+</sup> channels.....	28
<b>Chapter II: Methods.....</b>	<b>31</b>
2.1 Mouse introduction.....	31



2.2	X-gal staining.....	33
2.3	Immunohistochemistry (IHC).....	33
2.4	Quantitative reverse transcription PCR (RT-qPCR).....	35
2.5	Terminal deoxynucleotidyl transferase dUTP nick end labeling (TUNEL).....	36
2.6	Western Blot .....	38
2.7	Electrophysiology .....	40
2.8	Behavioral assays .....	42
2.9.	mRNA sequencing .....	45
	<b>Chapter III: Results .....</b>	<b>46</b>
3.1	The expression of <i>Shox2</i> in the thalamus.....	46
3.2	Tamoxifen injection successful induced <i>Shox2</i> KO in the thalamus.....	59
3.3	<i>Shox2</i> KO induced thalamus-related behavior deficits in adult mouse.....	62
3.4	<i>Shox2</i> KO altered intrinsic properties of thalamic neurons and induced cell Death.....	69
3.5	<i>Shox2</i> KO affected T-type calcium and HCN current in the PVA.....	79
3.6	<i>Shox2</i> KO decreased the mRNA and protein expression of Cav3.1 and HCN2/4 channel in the thalamus.....	90
3.7	mRNA sequencing results revealed that <i>Shox2</i> is essential for maintenance of thalamic neuron identity and survival.....	98

<b>Chapter IV: DISCUSSION .....</b>	<b>107</b>
4.1 Summary of results .....	107
4.2 <i>Shox2</i> KO impairs thalamus-related functions and thalamic physiological properties in young adult mice.....	114
4.3 The expression of <i>Shox2</i> in thalamic neurons provided new information for brain development study.....	119
4.4 <i>Shox2</i> is essential to maintain the thalamic neurons physiological properties and functions.....	126
<b>Reference.....</b>	<b>131</b>
<b>Appendix.....</b>	<b>150</b>

## LIST OF FIGURES

Figure 1.1 Schematic representation of a transverse view of adult mouse brain from rostral to caudal.....	15
Figure 1.2 Thalamic neurons (in dLGN) have two action potential patterns.....	23
Figure 1.3 The expression of HCN channels and T-type calcium channels in rodent brain.....	30
Figure 3.1 Brain sections demonstrating X-gal staining results from P56 days old male <i>Shox2<sup>LacZ/+</sup></i> mouse.....	47
Figure 3.2 Brain sections demonstrating X-gal staining results from P56 days old male <i>Shox2<sup>cre/+</sup>, Rosa26<sup>LacZ/+</sup></i> mouse.....	49
Figure 3.3 IHC results of coronal cryostat brain sections from P56 <i>Shox2<sup>cre/+</sup>, Rosa<sup>LacZ/+</sup></i> mouse.....	52
Figure 3.4 IHC results indicate that <i>Shox2</i> expression is restricted in the thalamus.....	53
Figure 3.5 <i>Shox2</i> expression is restricted to NeuN+ neurons in the thalamus.....	56
Figure 3.6 The distribution of GFAP+ glia and <i>Shox2</i> -expression cells in coronal cryostat sections from <i>Shox2<sup>cre/+</sup>, Rosa<sup>LacZ/+</sup></i> mouse.....	57
Figure 3.7 The co-staining results indicate that <i>Shox2</i> does not express in GFAP+ glia	

cells.....	58
Figure 3.8 Tamoxifen injection decreased <i>Shox2</i> mRNA expression and body weight in <i>Shox2</i> KO mice.....	61
Figure 3.9 <i>Shox2</i> KO altered mouse performance in open field test and impaired mouse performance in paw sensation test.....	64
Figure 3.10 <i>Shox2</i> KO impairs mouse performance in novel object recognition test.....	67
Figure 3.11. No significant difference in mobility time in 5-minute force swim and 5-minute tail suspension test between CR mice and KO mice.....	68
Figure 3.12, <i>Shox2</i> KO decreased the ratio of cells with spontaneous action potentials in the anterior paraventricular thalamus (PVA).....	72
Figure 3.13. Current injection evoked fewer action potentials in PVA neurons of <i>Shox2</i> KO mice compared to that of CR mice.....	73
Figure 3.14 The time to the peak of rebounded calcium spike induced by -150pA hyperpolarization and the areas under spike traces at -70mV in PVA neurons are different between CR and KO.....	75
Figure 3.15. <i>Shox2</i> KO induced region-specific cell death in adult mouse brain.....	78

Figure 3.16. The activation properties of T-type calcium current in PVA neurons of CR and <i>Shox2</i> KO mice.....	82
Figure 3.17. The inactivation properties of T-type calcium current in PVA neurons of CR and <i>Shox2</i> KO mice.....	86
Figure 3.18. <i>Shox2</i> inducible KO decreased HCN current in PVA of neurons.....	89
Figure 3.19. <i>Shox2</i> KO decreased the mRNA expression of CACNA1G, HCN2 and HCN4.....	93
Figure 3.20. The mRNA expression of several genes in the PVA of CR and <i>Shox2</i> KO mice.....	96
Figure 3.21. <i>Shox2</i> KO decreased the protein expression of HCN2, HCN4 and Ca <sub>v</sub> 3.1 expression.....	97
Figure 3.22. Gene ontology (GO) study of significantly regulated gene by <i>Shox2</i> KO.....	102
Figure 3.23. The gene expression profiles in thalamus are highly regulated by <i>Shox2</i> .....	103
Figure 3.24. Potassium channels are involved in <i>Shox2</i> regulation pathway.....	106

## LIST OF TABLES

Table 1. The list of sequence and target band size of RT-qPCR primers.....	37
Table 2. Some insignificant intrinsic properties of PVA neurons of CR and <i>Shox2</i> KO mice.....	76
Table 3. The list of genes upregulated in the midline thalamus of <i>Shox2</i> KO mice.....	104
Table 4 The list of upregulated gene by <i>Shox2</i> KO.....	105

## Chapter I: Introduction

### 1.1 Introduction of *SHOX* and *SHOX2*

*SHOX*, the human short stature homeobox gene, and the homologous gene, *SHOX2*, also called paired-related homeobox protein *SHOT* or homeobox protein Og12X, are transcription factors that are involved in development of several organs in vertebrate species (Clement-Jones et al., 2000). In humans, *SHOX* is located on the pseudoautosomal region 1 of the sex chromosome X (Rosin, Abassah-Oppong, & Cobb, 2013). While *SHOX2* is located on chromosome 3 (De Baere, Speleman, Van Roy, De Paepe, & Messiaen, 1998). *Shox2* orthologues are detectable in almost all vertebrate species, while *Shox* exists in human but has not been detected in rodents, fish and frog. *SHOX* and *SHOX2* are highly conserved. Human *SHOX* and *SHOX2* have 79% amino acid identity and the same DNA-binding domain and putative phosphorylation sites. Importantly, the functional redundancy in the regulation of heart pacemaker cells differentiation between human *SHOX* and mouse *Shox2* has been demonstrated in mouse models (Liu et al., 2011). The extraordinary conservation of *Shox2* among species, 99% amino acid identity

between human *SHOX2* protein and mouse *Shox2* protein, and the ubiquitous existence of *Shox2* among vertebrate species indicates an indispensable role of *Shox2* during development and evolution. Therefore, *Shox2* function in mouse is studied to reveal the role of human *SHOX* and *SHOX2*.

In humans, mutation or lack of *SHOX* causes several diseases or symptoms in humans. The haploinsufficiency of *SHOX* contributes to the short stature and skeletal abnormalities of Turner Syndrome, which is caused by the complete or partial loss of the X chromosome (Kosho et al., 1999; Seo et al., 2015). The mutation or haploinsufficiency of *SHOX* also causes other types of skeletal abnormality diseases, such as Leri-Weill dyschondrosteosis (Belin et al., 1998; Hirschfeldova & Solc, 2017), Langer syndrome (Barca-Tierno et al., 2011; Robertson et al., 2000) and Mayer-Rokitansky-Kuster-Hauser syndrome (Gervasini et al., 2010). These abnormalities manifest in similar manners and patients share the same short and malformed forearms and lower legs as well as other bone development problems. Turner syndrome occurs in 1 of every 2000 to 5000 females (Lippe, 1991), and together with all other *SHOX*-related syndromes, approximately 1 in every 1000 to 5000 humans may be affected (Rosin et al., 2013).



*SHOX2* mutations are not found in adult diseases, and it is believed to be because *SHOX2* is critical for early heart development. A specific *SHOX2* mutation is lethal in early embryonic stage (Espinoza-Lewis et al., 2009), and a study of 2149 adults revealed that *SHOX2* single nucleotide polymorphisms (SNP) variants had the strongest association with heart rate irregularities measured in electrocardiography (ECG), and these variants are an indicator for several abnormal heart conditions (Kofler et al., 2017), suggesting the involvement of *SHOX2* in cardiac functions.

## **1.2 *Shox2* has critical roles in the development of bone, palate and joint in mouse.**

Studies in mouse models also revealed that *Shox2* has a critical role in bone development. The *Shox2* conditional KO in mouse limbs caused almost total loss of humerus and femur (Cobb, Dierich, Huss-Garcia, & Duboule, 2006), and *Shox2* can affect transcription of several chondrocyte proliferation and differentiation regulators, including *Tbx4* (Glaser et al., 2014), natriuretic peptide B (NPPB) (Aza-Carmona et al., 2014), and *bmp4/RUNX2* (Bobick & Cobb, 2012; Cobb et al., 2006). In addition, *Shox2* knock out (KO) studies demonstrated that *Shox2* is critical for the development of anterior palate (Yu

et al., 2005) and temporomandibular joint (Gu, Wei, Yu, Fei, & Chen, 2008).

These findings in the mouse model explained the mechanisms of the short stature and skeletal abnormalities detected in SHOX insufficiency diseases in human.

### **1.3 *Shox2* is critical for the development of heart pacemaker nodal-like cells in mouse.**

Most neurons and working myocytes fire action potentials because of external signal through electrical and chemical synapses, ligand-gated receptors or even physical stimulation. However, some cells, called pacemaker cells, have automaticity and they can generate action potentials or action potential bursts without any external stimulation at a specific rate, similar to an internal clock. The most typical example is pacemaker cells in the sinoatrial node (SAN) of the heart which have automaticity and are important to synchronize working myocytes in a stable firing rate (Greisas & Zlochiver, 2016). Brain areas also exhibit synchronized oscillatory functions, and neurons of the thalamus spike in a synchronized burst status at a specific rate and underlie conditions such as slow wave sleep and absence seizure (He et al.,

2015).

The pump function of the heart depends on proper generation and propagation of electrical activity, mainly action potentials, in the cardiac cells. In normal conditions, the action potentials are initiated in the pacemaker cells in the SAN and propagate down through the atrium, atrioventricular node to ventricle which leads to contraction of atrial and ventricular myocytes (Nerbonne & Kass, 2005). The cells in the SAN are the primary pacemaker site within the heart. The pacemaker cells in the heart generate spontaneous, regularly-timed, and continuous action potentials. Expression of ion channels important for this activity in the pacemaker cells in the SAN is different from other myocytes. Pacemakers have low expression of voltage-gated sodium channels. Instead, they have high expression levels of calcium channels, especially T-type calcium channels, which initiate slow calcium spikes instead of rapid sodium spikes shown in the working myocytes (Mangoni et al., 2006). Especially, previous studies have shown the most important ion channels underlying the pacemaking properties are hyperpolarization activated HCN channels and hyperpolarization de-inactivated T-type calcium channels (Cribbs, 2010; Ludwig et al., 1999). The HCN currents and T-type calcium currents are

activated at relatively hyperpolarized voltages and participate in sub-threshold depolarizations, which can lead to membrane oscillations. Thus, these currents are implicated in pace-making property.

When the pacemaker cells in SAN are repolarized/hyperpolarized more negative than  $-60\text{mV}$ , HCN channels, especially HCN2 and HCN4 channels, will be activated and conduct slow, inward depolarizing non-selective cation current. This HCN current depolarizes the membrane, which is called subthreshold depolarization (or phase 4) (Figure 1.2 A). HCN current initiates phase 4 and depolarizes the membrane to about  $-50\text{mV}$ , which reaches the activation threshold of another important channel, low voltage-gated T-type calcium channels, which conduct the depolarizing T-type calcium current. T-type calcium currents further depolarize the membrane up to the threshold of activation of L-type calcium current and maybe some voltage-gated sodium current, which mediate the main upstroke (phase 0) for pacemaker action potentials.

Different from the pacemakers of the SAN, atrial and ventricular cells do not have HCN or T-type calcium currents, therefore they don't possess automaticity. These cells receive upstream signals initiated from SA pacemakers and spike

immediately when they receive input. Besides, they have high voltage-gated sodium channel expression, so the upstroke of the action potential (phase 0) is very sharp (Figure 1.2 B). Most atrial and ventricular heart cells have a prolonged plateau (phase 2) which is caused by balance between L-type calcium current and voltage-gated potassium current. The plateau phase distinguishes working cardiac myocytes spikes from neurons and skeletal muscles and underlies the specific prolonged contraction function of the heart.

Besides the involvement of *Shox2* in the development of bone, palate and temporomandibular joint, several lines of evidence show that *Shox2* plays a critical function in determining pacemaker cell fate in mouse studies. First, *Shox2* expression is restricted to the pacemaker cells in the SAN (Ionta et al., 2015; Puskaric et al., 2010), dorsal mesenchyme protrusion (DMP) (Sun et al., 2015), and pulmonary vein (Ye et al., 2015). Second, knockout of *Shox2* causes impaired expression of channels important for pacemaker activity, such as HCN4 and loss of pacemaker action potential properties in these regions. In addition, *in vitro* studies showed that the majority of single cells isolated from embryoid bodies transfected with an adenoviral vector expressing human *SHOX2* exhibits pacemaker-like action potentials (Ionta et al., 2015). Finally,

*Shox2* KO mice suffer embryonic lethality because of impairment of the cardiac pace-making function in the SAN and DMP (Espinoza-Lewis et al., 2009; Sun et al., 2015). These studies elucidate the determined role of *Shox2* in the development of pace-making properties in the heart. Similar pace-making activities are observed in neurons throughout the nervous system.

#### **1.4 *Shox2* has important roles in the nervous system in mice.**

Previous studies have shown that *Shox2* has important functions in the nervous system. *Shox2* has been shown to be required for the differentiation of *tropomyosin receptor kinase B (TrkB)* positive touch sensory neurons in dorsal root ganglia (DRG) (Abdo et al., 2011). Another study found that *Shox2* is expressed in a subpopulation of excitatory interneurons in the ventral spinal cord (Dougherty et al., 2013). These *Shox2*-expressing interneurons are rhythmically active during locomotor-like activity, and conditional blockade of glutamate release in these cells affects the frequency and stability of locomotor-like rhythm activity. Further, research from the Cobb lab showed *Shox2* also expresses in the mouse hindbrain and is critical for the development of the facial motor nucleus (nVII) (Rosin, Kurrasch, & Cobb, 2015) and cerebellum

(Rosin, Kurrasch, et al., 2015). They found whole brain *Shox2* KO resulted in elevated cell death in the facial motor nucleus, and correlated impaired facial nerves projection at E12.5-E14.5 days, and a drastic reduction in the size of facial motor nucleus at P0. In another study, they found inducible knock-out of *Shox2* in cerebellum by *En2-CreERT2* at E9.5 caused impaired cerebellar development and deficits in motor coordination.

Interestingly, previous studies showed that *Shox2* is a direct binding target and under regulation of *Aristaless*-related homeobox gene (*Arx*) (Fulp et al., 2008; Poeta et al., 2013; Shoubridge, Tan, Seiboth, & Gecz, 2012). Different mutations in *ARX* in humans have been linked to at least nine distinct neurological disorders (Fulp et al., 2008) including X-linked infantile spasm disorders (Olivetti, Maheshwari, & Noebels, 2014), infantile epileptic encephalopathy (Guerrini et al., 2007; Kato et al., 2007), Partington syndrome disorders (Frints et al., 2002; Gronskov et al., 2014), autism (Turner, Partington, Kerr, Mangelsdorf, & Gecz, 2002) and impaired intellectual abilities (Sherr, 2003). Mouse studies have revealed that *Arx* is specifically expressed in interneurons and regulates interneuron migration and maturation (Colombo, Galli, Cossu, Gecz, & Broccoli, 2004; Marsh et al., 2016; Poirier et al., 2004).

*Arx* has been found to express in the ventral thalamus and repress *Shox2* expression from embryonic to postnatal stage and postnatal estradiol application decreased *Arx* mutant-induced *Shox2* upregulation and prevented *Arx* mutant-induced infantile spasms (Olivetti et al., 2014). Although, forebrain tissue is the main resource of brain tissue used in these studies, the detailed expression of *Shox2* at the brain area-specific level and in cell-specific levels is not studied.

### ***1.5 The anatomy and function of the greater thalamus***

The thalamus is a gray matter region located in the dorsal part of the diencephalon of the brain. The thalamus is best known as the main relay center linking different regions of neocortex with peripheral sensory input, subcortical nuclei, and the midbrain. Since the thalamus is located centrally in the brain and is important for overall brain function, the term thalamus derives from the Greek word that means 'inner chamber' or 'meeting place' describing the location and function of the thalamus (Mashour & Alkire, 2013; Mishra & Mishra, 2012). Historically, the thalamus was recognized as encompassing a larger brain region, and the term of 'thalamus' in some scientific papers is still



ambiguous. In this dissertation, we refer to the traditional 'thalamus' as 'the greater thalamus'. The greater thalamus has been found to play an important role in sensory and motor information relay and processing, the generation and maintenance of brain rhythms, and limbic cognitive functions including emotion regulation and memory formation.

The greater thalamus is the central core nuclear complex surrounded by the cerebral hemispheres, and connected dorsally to hypothalamus and midbrain (Figure 2.1). It contains three main parts: epithalamus, thalamus and prethalamus (ventral thalamus). Nissl first proposed that the epithalamus is not part of thalamus because the epithalamus connects the hypothalamus and interpeduncular regions rather than cerebral hemisphere and midbrain (Edward G Jones, 2012). Later it was proposed that ventral thalamus is developmentally more similar to the subthalamus and hypothalamus, so ventral thalamus should not be considered as part of thalamus (Edward G Jones, 2012; Martinez-Ferre & Martinez, 2012). Only the dorsal thalamus typically connects cerebral hemispheres and midbrain and is referred to as the thalamus. Therefore, for simplicity in this dissertation, 'thalamus' means the dorsal part of greater thalamus, excluding prethalamus and epithalamus.

Epithalamus is located mediodorsally of the thalamus and forms an important part of third ventricle walls. It consists of two main nuclei, the pineal body and habenula (Concha & Wilson, 2001). The pineal gland is a small, pinecone-shaped endocrine gland. It produces and secretes melatonin, which plays an important role in an animals' circadian rhythm and seasonal cycles (Fraschini, Mess, & Martini, 1968). The habenula nuclei, consist of two distinct regions called lateral habenula (LH) and media habenula (MH). These nuclei receive primary afferents from septum and *stria medullaris* and project to midbrain. The habenular nuclei have been demonstrated to play an important role in pain processing, learning and memory (Mathis & Lecourtier, 2017; Tomaiuolo, Gonzalez, Medina, & Piriz, 2014), emotion (J. Li, Li, Zhang, Shen, & Zhao, 2016), and motivation and reward (Hikosaka, 2010; Proulx, Hikosaka, & Malinow, 2014). Dysfunction of habenula can cause cognitive impairment, attention deficits, schizophrenic-like symptoms and mood disorders (Lecourtier, Neijt, & Kelly, 2004).

Prethalamus (or also called ventral thalamus) forms a shell ventral and lateral to the thalamus. The main nuclei of the prethalamus are reticular nucleus of thalamus (RT), ventral lateral geniculate nucleus (LGN), subgeniculate

nucleus (SG), and zona incerta (ZI) (Watson et al., 2017). Unlike the thalamus, the prethalamus does not project excitatory afferents into cerebral cortex. Generally, most nuclei in the prethalamus connect with other thalamic nuclei and play an important role in brain rhythm generation, synchronization and maintenance (Avanzini et al., 1992).

The RT is located between the external medullary lamina and the internal capsule white matter, forming a ventral and caudal shell for the thalamus. RT consists of GABAergic interneurons and is typically labeled with parvalbumin (PV), a marker for fast-spiking interneurons. RT has been found to have at least seven sectors including five sensory, one motor and one limbic (Pinault, 2004) with a similar topographic organization of somatosensory, auditory and visual sectors, similar to the neocortex and thalamus (Shosaku, Kayama, & Sumitomo, 1984). For example, the sensory afferents of the whiskers on the mystacial pad of the rodent snout project to a specific barreloid region of the ventral basal (VB) nucleus of the thalamus. The primary relay neurons in these regions of the thalamus project to the specific regions of the somatosensory cortex, called the barrel cortex, while branching to a specific region of Rt. While the specific reciprocal projections from corticothalamic neurons in the barrel cortex reach

the same barreloid region and branch to the same region in the Rt. Neurons in Rt receive the excitatory inputs from specific cortical and thalamic regions and send inhibitory input the same thalamus regions. Thus, Rt is an important region to regulate thalamocortical connectivity. Rt may regulate almost all thalamus cell excitability, and also the thalamocortical and corticothalamic projections.

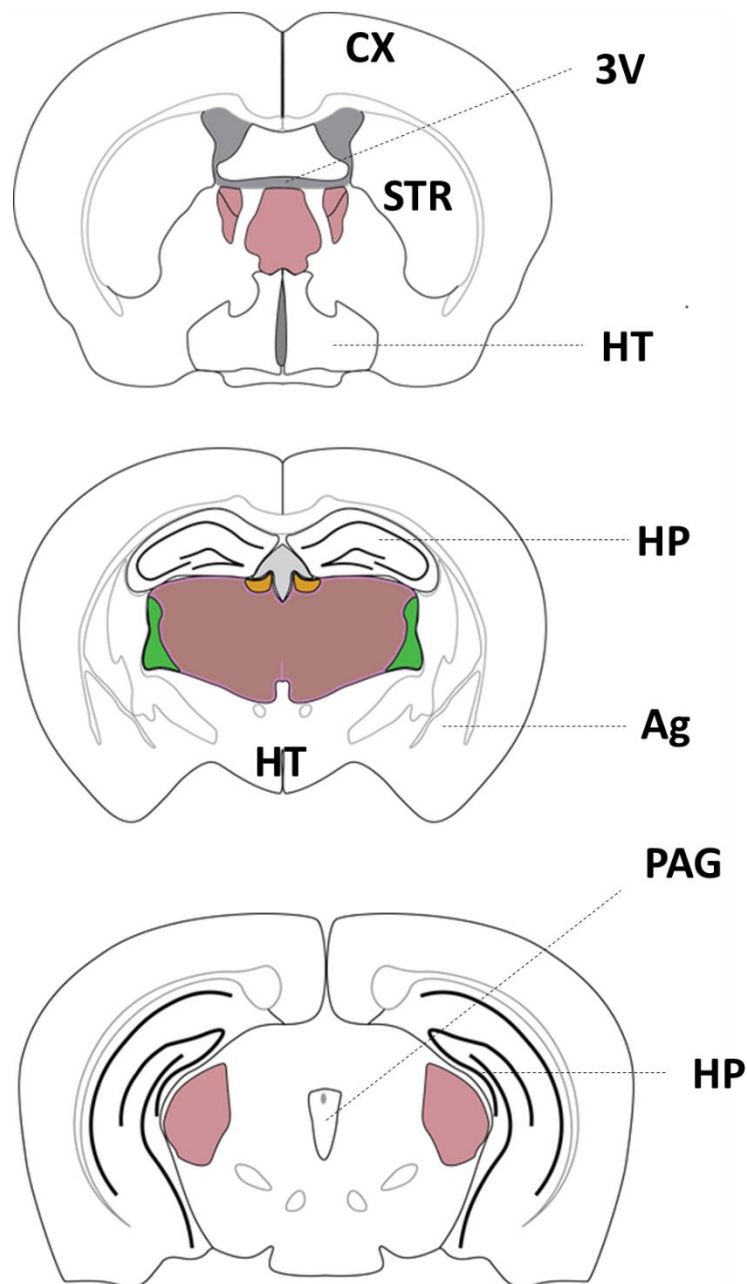


**Figure 1.1 Schematic representation of a coronal view of adult mouse brain from rostral to caudal.** The greater thalamus, consisting of epithalamus (yellow), thalamus (purple) and ventral thalamus (green), is connected ventrally to the hypothalamus, and surrounded laterally by forebrain and midbrain bundle systems, and bordered dorsally by hippocampus.

## 1.6 The anatomy and function of the thalamus

The thalamus is the largest component derived from prosomere 2 (p2) of the diencephalon (Martinez-Ferre & Martinez, 2012). It consists of more than 50 nuclei (Herrero, Barcia, & Navarro, 2002). Based on common function and anatomical location, the thalamus can be divided into three main groups of nuclei by the internal medullary lamina: anterior thalamus (ATN), medial and midline thalamus, and lateral thalamus. The neurons of most thalamic nuclei project to the layer IV of the cortex, but some project rather diffusely to upper cortical layers, including layer I (Cruikshank et al., 2012; Kloc & Maffei, 2014). Almost all incoming sensory information from the periphery passes through the thalamus on the way to the cortex, so the thalamus has a critical role in processing and gating the flow of the information (Sherman, 2007). Some diffuse connections between the thalamus and cortex work as a delay and control center for cortex and cortex connection (Guillery, 1995; Sherman, 2016). In addition, the typical burst firing properties of the thalamic neurons and the reciprocal connection between the thalamus and prethalamus are critical for brain rhythm generation and maintenance.

The anterior thalamus nuclei group consists of anterodorsal nucleus (AD),

anteromedial nucleus (AM), anteroventral nucleus (AV) and laterodorsal nucleus (LD). ATN is considered an important part of limbic system (Seki & Zyo, 1984), and it connects with other parts of limbic system, mainly mammillary bodies, prefrontal cortex, hippocampus, and hippocampal formation (Irle & Markowitsch, 1982). Many of these connections are reciprocal and region specific, such as the connection between AD and retrosplenial cortex, AV and anterior cingulate cortex, and AM and entorhinal cortex (Jankowski et al., 2013). The connections and functions of cells in the ATN can be considered as three parts: 1) Head direction cells, which fire only when an animal's head points in a specific direction (Taube, 1995). These cell have been found to mainly distribute in the AD projection pathway, including AD, LD, postsubiculum, parasubiculum, lateral MB and dorsal tegmental nucleus of Gudden (Clark & Taube, 2012). This pathway has been proposed and demonstrated to merge external and internal sources of information, especially head direction signals, and contribute to spatial navigation; 2) All nuclei of ATN but mainly AM, receive a large input from hippocampal formation and project to the prefrontal cortex and take part in the loop of hippocampus-ATN-prefrontal cortex-hippocampus for higher cognitive and executive function (M. Li, Long, & Yang, 2015). 3) The

feedback loop between AV and the hippocampal formation is proposed to be important for generation, propagation and maintenance of brain rhythms between hippocampal formation and the thalamus, and these rhythms are important in limbic cognitive function (Jankowski et al., 2013; Tsanov et al., 2011).

The middle part of the thalamus consists of three main groups of nuclei: medial thalamus, midline thalamus and intralaminar nuclei of thalamus. Mediodorsal (MD) nucleus locates medial to the internal medullary lamina and is the main medial nucleus of the thalamus (Mitchell, 2015). MD is the most studied limbic thalamic nucleus. Different sub-regions of MD have specific and reciprocal connections between different regions of prefrontal cortex. The MD-PFC synchronization is thought to be critical for the function of PFC which is considered the core for higher cognitive function including working memory, selective attention and decision making (Cardoso-Cruz, Sousa, Vieira, Lima, & Galhardo, 2013; Parnaudeau et al., 2013).

The midline thalamus consists of paraventricular (PVT), paratenial (PT), reuniens (RE) and rhomboid (RH) nuclei and is located essentially within the middle of the whole brain. Generally, the function of the middle thalamus is



related to higher cognitive functions, including memory processing, attention and orienting as well as reward-based behavior (Van der Werf, Witter, & Groenewegen, 2002). PVT and PT nuclei of the midline thalamus mainly project to the amygdala and nucleus accumbens (Vertes, Linley, & Hoover, 2015), and are involved in stress response (Bhatnagar, Huber, Nowak, & Trotter, 2002), feeding behavior (Choi et al., 2012) and circadian regulation (Salazar-Juarez, Escobar, & Aguilar-Roblero, 2002). RE and RH of midline thalamus mainly project to hippocampus and medial PFC. Given their connection with the hippocampus and mPFC, RE and RH play a role in processes such as working memory, long-term memory persistence and strategy shifting in memory task (Cholvin et al., 2013; Hallock, Wang, & Griffin, 2016; Loureiro et al., 2012).

The intralaminar nuclei group locates within the internal medullary lamina and consists of several nuclei, including parafascicular nucleus (PF), central lateral nucleus (CL), paracentral nucleus (PCN), central medial nucleus (CM) and rhomboid nucleus (RH). Intralaminar nuclei project to a wide range of cortical and sub-cortical structure including prefrontal cortex and posterior cingulate (Saalman, 2014), so are involved in a broad variety of functions, including arousal (Van der Werf et al., 2002), attention (Kinomura, Larsson,

Gulyas, & Roland, 1996), working memory (Newman & Burk, 2005), saccade generation and movement monitoring (Koch, 1995).

The lateral thalamus nuclei group is defined as all nuclei between internal medullary lamina and external medullary lamina, including dorsal and posterior subgroup nuclei such as posterior complex (PO), lateral posterior nucleus (LP), ventral subgroup such as ventrobasal nucleus (VB), ventral medial nucleus (VM), ventral lateral nucleus (VL), ventral anterior nucleus (VA) and geniculate group, such as dorsal LGN and medial geniculate nucleus (MGN) (Takahashi, 1985). Lateral thalamus nuclei have the most typical sensory relay functions. All peripheral sensory inputs except olfactory information are relayed through the lateral thalamus: dLGN relayed visual information (Dan, Alonso, Usrey, & Reid, 1998; Reinagel, Godwin, Sherman, & Koch, 1999), MGN relayed auditory and balance information (Wehr & Zador, 2003), VB relayed somatosensory and taste information (Cechetto & Saper, 1987; E. G. Jones & Friedman, 1982). In addition, most motor information from the Globus Pallidus is relayed by VA and VL to the primary motor cortex (Shipp, 2005).

Most parts of lateral thalamus, including LGN, MGN, VB, VA and VL relay specific input into the specific region of the cortex and are called first order relay

nuclei. The relay neurons located in first order relay nuclei are also called thalamocortical relay neurons or principal relay neurons. They provide the main specific thalamocortical projection to specific primary sensory or motor cortex and receive reciprocal projections from the same specific cortex. They form thalamocortical reciprocal connection circuits which are critical for sensory information propagation and processing (Basso, Uhlrich, & Bickford, 2005).

Other than these first order relay neurons, LP and PO, along with MD in medial thalamus, LD in anterior thalamus and intralaminar nuclei, are typical higher order relay neurons. They usually receive projections from primary sensory cortex or subcortical nuclei and project to higher order cortex such as medial PFC. They have important role in relaying and processing information between cortex. Higher order relays form important cortico-thalamo-cortico circuit which is essential for cortex information processing (Theyel, Llano, & Sherman, 2010). LP and PO are the higher order relay nuclei implicated in multisensory processing including visual and nociceptive information processing (Allen, Procyk, Howarth, Walmsley, & Brown, 2016).

## **1.7 Electrophysiological properties of thalamus neurons**

The thalamus is critical in controlling brain function. Electroencephalogram

(EEG) recordings show that mammalian brains have two distinct states. During wake state, especially when closing eyes and without any interruption, the typical EEG signal is 8-13Hz low amplitude activity (alpha waves). However, during deep sleep or absence seizures, the typical EEG signal is 0.5 - 4 Hz high amplitude activity (delta waves)(Giordano, Foppiani, Minuto, Marugo, & Barreca, 1973). Because of the low frequency of delta waves compared to alpha waves, exhibited during sleep are also called slow-wave sleep. The *in vivo* electrophysiological recording from LGN of cat revealed that thalamus cells have two distinct states of action potential patterns. During slow-wave sleep, thalamus neurons are hyperpolarized and exhibit bursts of action potentials, while during wave and rapid eye movement sleep (REM), thalamic neurons are depolarized and exhibit high frequency trains of single action potentials (Hirsch, Fourment, & Marc, 1983). During slow-wave sleep and absence seizure, thalamic neurons are relatively hyperpolarized and exhibit burst action potential firing patterns (Figure 2.2). Besides, the finding that the transition from sleep to waking is associated with the depolarization of thalamus neurons by ascending arousal neurotransmitters such as acetylcholine (ACh) and norepinephrine (NE) further indicates the critical role of the thalamus in controlling the status of the

whole brains (Kayama & Koyama, 2003; McCormick & Prince, 1987).

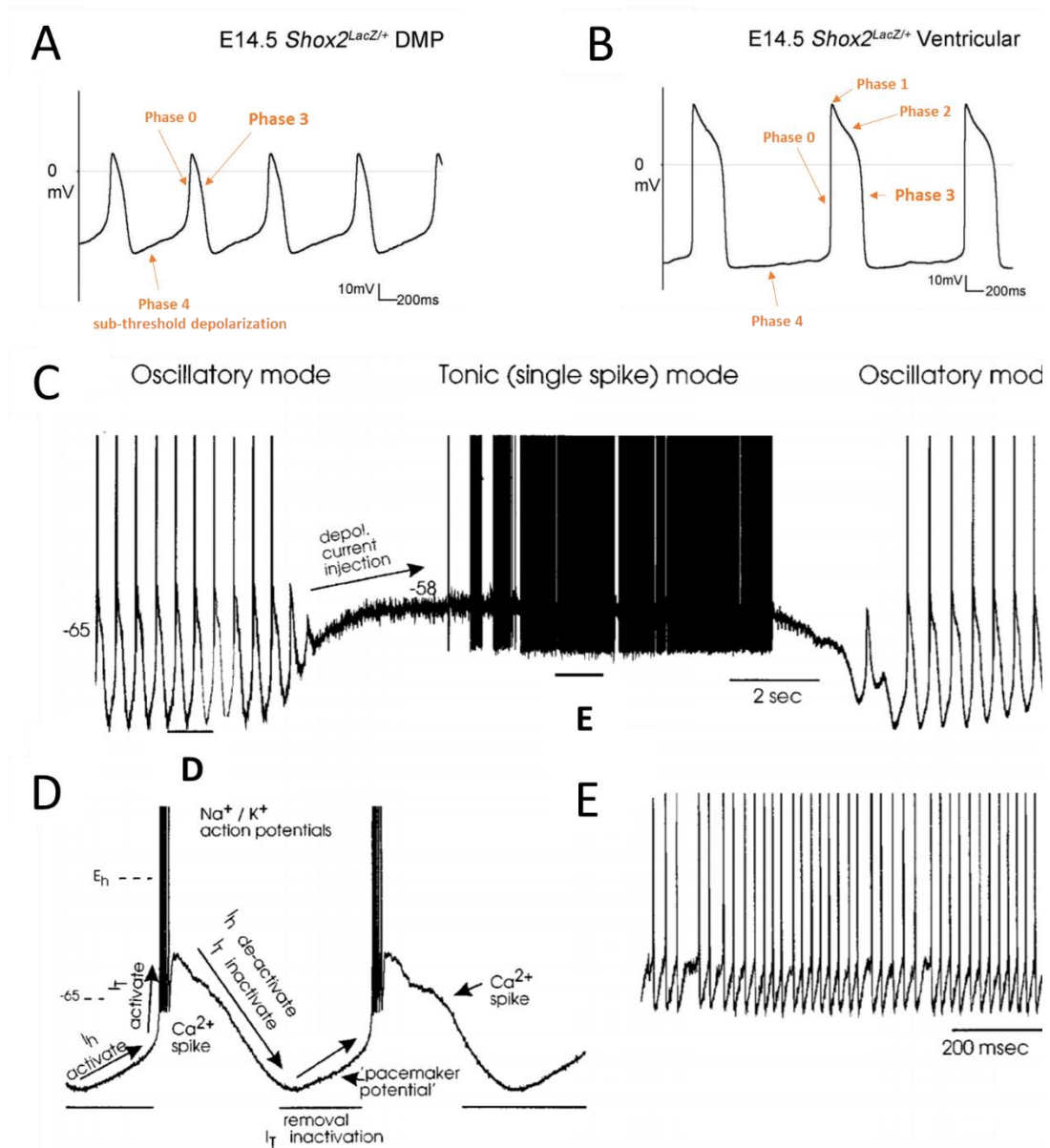


**Figure 1.2 The morphology of typical action potentials in heart and thalamus.** A-B. In heart, action potentials in pacemakers and working myocytes have distinct morphology. A. Typical action potentials in pacemakers have 3 phases. Phase 4 has sub-threshold depolarization mediated by HCN current and T-type calcium current. Phase 0 is a slow upstroke phase mediated by calcium current. Phase 3 is a smooth repolarization phase led by potassium current. B. Typical ventricular action potentials have 5 phases. Phase 4 has no sub-threshold depolarization. Phase 0 is a rapid upstroke phase mediated mainly by fast voltage-gated sodium current. Phase 1 is a quick and sharp repolarization phase mediated by A-type potassium current. Phase 2 is a balanced 'plateau' by calcium current and potassium current. Phase 3 is the same repolarization phase as that in pacemakers dominated by potassium current. D-E, Thalamic neurons (in dLGN) have two action potential patterns. C. Thalamic neurons

exhibit two different patterns of action potentials: tonic spikes (enlarged in Figure E) pattern and burst spikes pattern (enlarged in Figure D). When the membrane of thalamic neurons is depolarized (-58 mV in Figure), thalamic neurons exhibit tonic action potential pattern similar as other types of neurons. When the membrane of thalamic neurons is hyperpolarized (negative than -65 in Figure), thalamic neurons exhibit burst action potential pattern with a delta frequency (0.5Hz-4Hz). D) HCN current ( $I_h$ ) and T-type calcium current ( $I_T$ ) mediate the thalamic burst spike pattern. HCN current is activated in hyperpolarized membrane potential and depolarized the membrane. The potential of membrane depolarized by HCN current reaches the threshold of and is further depolarized by T-type calcium current to the threshold of voltage-gated sodium current and L-type calcium current, therefore exhibit multiple fast  $\text{Na}^+$  spikes and a slow  $\text{Ca}^{2+}$  spike in each burst. The depolarization de-activated HCN current and inactivated T-type calcium current immediately before spikes and voltage-gated potassium current repolarizes and hyperpolarizes the membrane back under -65mV, at which HCN current will be activated again and the inactivation of T-type calcium current will be removed and induced the next burst. E) The burst spike pattern of action potentials when the membrane of thalamic neurons is relatively depolarized. Figures are adapted from Dr. Sun and Dr. McCormick's paper (McCormick & Bal, 1997; McCormick & Pape, 1990; Sun et al., 2015).

## **1.8. HCN2/4 channels and T-type calcium channels are important currents implicated in pacemaking function.**

### **1.8.1 HCN channels**

Hyperpolarization-activated cyclic nucleotide-gated (HCN) channels are non-selective cyclic adenosine monophosphate (cAMP)-gated cation channels mainly distributed in the heart and brains of vertebrate animals and play roles in oscillatory firing patterns (Luthi & McCormick, 1998). HCN channels are usually activated at a hyperpolarized potential typically more negative than -50mV with existence of Camp. The channels are permeable to non-selective cation ions, mainly Na<sup>+</sup> and K<sup>+</sup>, and thus the HCN currents usually have a reverse potential around -30mV (Wahl-Schott & Biel, 2009). The specific properties of HCN channels provide interesting physiological functions, and their activation at hyperpolarized potential allows for depolarized membrane voltage. In this way, HCN channels can reverse an inhibitory input to an excitatory one. This transition of inhibition to excitation makes HCN channels allow pacemaking properties, so the channels are also called pacemaker channels and HCN channels underlie the automaticity properties in the heart and brain. The HCN currents are also called h-currents (or I<sub>h</sub>), funny currents



(I<sub>f</sub>), or pacemaker currents.

There are four subtypes of HCN channels from HCN1 to HCN4. The voltage-dependent activation properties differ quantitatively among these four subtypes. The typical value of midpoint of activation voltage ( $V_{1/2}$ ) of HCN1 is around -70mV, while that of HCN2 and HCN4 is around -100mV in the presence of 1mM cAMP (Altomare et al., 2003). The activation kinetics are also different among these four subtypes. HCN1 is the fastest channel with a range of activation time constant ( $\tau$ ) from 25ms to 300ms depending on the voltage, temperature, and cAMP concentration. HCN4, on the other hand, is the slowest HCN channels with a 40-fold slower  $\tau$  compared to HCN1 at -35 °C, -100 mV and 1mM cAMP (Ishii, Takano, & Ohmori, 2001). The  $\tau$  of HCN4 can be up to several seconds at -70mV (Wahl-Schott & Biel, 2009). The properties of HCN2 and HCN3 channels fall between HCN1 and HCN4.

HCN1 channels are the main HCN channels in most regions of the brains, including hippocampus, layer IV cells of the neocortex, and Purkinje cells of the cerebellum (Ludwig et al., 2003). HCN1 channels in cerebellar Purkinje cells have been found to be important in motor learning and postsynaptic neuronal signal integration (Nolan et al., 2003), and in the hippocampal network are

important for theta (4-9Hz) field oscillation potentials recorded *in vivo* from CA1 pyramidal layer (Nolan et al., 2004).

The HCN2/4 channels are the most typical channels in the pacemaker cells of heart SA node (Ludwig et al., 1999). Compared to HCN1 channels, HCN2 and HCN4 channels are activated at the most hyperpolarized voltage and have the slowest activation/inactivation kinetic (Altomare et al., 2003). These properties make HCN2/4 channels critical for low-frequency automaticity in the heart for several reasons. First, the hyperpolarized activation threshold of HCN2/4 makes these channels not respond to small hyperpolarization inputs or subtle membrane voltage fluctuation, but only to deep hyperpolarization, so h-current is more stable and develops its own automaticity. Secondly, the slower activation/inactivation kinetics of HCN2/4 make h-currents last longer and thus control the rhythmic oscillations at a lower frequency. Interestingly, different from the cortex and hippocampus with predominately HCN1 expression, HCN2 and HCN4 expression are highly expressed in the thalamus (Fig. 1.3) (Abbas, Ying, & Goldstein, 2006; Notomi & Shigemoto, 2004). This high HCN2/4 expression is very similar to that in SA node of the heart. The burst action potential patterns in the thalamus are also very similar like action potential

pattern in the SA node of the heart. The same specific expression pattern of HCN channels and action potential patterns suggest the possibility of same master gene controlling expression of these channels in the thalamus and SA nodal cells.

### **1.8.2 T-type Ca<sup>2+</sup> channels**

Transient-opening (T-type) calcium channels are low voltage-activated Ca<sup>2+</sup> channels relative to long opening (L-type) calcium channels with higher activation voltage. The activation voltage threshold of T-type calcium channels is typically around -55 mV, compared to L-type calcium channels with an activation voltage threshold above -20mV (Zhou & January, 1998). T-type calcium channels have a rapid inactivation time and small single-channel current, so the T-type calcium current is a transient current at the whole cell level (Cheong & Shin, 2013). Although there are other subunits such as  $\beta$ ,  $\alpha 2\delta$  and  $\gamma$  subunits, the main properties of T-type calcium channels are determined by the pore-forming  $\alpha 1$  subunit (Perez-Reyes, 2003). There are three types of T-type calcium channels in the vertebrate called Cav3.1, Cav3.2 and Cav3.3 respectively, each of which associated with a specific  $\alpha 1$  subunit  $\alpha 1G$ ,  $\alpha 1H$ , and  $\alpha 1I$ , coded by the respective genes *CACNA1G*, *CACNA1H*, and *CACNA1H*

(Iftinca, 2011). T-type calcium currents are important pace-making currents in the nodal like cells in the heart (Cribbs, 2010; Zhou & January, 1998). Besides, T-type calcium channels are expressed in the thalamus (Fig. 1.3) and the currents are implicated in several thalamus-related physiological and pathological process such as sleep regulation, sensory information relay and absence seizure (Cheong & Shin, 2013). Because T-type calcium channels are inactivated at depolarized voltages and hyperpolarization can remove this inactivation and possess slower characteristics than voltage-gated sodium channels, the T-type calcium channels are usually activated when the membrane voltage recovers from hyperpolarization. T-type calcium currents can induce long rebound calcium spikes which usually cause depolarization sufficient to reach threshold and cause multiple Na<sup>+</sup> spikes (Perez-Reyes, 2003). These properties implicate T-type calcium channels in slow frequency automaticity.

This dissertation investigates the expression pattern of *Shox2* and the role of *Shox2* in regulation of genes important for pace-making activity and neuronal functions in the thalamus. Further, I go on to demonstrate that *Shox2* KO affects the physiological properties of thalamic neurons.

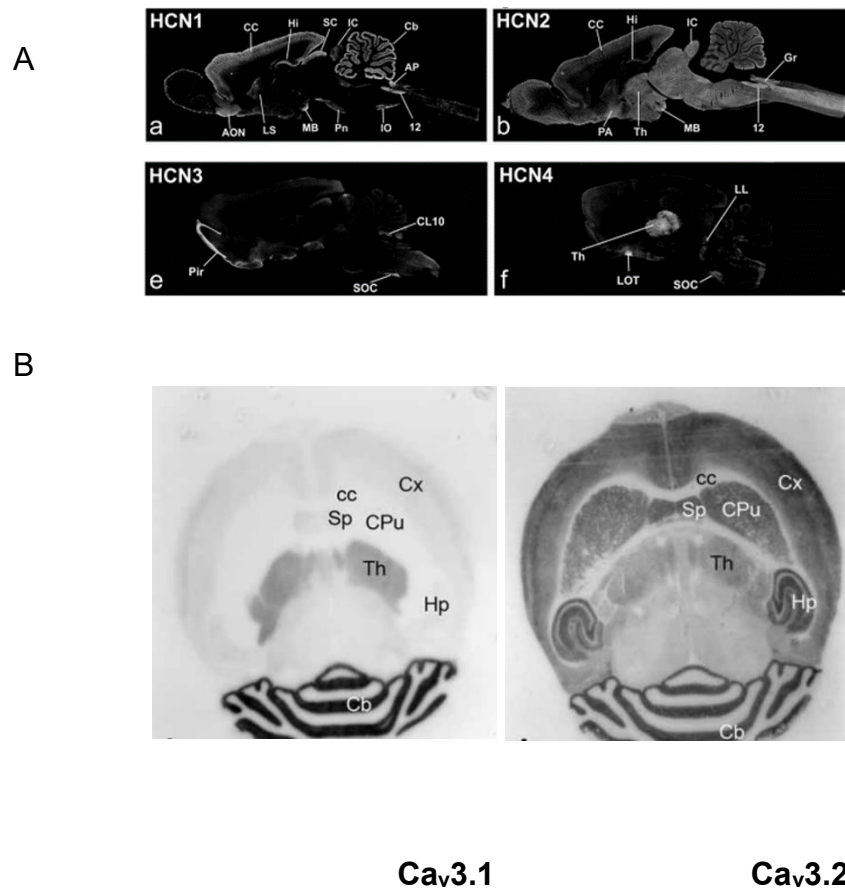


**Figure 1.3 The expression of HCN channels and T-type calcium channels in rodent brain.** A) HCN1 is the main HCN channel expressing in the cortex, hippocampus and cerebellum in rat brain. HCN2 is expressed in the cortex, thalamus, midbrain and hindbrain. HCN3 is mainly expressed in piriform area. HCN4 is specifically expressed in the thalamus (Notomi & Shigemoto, 2004). B) The protein expression of Ca<sub>v</sub>3.1 and Ca<sub>v</sub>3.2 in mouse brain. Ca<sub>v</sub>3.1 is specifically expressed in the thalamus while Ca<sub>v</sub>3.2 has relatively low expression in the thalamus (Aguado, Garcia-Madrona, Gil-Minguez, & Lujan, 2016).

## Chapter II: Methods

### 2.1 Mouse introduction

All procedures involving mice are approved by Tulane University Institutional Animal Care and Use Committee (IACUC) according to National Institutes of Health (NIH) guidelines. All *Shox2* transgenic mice were generously given by Dr. Yiping Chen's lab. All C57/Bl6 mice were ordered from Charles River. *Rosa26<sup>LacZ/+</sup>*, *Gbx2<sup>CreERT/+</sup>* breeders were ordered from Jackson Lab.

The first two exons in a *Shox2* allele in *Shox2<sup>LacZ/+</sup>* and *Shox2<sup>cre/+</sup>* mice were partially replaced by LacZ and Cre genes so the transcriptional product under the *Shox2* promoter in that allele is LacZ mRNA and Cre mRNA, while the unaffected alleles work normally (Sun, Zhang, Liu, Gu, & Chen, 2013). *Rosa<sup>CreERT/+</sup>* mice were a transgenic mouse line with tamoxifen-inducible creERT inserted in the *Rosa26* loci. Cre-loxP recombination may occur ubiquitously among the organism once tamoxifen is injected to induce free Cre protein from CreERT under the constitutively and ubiquitously-activated *Rosa26* promoter. *Gbx2<sup>CreERT/+</sup>*, in which CreERT is specifically expressed in the midline thalamus

of adult mouse, was used for KO of *Shox2* in a specific region of the thalamus for a better comparison between control region of thalamus and KO region of thalamus. *Rosa26<sup>LacZ/+</sup>* mice are a transgenic mouse line with inserted floxed stop signals followed by LacZ gene in *Rosa26* loci (Soriano, 1999). This mouse strain is used to test the expression of the Cre transgene in any transgenic strain carrying Cre under the regulation of a specific promoter, so it is called 'Cre reporter' strain in the dissertation.

In inducible KO experiments, we crossed *Rosa26<sup>CreERT/+</sup>*, *Shox2<sup>ff</sup>* or *Rosa26<sup>CreERT/CreERT</sup>*, *Shox2<sup>ff</sup>* or *Gbx2<sup>CreERT/+</sup>*, *Shox2<sup>ff</sup>* female mice with *Shox2<sup>-/+</sup>* male mice. The litters were labelled and genotyped PND10. The knock-out group was the *CreERT/+*, *Shox2<sup>ff</sup>* mice or *CreERT/+*, *Shox2<sup>ff</sup>* mice and the control (CR) group was the littermate *CreERT/+*, *Shox2<sup>+/f</sup>*. Tamoxifen (20 mg/mL) was dissolved in sterile corn oil (sigma, C8267) with 10% alcohol and aliquoted. In the tamoxifen-inducible knock out (KO) experiments, pre-warmed tamoxifen (160 mg/kg) was injected to KO mice and control littermates intraperitoneally (IP) at the same time every day for five consecutive day. The littermate KO mice and CR mice of the the same sex are housed together and received the same handling and their individual genotypes are blinded to the experimenter. RT-

qPCR experiments with tissue from brain stem was used to confirm the efficiency of *Shox2* KO in brains in every animal tested.

## 2.2 X-gal staining

Adult *Shox2*<sup>LacZ/+</sup> or *Shox2*<sup>cre/+</sup>, *Rosa*<sup>LacZ/+</sup> male mice were anaesthetized and sacrificed by decapitation, and the brains were removed. Brains were sliced at 200  $\mu$ m using a Vibratome Series 3000 Plus Tissue Sectioning system. Brain slices were placed into ice-cold artificial cerebrospinal fluid (aCSF) in a 24-well plate, and fixed with 0.5% glutaraldehyde and 4% paraformaldehyde in PBS for 15 minutes. After 3X wash with ice-cold aCSF, the slices were stained with X-gal staining solution (X-gal (1mg/ml), potassium ferrocyanide (4 mM), potassium ferricyanide (4mM), MgCl<sub>2</sub>(2 mM)) and covered by aluminum foil at 37 °C overnight. All slices were washed and post-fixed, then images were taken under stereoscope.

## 2.3 Immunohistochemistry (IHC)

Mice were deeply anaesthetized by injection with ketamine (80 mg/kg) mixed with xylazine (10 mg/Kg), transcardially perfused with PBS followed by



4% paraformaldehyde in PBS and decapitated for brain collection. Mouse brains were placed in 4% paraformaldehyde at 4 °C overnight for post-fix, 15% and 30% sucrose in PBS respectively at 4 °C overnight for cryostat-protection. Brain samples were embedded with optimal cutting temperature compound (O.C.T.) and stored at -20 °C and cryo-sectioned to 20 µM coronal slices with *Leica CM3050S*. The brain slices were collected and placed on microscope slides (Superfrost, Fisher Scientific, 22-037-246). For IHC staining, slides with cryostat slices samples were washed with 50 mM Tris buffered saline with 0.025% Triton X-100 (TTBS) and blocked in 2% Bovine serum albumin (BSA) in TTBS for 2 hours at room temperature. Primary antibodies were diluted in blocking solutions and applied on slides overnight at 4 °C. Fluorescence conjugated secondary antibodies were diluted 1:1000 in blocking solutions and applied on slides for one hour at room temperature. 1:1000 DAPI were applied for 5 minutes at room temperature for nuclei staining. After wash, the slides were mounted with H-1000 mounting media and imaged under confocal microscope.

Antibody list: Chicken anti  $\beta$ -galactosidase antibody (abcam, ab9361): 1:500; rabbit anti NeuN antibody conjugated with Cy3 (Millipore sigma, ABN78): 1:500; mouse anti parvalbumin antibody (Millipore sigma, MAB1572): 1:500;

Rabbit anti GFP antibody (Novus Biologicals, NB 600-308): 1:300; Rabbit anti-

GFAP antibody (PhosphoSolutions, 620-GFAP): 1:300;

Alexa Fluor 488 Goat anti-mouse (Life technologies), 1:1000; Alexa Fluor 594

Goat anti-rabbit (Life technologies): 1:1000; Alexa Fluor 647 Goat anti-chicken

(Life technologies): 1:1000;

## **2.4 Quantitative reverse transcription PCR (RT-qPCR)**

The whole thalamus was collected from adult mouse brains and immediately stored in *RNAlater™ RNA stabilization reagent* (Qiagen, 76104). RNA was extracted from thalamus tissue using *RNeasy Mini Kit* (Qiagen, 74104) following the standard protocol provided in the manual. The RNA concentration and quality were tested using *Nanodrop Microvolume Spectrophotometers and Fluorometer* and gel investigation. Reverse transcription was conducted using *iScript™ Reverse Transcription Supermix* (Bio-rad, 1708840). Quantitative PCR was conducted with *iTaq™ Universal SYBR<sup>R</sup> Green Supermix* (Bio-rad, 1725121) in *Bio-Rad<sup>R</sup> CFX96 Touch™ PCR system*. Data analysis was done with *CFX Manager software*. The primer sequences of all tested genes including reference gene ACTB and TBP were listed in *Table 1*.

## 2.5 Terminal deoxynucleotidyl transferase dUTP nick end labeling (TUNEL)

The TUNEL experiments were conducted with *In Situ Cell Death Detection Kit, Flurescein* (Roche, 11684795910) following the standard protocol provided in the manual. Briefly, 20  $\mu$ M cryostat coronal brain slices on slides were dried at room temperature and washed with phosphate buffered saline (PBS) with 0.025% Triton X-100. All slides were merged in the antigen retrieval buffer (10mM sodium citrate, pH= 6.0, 0.5% Triton X-100) at 95 °C for 5 minutes. After cooling and washing, 2% BSA in PBS was applied on slides for 1 hour at room temperature to block all slides. After blocking, the staining mix was applied to slides under the instruction of the manual. 1:1000 DAPI were applied for 5 minutes for nuclear staining. All slides were mounted *with H-1000 mounting media* and store at 4 °C and then imaged using confocal microscope.

**Table 1. The list of sequence and target band size of RT-qPCR primers**

<b>Gene</b>	<b>Forward Primer</b>	<b>Reverse Primer</b>	<b>Band size</b>
<b><i>Shox2</i></b>	CCGAGTACAGGTTTGGTTTC	GGCATCCTTAAAGCACCTAC	147 bp
<b><i><math>\beta</math>-actin</i></b>	CTAGACTTCGAGCAGGAGAT	GATGCCACAGGATTCCATAC	161 bp
<b><i>Hcn1</i></b>	CTTCGTATCGTGAGGTTTAC	GTCATAGGTCATGTGGAATATC	111 bp
<b><i>Hcn2</i></b>	CTTTGAGACTGTGGCTATTG	GCATTCTCCTGGTTGTTG	114 bp
<b><i>Hcn4</i></b>	ATACTTATTGCCGCCTCTAC	TGGAGTTCTTCTGCCTATG	132 bp
<b><i>Cacna1g</i></b>	GACACCAGGAACATCACTAAC	CACAAACAGGGACATCAGAG	111 bp
<b><i>Cacna1h</i></b>	TTTGGAACATATGTGCTCTTC	TCTAGGTGGGTAGATGTCTTATC	116 bp
<b><i>Gria2</i></b>	GGAATGGTATGGTTGGAGAAC	GGCTTCGAGAAGTCAATCAC	103 bp
<b><i>Bcl-2</i></b>	ATGGTGTGGTTGCCTTATG	TCCTGTGCAAAGAACTTACTG	105 bp
<b><i>Bcl-xl</i></b>	GAGAACCACTACATGCAACTC	GAAGGTGGCTTTCACAGAAG	113 bp
<b><i>Bax</i></b>	GATGCGTCCACCAAGAAG	GTGTCCACGTCAGCAATC	98 bp
<b><i>TrkB</i></b>	GATGACAGTGGAAGCAAATC	GAGACTCGAGAAACGTGATAG	112 bp
<b><i>TBP</i></b>	CCGTGAATCTTGCTGTAACTTG	GTTGTCCGTGGCTCTCTTATTCTC	115 bp

## 2.6 Western Blot

The thalamus was collected from the adult mouse brains and immediately stored in dry ice or -80 °C until use. The thalamus samples were lysed with *RIPA lysis buffer* (150 mM Sodium chloride, 1% Triton X-100, 0.5% sodium deoxycholate, 0.1% SDS, 50 mM Tris, pH 8.0) with fresh added *Halt<sup>TM</sup> protease inhibitor cocktail* (ThermoFisher Scientific, 78430). Then the samples were centrifuged at 12,000 rpm at 4 °C for 20 minutes and the supernatant protein samples were collected. The protein concentration was determined using the *Bio-Rad DC protein assay* (Bio-Rad, 500-0116), balanced with the same lysis buffer and aliquot stored at -80 °C until use. Before loading, 5X sample buffer (ThermoFisher Scientific, 39001) was added into each protein sample and dithiothreitol (DTT) was added at the same time to a final concentration of 50 mM. Sample mixtures were left at room temperature for 30 minutes. Protein (20-30 µg) was loaded to each well of SDS-PAGE gel (4% stacking gel and 8% separating gel), together with 3 µL prestained protein ladder (ThermoFisher Scientific, 26619). To get the best separation of large protein bands, the gels were run under 70 mV for 3 hours. Then the proteins were transferred to a pre-activated PVDF membrane (Millipore, IPFL00005) at -70 mV for 3 to 4 hours.

Sodium dodecyl sulfate (SDS) and methanol were added into transfer buffer at a final concentration of 0.1% and 10%, respectively. The gels were stained with Coomassie Brilliant Blue solution (0.1% Coomassie Brilliant Blue, 50% methanol, 10% Glacial acetic acid) and no obvious proteins remained under these transfer conditions. Membranes were incubated in blocking solution with 5% non-fat dry milk and 3% BSA in TTBS at room temperature for one hour. Primary antibody is diluted in *Odyssey<sup>R</sup>* Blocking Buffer in TBS and applied on the membrane at 4 °C overnight. After washing the membrane with TTBS, fluorescence-conjugated secondary antibody is diluted and applied on the membrane at room temperature for one hour. The images of staining results were collected by *Odyssey CLx Infrared Scanner* and analyzed by *Image Studio Lite Ver 5.2*.

Antibody list: mouse anti-HCN2 antibody (Neuromab, N71/37): 1:1000; mouse anti-HCN4 antibody (Neuromab, N114/10): 1:1000; mouse anti-Cav3.1 antibody (Neuromab, N178A/9): 1:1000; IRDye 680RD Goat anti-mouse (Li-cor, P/N 926-68070): 1: 10,000; IRDye 800CW Goat anti-rabbit IgG(H+L) (Li-Cor, P/N 926-32211): 1: 10,000;

## 2.7 Electrophysiology

At the same time of the day (11 am summer time and 10 am winter time), mice were anaesthetized with isoflurane and decapitated. Brains were quickly removed and immersed in oxygenated (95% O<sub>2</sub> and 5% CO<sub>2</sub>), ice-cold N-methyl-D-glucamine (NMDG)-based aCSF solution (in mM, 110 NMDG, 110 HCl, 3 KCl, 1.1 NaH<sub>2</sub>PO<sub>4</sub>, 25 NaHCO<sub>3</sub>, 25 Glucose, 10 ascorbic acid, 3 pyruvic acid, 10 MgSO<sub>4</sub>, 0.5 CaCl<sub>2</sub>). The first 350  $\mu$ m coronal brain section with the most anterior paraventricular thalamus (PVT) was obtained with a Vibratome Series 3000 Plus Tissue Sectioning system. The collected brain slices were transferred and incubated in bubbled standard aCSF (in mM, 125 NaCl, 2.5 KCl, 26 NaHCO<sub>3</sub>, 1.24 NaH<sub>2</sub>PO<sub>3</sub>, 25 Dextrose, 2 MgSO<sub>4</sub>, 2 CaCl<sub>2</sub>) at 37 °C for 30 minutes, then incubated at room temperature until use.

During the recording, individual slice was transferred to a recording chamber and perfused with oxygenated external solution at a speed of 1 mL per minute at room temperature. If not specifically mentioned, standard aCSF was perfused as external solutions. For specific current isolation, different pharmacological antagonists were applied in the external solution as stated in the results. PVA was identified under infrared differential interference contrast

(DIC) microscopy as the enclosed nuclei near the border of the third ventricle by *stria medullaris* white matter fiber structure. Attached cell and whole cell recording were obtained using *MultiClamp 700B amplifier*, *Digidata 1322A digitizer*, and a PC running *Clampex 10.3* software (Molecular Device). For attached-cell recording, glass pipettes had resistances of 2.5 – 3.5 M $\Omega$  filled with standard aCSF. To keep all cells under the same physiological conditions, giga seals were obtained in every cell by application of a small negative pressure for spontaneous action potential recording. For intracellular whole-cell patch clamp recording, glass pipettes had resistances of 3.5 – 6 M $\Omega$  filled with internal pipette solution (in mM, 120 Kglu, 20 KCl, 0.2 EGTA, 10 Hepes, 4 NaCl, 4 Mg<sup>2+</sup>ATP, 14 phosphocreatine, 0.3 Tris GTP (pH was adjusted to 7.2-7.25 by KOH, osmolarity was adjusted to 305-315mOsm by sorbitol). Series resistance was monitored and only cells with series resistance less than 20 M $\Omega$  during the whole recording were further analyzed. For spontaneous action potential recording, the injected current was held at 0 mV under current clamp for 5 minutes recording. Cells with no action potentials identified in 5 minutes are classified as 'not active' cells.

HCN or T-type calcium currents were isolated under voltage- clamp. The



external solution for HCN current isolation contained 0.5  $\mu\text{M}$  TTX, 1 mM  $\text{NiCl}_2$ , 1 mM  $\text{CdCl}_2$ , 2 mM  $\text{BaCl}_2$ , 10  $\mu\text{M}$  DNQX and APV to block voltage-gated sodium channels, voltage-gated calcium channels, inwardly-rectifying potassium channels and excitatory synaptic current, but no  $\text{NaH}_2\text{PO}_4$  to prevent precipitation with big cations. The external solution for T-type calcium current isolation was standard aCSF containing 0.5  $\mu\text{M}$  TTX to block voltage-gated sodium channels.

## 2.8 Behavioral assays

**Open field test** was applied to test mouse exploratory behavior and anxiety behavior. All mice have received routine handling for a week and have put in the same room for 1 hour each day for three days before experiments. Each mouse was placed in the open field and allowed to explore freely under dim red light for 5 minutes. Infrared beams and computer-based software *Fusion* was used to track mice and calculate mice activity and time spent in the center (4x4) of total open field (8x8).

In **novel object recognition (NOR) experiments**, all mice have received routine handling and three days room habituations before experiments. On the

day before familiarization trial, each mouse was placed in the open field in the absence of objects and allowed to explore it freely for open field habituation, the behaviors of which were recorded and analyzed further as open field test data. In the familiarization trial, each mouse was placed in the open field containing two identical 100 ml beakers in the neighboring corners for 5 minutes. Twenty-four hours later, each mouse was placed back in the same open field with two objects, one of which was the identical 100 ml beaker and the other one was replaced with a novel object (a lock in a similar dimension) for 5 minutes testing trial. To prevent coercion to explore the objects, mice were always released against the center of the opposite walls in both familiarization and testing trials. The mouse behaviors in the testing trials were taped and analyzed by experimenters who are blinded to the genotypes of the mice. The exploration was defined as the nose of the mouse is sniffing and touching it with attention, while running around the object, sitting or climbing on it was not recorded as exploration (Antunes & Biala, 2012).

The **paw sensation test** was applied to assess mouse paw sensorimotor response (Arakawa et al., 2014). A small piece of round sticky paper tape (Tough-spots, for microtube cap ID,  $\sim 1\text{cm}^2$ , Research Products International

Corp. 247129Y) was applied to the plantar surface of the right hindpaw of each mouse and the mouse was placed back to its home cage. The latency to the first response to the paper of each mouse was measured and analyzed.

The **tail suspension test** and **forced swim test** were applied to assess and evaluate mouse depressive-like behaviors (Can, Dao, Arad, et al., 2012; Can, Dao, Terrillion, et al., 2012). In tail suspension test, each mouse was suspended by the tail for 5 minutes under dim red light and a 5-cm truncation from a Falcon 15 mL conical centrifuge tube was placed around the tails to prevent tail climbing. The behavior of the mouse was taped and analyzed by experimenters who were blinded to the genotypes of the mice. The escape related struggling time for 5 minutes experiments was measured as mobility time. In forced swim test, each mouse was placed in a 1000 ml beaker with ~800 ml water for 5 minutes. The behavior of the mouse was taped and analyzed by experimenters who were blinded to genotypes of the mice. The escape- related mobility behavior was measured In both tests, the small movements confined to only front or hind legs were not counted as mobility. Only intentional movements with four legs or body were timed for mobility time.

## 2.9 mRNA sequencing

Midline thalamus was identified in the first anterior-PVT coronal slice as described in electrophysiological experiments. Landmarks included the third ventricle, *stria medullaris*, and *columns of the fornix*. 1200  $\mu$ M-thick midline thalamus truncations were collected as midline thalamus tissue. Midline mRNA was extracted from five  $Gbx2^{CreERT/+}$ ,  $Shox2^{f/-}$  KO mice and five  $Gbx2^{CreERT/+}$ ,  $Shox2^{f/+}$  CR mice and sent to *BGI Americas Corporation (Cambridge, MA, USA)* for RNA-seq Quantification. More than 26 million single-end 50-bp reads by BGISEQ-500 Sequencing Platform have gotten per sample and further analyzed using EBseq method by *BGI Americas Corporation*. We screened out differentially expressed genes (DEGs) according to the post probability of equally expressed (PPEE) value and fragment reads per kilobase per million mapped reads (FPKM) *BGI Americas Corporation* provided and conducted gene ontology (GO) analysis.

## Chapter III: Results

### 3.1 The expression of *Shox2* in the thalamus

To investigate *Shox2* expression in the adult mice, we conducted X-gal staining experiments with coronal brain slices from P56 *Shox2*<sup>LacZ/+</sup> mice, in which the expression of LacZ indicated the expression of *Shox2*. In the cerebrum, no *Shox2* expression was found in the cortex (Figure 3.1 A-G), subcortical regions of the forebrain (Figure 3.1 A-C), amygdala (Figure 3.1 E), or cerebellum (Figure 3.1 H). Interestingly, *Shox2* was expressed throughout the thalamus from rostral to caudal, including anterior thalamus, midline thalamus, VB, dLGN and MGN (Figure 3.1 B-G). The only exception is that the X-gal staining signal in LD is, if any, relatively weak. Moreover, no expression of *Shox2* was observed in the HB and Rt, which are the representative regions of the epithalamus and prethalamus (Figure 3.1 D-F).

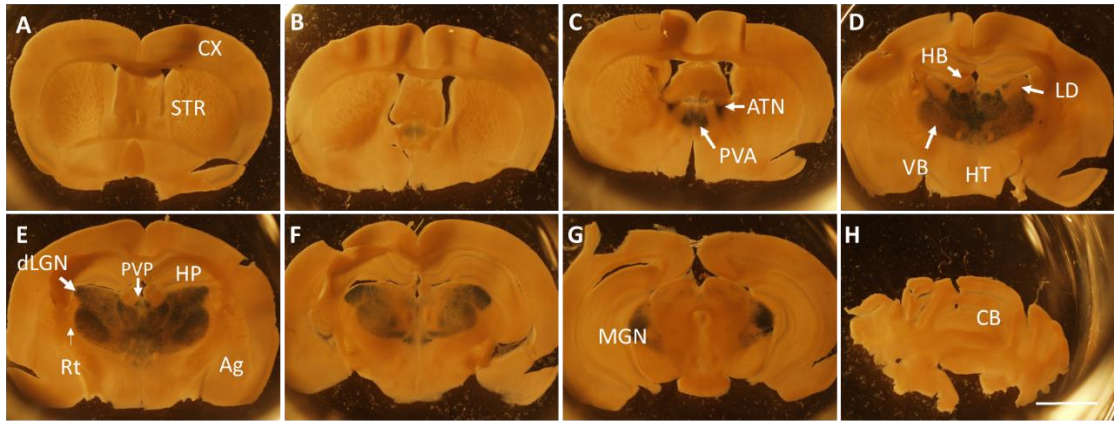


**Figure 3.1 Brain sections demonstrating X-gal staining results from P56 days old male *Shox2*<sup>LacZ/+</sup> mouse.** The results showed that *Shox2* expression was restricted in most nuclei of the thalamus from rostral to caudal including anterior thalamus nuclei (ATN), anterior paraventricular thalamus (PVA), posterior paraventricular thalamus (PVP), ventrobasal nucleus (VB), dorsal lateral geniculate nucleus (dLGN) and medial geniculate nucleus (MGN) in adult mouse brain. The only thalamic nucleus showing low *Shox2* expression was lateral dorsal (LD) nuclei in Figure D. The *Shox2* does not express in the cortex (CX), hippocampus (HP), striatum (STR), amygdala (Ag), hypothalamus (HT) and cerebellum (CB) in adult mouse. Error bar shows 2  $\mu$ M.

To determine if the *Shox2* expression pattern changes during development, we conducted X-gal staining with coronal brain slices from P56 *Shox2*<sup>cre/+</sup>, *Rosa26*<sup>LacZ/+</sup> mice. X-gal staining in these animals will identify any cells that have expressed *Shox2* at any time during development. In the *Shox2*<sup>cre/+</sup>, *Rosa26*<sup>LacZ/+</sup> mice, no signal was detected in the cortex (Figure 3.2 A-F), subcortical regions of the forebrains (Figure 3.2 A, B), amygdala (Figure 3.2 C, D), hypothalamus (Figure 3.2 B-D), the ventral part of the midbrain (Figure 3.2 F), and especially hippocampus and reticular thalamus (Figure 3.2 C-F). Cells of the habenula nuclei (Figure 3.2 C D) and superior colliculi (Figure 3.2 F) do express *Shox2* at timepoints throughout development, but not in the adult animal (Figure 3.1).

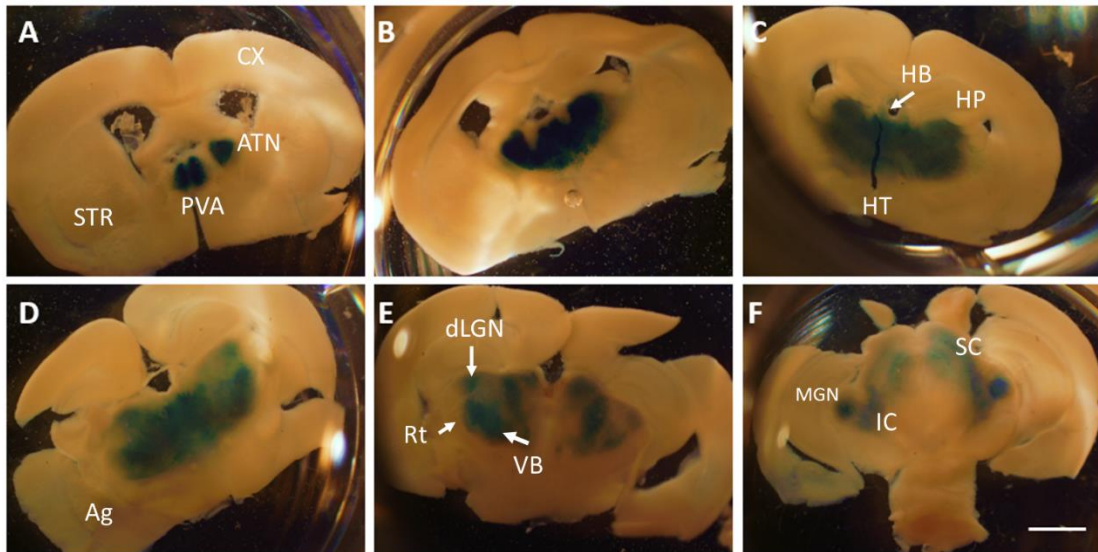


**Figure 3.2 Brain sections demonstrating X-gal staining results from P56 days old male *Shox2*<sup>cre/+</sup>, *Rosa26*<sup>LacZ/+</sup> mouse.** The results show that *Shox2* expression was restricted to the greater thalamus throughout development. In these animals, X-gal staining covered all *Shox2* expression regions detected in *Shox2*<sup>LacZ/+</sup> mouse in Figure 2.1, such as anterior thalamus nuclei (ATN), anterior paraventricular nucleus (PVA), ventrobasal thalamus (VB), dorsal lateral geniculate nucleus (dLGN) and medial geniculate nucleus (MGN), but was still not observed in the cortex (CX), striatum (STR), hippocampus (HP), amygdala (Ag) or hypothalamus (HT). During development, *Shox2* did express in in habenula (HB), and some areas of the midbrain including superior colliculus (SC) and inferior colliculus (IC), but this expression is decreased during development, as shown in Figure 2.1. Scale bar indicates 2  $\mu$ M.



To investigate the cellular expression profile of *Shox2* in *Shox2*<sup>cre/+</sup>, *Rosa26*<sup>LacZ/+</sup> adult mice, we conducted IHC experiment with cryostat coronal brain sections. Parvalbumin is highly expressed in interneurons of reticular nucleus of thalamus, therefore, we used PV labeling to determine the specific location of the reticular nucleus border of the thalamus. The PV IHC staining results showed very few PV-positive cells in the thalamus, which is consistent with previous findings that most nuclei of the mouse thalamus possess very few inhibitory interneurons in most nuclei of mouse thalamus (Arcelli, Frassoni, Regondi, De Biasi, & Spreafico, 1997; Bodor, Giber, Rovo, Ulbert, & Acsady, 2008). The main PV+ neurons located at the lateral and ventral borders of the thalamus defined the exact border of Rt and our results indicated that *Shox2* was never expressed in Rt (Figure 3.3 H and Figure 3.4 E-H). We detected very sparse PV+ cells in the thalamus and these cells never expressed *Shox2*. In addition, the IHC results confirmed that *Shox2* was never expressed in cells from the cortex (Figure 3.3 A E and Figure 3.4), hippocampus (Figure 3.3 A, F and Figure 3.4), hypothalamus (Figure 3.3 A), and amygdala (Figure 3.3 A). *Shox2* expressed ubiquitously in the cells in the thalamus (Figure 3.3 A-D and Figure 3.4) and sparsely in the habenula (Figure 3.3 G and Figure 3.4 E-H).

According to the results of X-gal staining and IHC staining, we can conclude that *Shox2* was expressed restrictedly in the whole mouse thalamus, and not in PV+ neurons. In the thalamus, *Shox2* is not expressed in the PV+ neurons (Figure 3.3 G).

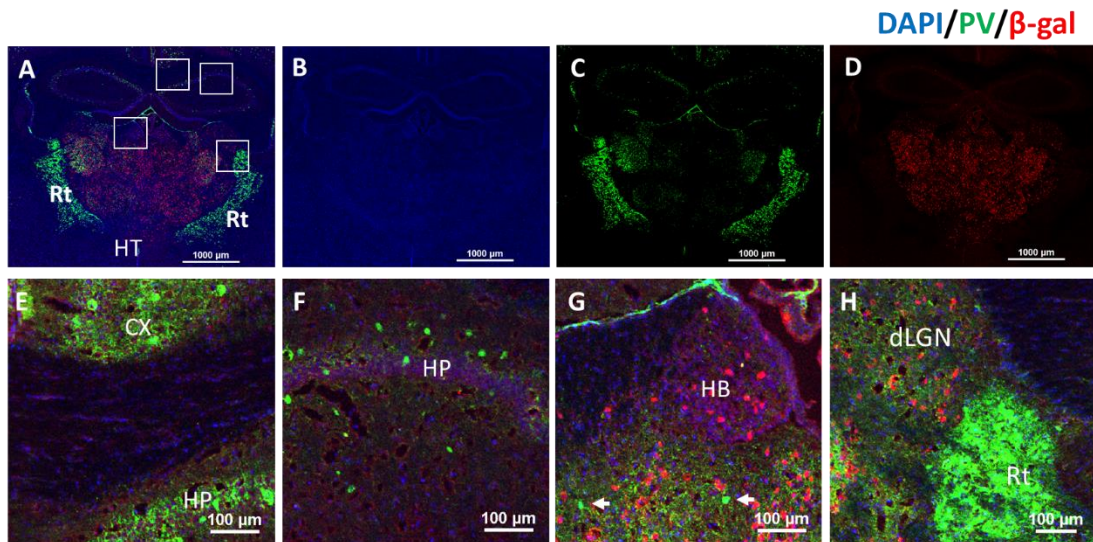


**Figure 3.3.** IHC results of coronal cryostat brain sections from P56 *Shox2*<sup>cre/+</sup>, *Rosa*<sup>LacZ/+</sup> mouse. PV staining (A, C) shows the border of reticular thalamus (Rt) which has high density of PV+ interneurons.  $\beta$ -gal staining (A, D) in coronal sections from *Shox2*<sup>cre/+</sup>, *Rosa*<sup>LacZ/+</sup> mice labels all cells that used to express *Shox2*. The merged imaging (A) of DAPI, PV and  $\beta$ -gal indicates the *Shox2* expression is restrictedly bordered by PV expressing Rt (A, H). Boxed areas in Figure A are amplified, from top to bottom, in figure E, F, G, H. The results indicate that *Shox2* never expressed in the cortex (CX, E), hippocampus (HP, E, F) and Rt (A, H), but has sparsely expressed in habenula (HB, G). We can detect some PV expressing cells in the thalamus and *Shox2* did not co-express in these cells (G, arrows).

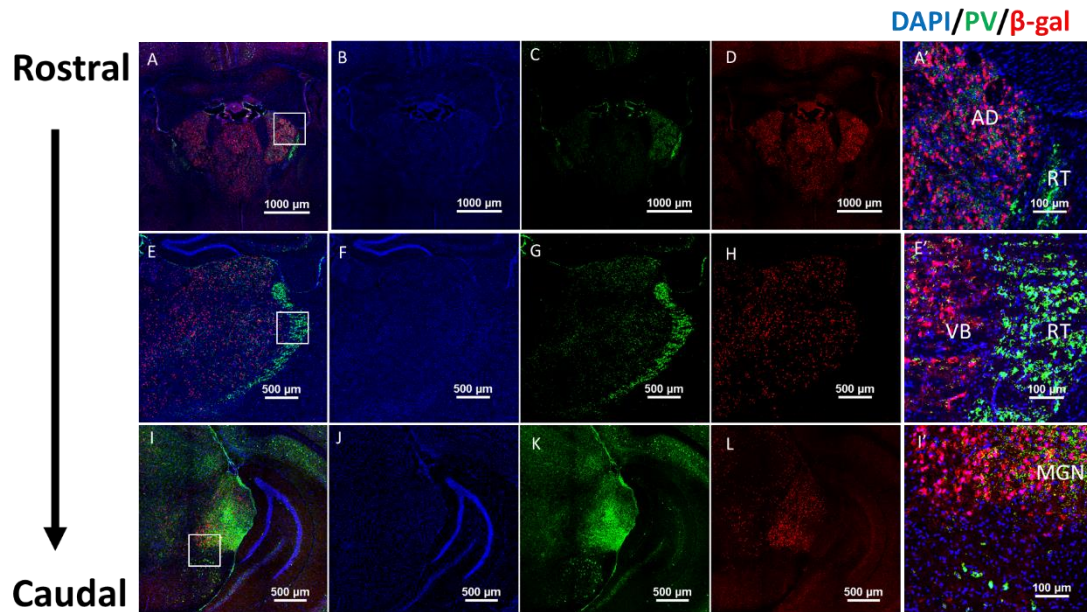


**Figure 3.4.** IHC results indicate that *Shox2* expression is restricted in the thalamus. The co-staining of PV and  $\beta$ -gal indicated that *Shox2* expression is restricted to the thalamus in all coronal sections from rostral (A-D), middle (E-H) to caudal (I-L). Boxes in Figure A, E, I are amplified in Figure A', E' and I'.

The IHC results also indicated that *Shox2* did not express in every DAPI labeled cell in the thalamus (Figure 3.3 and Figure 3.4). Therefore, to investigate which cell-type *Shox2* expresses in, either neurons or glia, we labeled all neurons with the antibody anti-neuronal nuclear protein (NeuN) which is specifically expressed in neurons (Gusel'nikova & Korzhevskiy, 2015; Herculano-Houzel & Lent, 2005)(Figure 3.5). We found that the *Shox2*<sup>cre</sup> reporter gene LacZ was expressed in NeuN positive neurons throughout the thalamus from rostral to caudal (Figure 3.5). But not every NeuN positive neurons expressed the LacZ reporter. The ratio of *Shox2* expressing cells and total neurons varied among the thalamic nuclei (Figure 3.5 M). It is important to point out that our results further confirmed the previous result that *Shox2* was not expressed in cells in the reticular thalamus, hippocampus, cortex or other regions beyond the greater thalamus. Within the thalamus, *Shox2* was expressed in more than 50% neurons in the PVT, AD, VB and MGN. The lowest percentage of *Shox2*-expressing cells was found in the LD of the thalamus, which is consistent with our previous X-gal staining results which showed a low staining signal in the LD (Figure 3.1, 3.2).

To confirm that *Shox2* did not express in the glia cells, we stained glia with

antibody anti- Glial Fibrillary Acidic Protein (GFAP), which is expressed specifically in glia, especially astrocytes which are the main type of glia, and has been used as a marker for glia (Eng, 1985; Yang & Wang, 2015). Interestingly, our results indicated that the GFAP expression showed a negative correlation with *Shox2* expression (Figure 3.6 and Figure 3.7). In brain areas where *Shox2* was not expressed, such as the cortex, hippocampus (Figure 3.7 A B) and hypothalamus, GFAP had relatively high expression. However, the number of cells with GFAP expression in the thalamus was relatively low in (Figure 3.6 A C). Figure 3.7 shows that GFAP and *Shox2* co-expression in different nuclei from rostral to caudal thalamus. Importantly, these results indicated that *Shox2* did not express in the GFAP-positive glia cells.

In summary, the results from our X-gal staining and IHC experiments indicated that *Shox2* expression during development was restricted to neurons in mouse thalamus, habenula and superior colliculus during development. In the adult stage, the expression of *Shox2* is limited to the thalamus neurons.

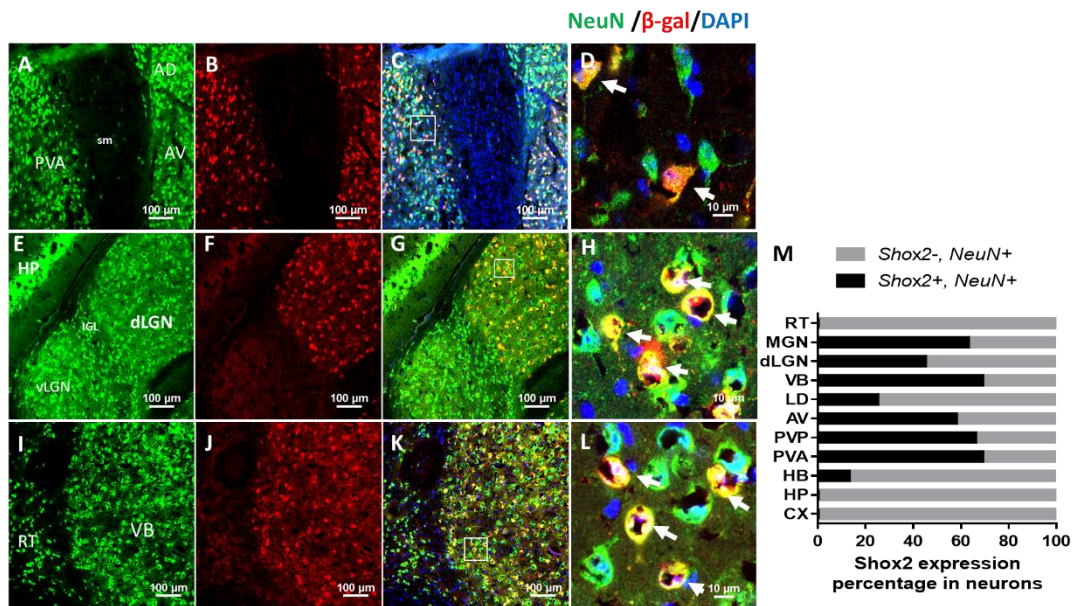


**Figure 3.5. *Shox2* expression is restricted to NeuN<sup>+</sup> neurons in the thalamus.** Double immunofluorescence for NeuN (green, A, E, I) and  $\beta$ -gal (red, B, F, J) which is the reporter of *Shox2* expression history profile indicated *Shox2* only expresses in the NeuN<sup>+</sup> neurons (merged C-D, G-H, K-L). Three typical thalamic regions including anterior paraventricular thalamus (PVA) (A-D), dorsal lateral geniculate nucleus (dLGN) (E-H) and ventrobasal nucleus (VB) (I-L) are shown to indicate that *Shox2* only expresses in NeuN<sup>+</sup> neurons. Boxed regions in merged figure C, G, K are amplified in figure D, H, L and arrows in D, H, and L show the cells co-expressed *Shox2* and NeuN. The percentage of *Shox2*<sup>+</sup> cells in NeuN<sup>+</sup> neurons in some typical thalamic nuclei are shown in Figure M. sm: stria medullaris; vLGN, ventral LGN; IGL: intergeniculate leaflet of the LGN; RT: reticular thalamus. AV: anteroventral nucleus of the thalamus; AD: anterodorsal nucleus of the thalamus. HB: habenula; HP: hippocampus; CX: cortex.



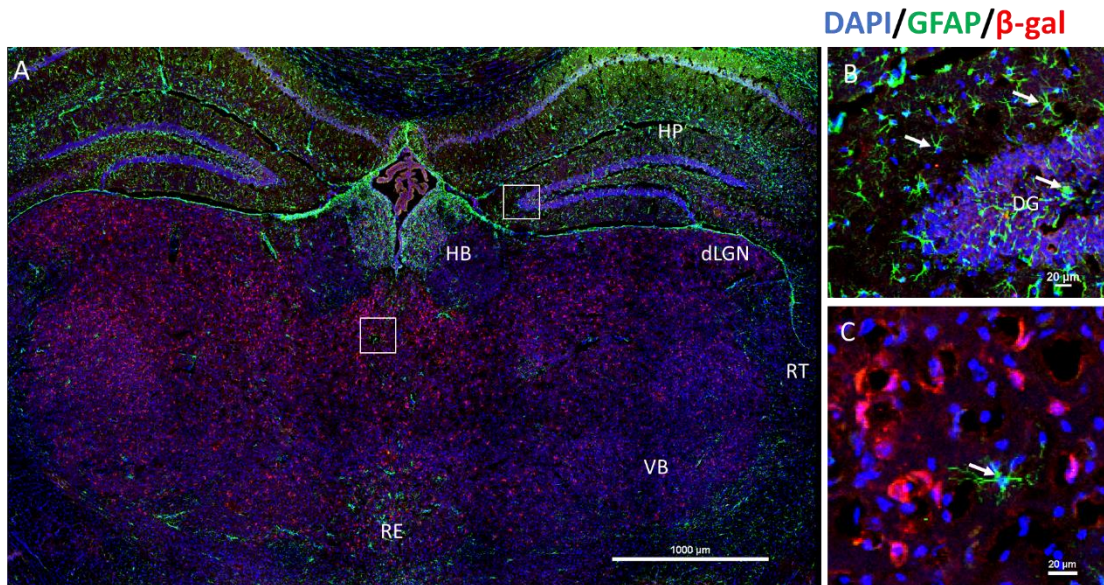


**Figure 3.6** The distribution of GFAP+ gliia and *Shox2*-expression cells in coronal cryostat sections from *Shox2*<sup>cre/+</sup>, *Rosa*<sup>LacZ/+</sup> mouse. Our results showed that gliia, which is reflected by GFAP staining (green), has high distribution in the hippocampus (HP, A and B) and the neighboring regions of thalamus, including habenula (HB) and reticular thalamus (RT). But the GFAP+ gliia cells are rare (A and C) in most nuclei in the thalamus, except ventral part of midline thalamus, such as nucleus of reunion (RE). The top box in Figure A is enlarged in Figure B, and the bottom one is enlarged in Figure C. We did not detect any cells having immunoreactivity to both *Shox2* and GFAP.



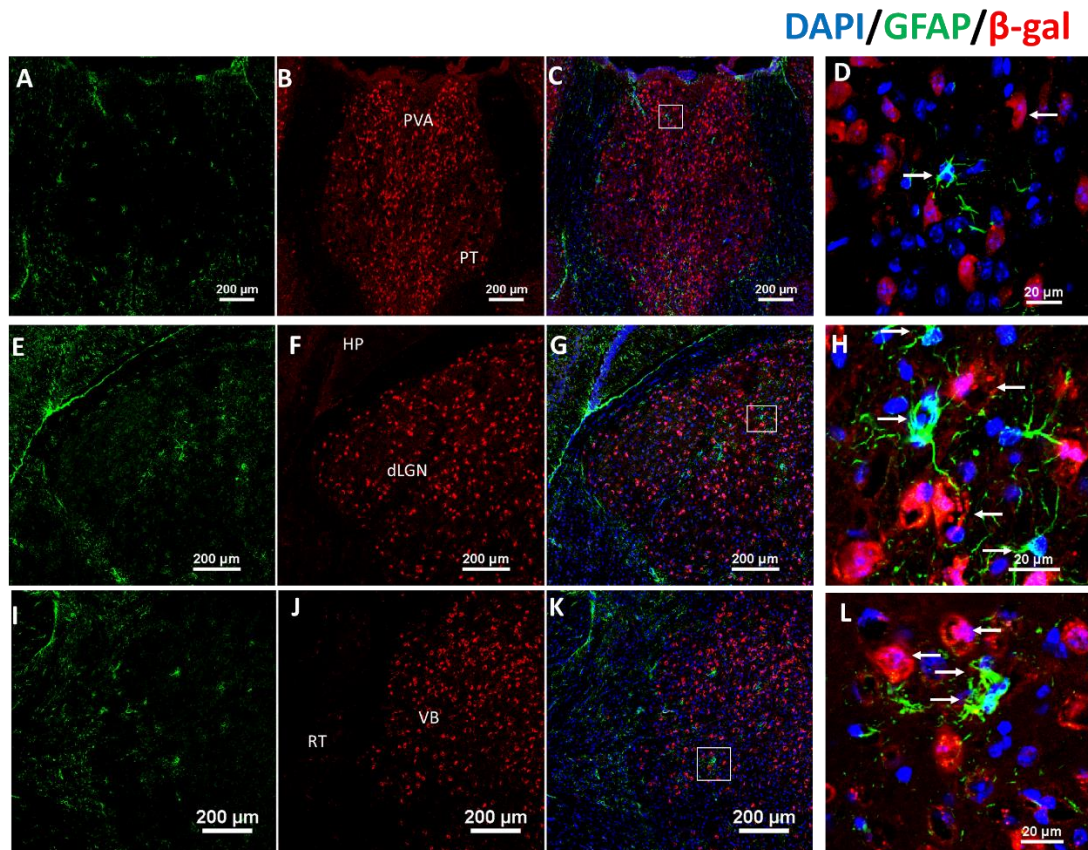


**Figure 3.7.** The co-staining results indicate that *Shox2* does not express in GFAP+ glia cells. The figures show the co-expression of glia marker GFAP (green, A, E, I) and  $\beta$ -gal (red, B,F,J), which reflects *Shox2* expression history profile, in three typical thalamus regions: PVA (A-D), dLGN (E-H) and VB (I-L). The box regions in merged staining figures (C, G, K) are magnified in Figure D, H and L. The right arrows show the GFAP+ glia and the left arrows show *Shox2* expression cells. We did not see any cells expressed both GFAP and *Shox2*. PT: parataenial nucleus.

### **3.2. Tamoxifen injection successfully induced *Shox2* KO in the thalamus.**

Previous studies found that *Shox2* plays a decisive role in the differentiation of pacemaker cells in the sinoatrial node of the heart and pulmonary vein (Puskaric et al., 2010; Sun et al., 2015; Ye et al., 2015). These areas of the cardiovascular system possess pace-making automaticity mediated by the prominent expression of pacemaker-related HCN channels and T-type calcium channels (Cribbs, 2010; Ludwig et al., 2003). Our studies revealed that *Shox2* expression is restricted to the thalamus. Interestingly, the thalamus also has high HCN2/4 expression but low HCN1 expression, which is different from other regions of cerebrum, but similar to heart pacemaker cells. The thalamus is believed to be an important area of the brain generating rhythmic oscillations, especially the slow oscillation wave generated in the thalamus during slow-wave sleep and absence seizure. Moreover, although *Shox2* does express during development in some other brain regions, including the habenula and midbrain, *Shox2* expression in the adult mouse thalamus remains into adulthood. Given *Shox2*'s role in controlling expression of channels important for pacemaker function and its prominent expression in the

thalamus, we hypothesized that *Shox2* is necessary to maintain physiological properties and functions by regulating HCN current and T-type calcium current in the neurons of the adult mouse thalamus. To study the involvement of *Shox2* in the adult thalamic physiological properties and behavioral functions, we used the tamoxifen-inducible Cre-loxP recombination system to ablate the expression of *Shox2* in the adult mouse. We used Rosa26<sup>CreERT</sup>, the whole body expressed CreERT, to inducible KO of *Shox2* in the whole thalamus to study both the effects of *Shox2* KO on behavioral functions and cellular physiological properties. Mice from both groups were injected with tamoxifen (160 mg/kg, IP) at the same time every day for five successive days. The *Shox2* mRNA expression level was checked using PCR and RT-qPCR for all animals used in the experiments to make sure the correct genotypes and knockout process (Figure 3.8). Interestingly, we found that the *Shox2* KO mice weighed significantly less than the CR mice (Figure 3.8).

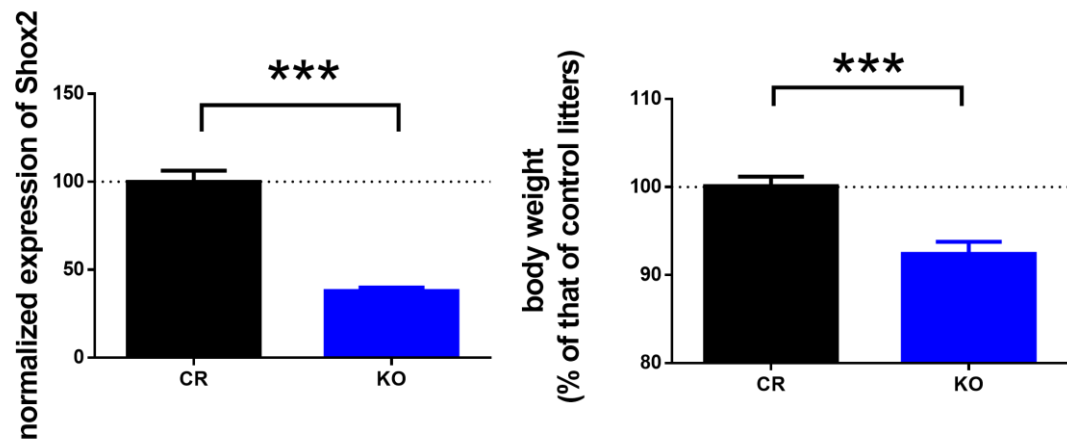


**Figure 3.8 Tamoxifen injection decreased *Shox2* mRNA expression and body weight in *Shox2* KO mice.** The mRNA expression decreased in the whole thalamus of Rosa26<sup>CreERT</sup> KO mice ( $t(19) = 9.04$ ,  $P < 0.001$ ) and decreased mice body weight ( $t(15) = 4.48$ ,  $P < 0.001$ ).

### **3.3 *Shox2* KO induced thalamus-related behavior deficits in adult mouse.**

The thalamus plays a critical role in sensory and motor information relay and processing, sleep and arousal, learning and memory, and other cognitive functions as described in the section of introduction. We tested both cognitive and somatosensory functions in adult Rosa26<sup>CreERT</sup> mice.

First, we conducted an open field test to investigate the overall activity and general anxiety level of CR and *Shox2* KO mice. We found that the total distance travelled by *Shox2* KO mice was significantly decreased compared to CR mice (Figure 3.9 A,  $t(44) = 2.03$ ,  $P = 0.05$ ). In addition, we found that the KO mice spent a significantly larger percentage of time spent in the center of the open field compared to CR mice (Figure 3.9 B,  $t(26) = 2.22$ ,  $P = 0.04$ ). Together, these results suggested that the *Shox2* KO mice traveled less distance, and the anxiety levels were decreased compared to littermate controls.

To test the performance of mice in general somatosensory function, we conducted the paw sensation test, in which sticky tape was applied to the plantar surface of the right hindpaw of each mouse, and the latency for the mouse's first reaction to the tape was measured (Arakawa et al., 2014; Bouet

et al., 2009). We found the latency to react to the tape of KO mice was significantly longer than that of CR mice (Figure 3.9 C, Student's t-test,  $t(26) = 2.38$ ,  $P = 0.03$ ). The results suggested that *Shox2* KO induced somatosensory deficits in adult mice.

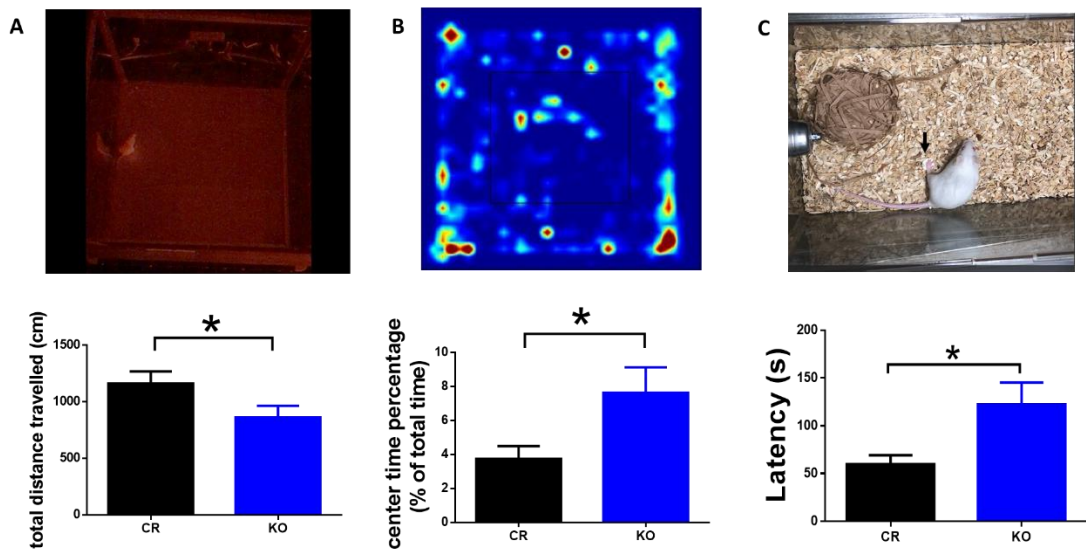


**Figure 3.9 *Shox2* KO altered mouse performance in open field test and impaired mouse performance in paw sensation test.** A. Top, mice were placed in the open field and monitored by infrared beam and computer software *Fusion*. Bot, the activity of *Shox2* KO mice was significantly decreased than CR mice ( $t(44) = 2.03$ ,  $P = 0.05$ ). B. Top, the heat map shows mice activity recorded by *Fusion* and analyzed via *Matlab*. Bot, *Shox2* KO mice spent more percentage of time in the center of open field than CR mice (student's t-test,  $t(26) = 2.22$ ,  $P = 0.04$ ). C. Top, mice with a  $\sim 1$  cm<sup>2</sup> sticky tapes on the right hind paw were placed back to the home cage and tested the latency for the mice to first react the tapes. Bot, the results showed that *Shox2* KO mice had a longer latency to respond to the tapes than CR mice (student's t-test,  $t(26) = 2.38$ ,  $P = 0.03$ )

Anterior thalamus and medial thalamus are critical for learning and memory process (Jankowski et al., 2013; Mitchell, 2015). To test if *Shox2* KO impairs learning and memory function, we conducted the novel object recognition experiments (Antunes & Biala, 2012) (Figure 3.10). In the familiarization trial, mice were placed in the open field with two identical 100 ml beakers for 5 minutes for learning process. Twenty-four hours later, the mice were placed in the same open field but one of the beakers was replaced by a similar-dimension lock for memory test. Our results indicated that the total exploratory time around both objects in 5 minutes testing trial of CR and *Shox2* KO mice was not significantly different (Figure 3.10 B,  $P=0.26$ ). Two-way repeated ANOVA test of the exploratory time spent around each object by CR and *Shox2* KO mice indicated a significant interaction between genotype (CR vs KO) and object novelty (novel vs familiar) ( $F(1, 25) = 5.78, P = 0.02$ ). Post-hoc Bonferroni's test indicated that CR mice spent more time around the novel object than the familiar one ( $P=0.01$ ), but KO mice did not ( $P>0.99$ ). In addition, the percentage of time *Shox2* KO mice spent around novel object was significantly decreased compared to that of CR mice (Figure 3.10 D, Student's t-test,  $t(25) = 2.80, P<0.01$ ). Our results indicating that *Shox2* KO impaired mice performance in



novel object recognition task suggests the impairment of learning and memory ability of *Shox2* KO mice.

Because our open field test results suggested that *Shox2* KO mice exhibited lower anxiety, we went on to further investigate depressive-like behaviors using tail suspension test and forced swim test, in which test mice are put in an uncomfortable but non-escapable situation and the active struggling time was measured as mobility time to describe their depressive-like behaviors (Can, Dao, Arad, et al., 2012; Can, Dao, Terrillion, et al., 2012) (Figure 3.11). The results showed no significant difference in mobility time between CR and KO mice in either test (forced swim test,  $t(20) = 0.39$ ,  $P = 0.70$ ; tail suspension,  $t(20) = 0.85$ ,  $P = 0.40$ ), suggesting *Shox2* KO did not significantly affect depressive-like behaviors.

In summary, our results indicated that the *Shox2* KO mice showed decreased activity and anxiety levels in the open field test, impaired learning and memory in novel object recognition test, and impaired somatosensory function in paw sensation test. Therefore, all behavior results suggest that *Shox2* is important to maintain the proper function of adult thalamus.

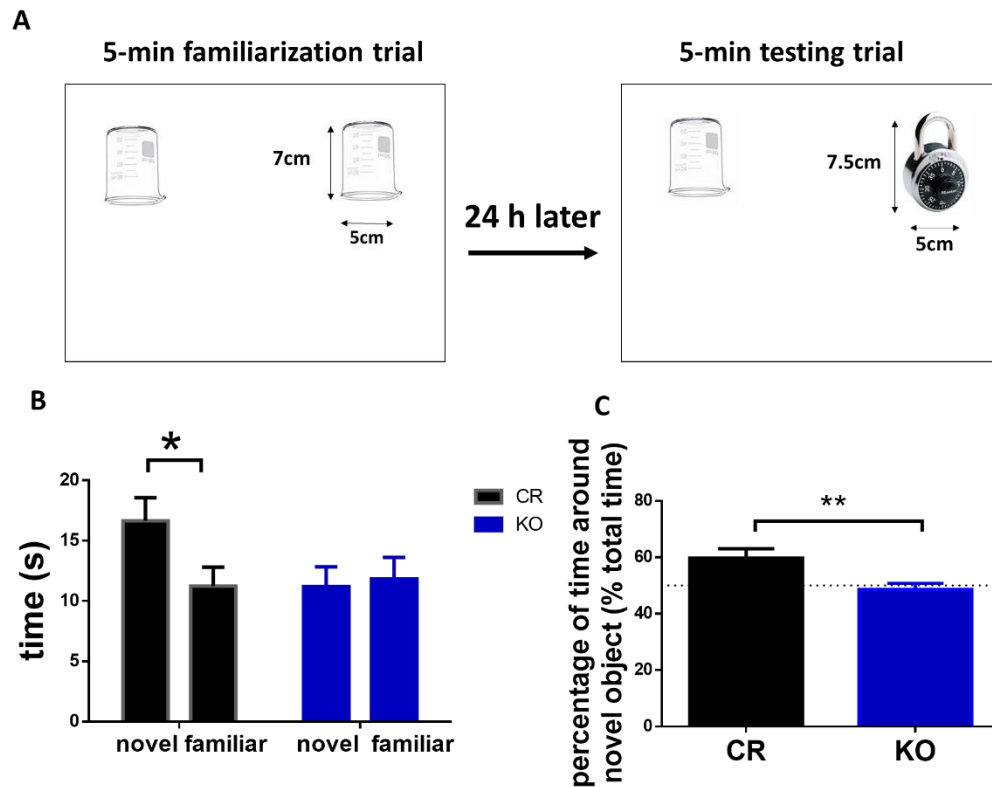


**Figure 3.10. *Shox2* KO impairs mouse performance in novel object recognition test.**

A. Mice were placed in the open field with two identical 100 mL beaker (diameter, ~5cm; height, ~7cm) in the 5-minute familiarization trials (left), and 24 hours later, mice were placed in the same open field but one beaker (familiar object) was replaced by a similar-dimension lock (novel object, 7.5cm x 5 cm) for 5 minutes in the testing trial and the exploratory time of the mouse spent around each object was measured (right). B. In the testing trial, Two-way repeated measures ANOVA showed an interaction in the time spent around two objects between genotypes (CR vs KO) and object novelty (familiar vs novel) ( $F(1, 25) = 5.78, P = 0.02$ ) and post-hoc Bonferroni's test indicated that CR mice spent more time around novel object than that around familiar one ( $P = 0.01$ ), but KO mice do not ( $P > 0.99$ ). D. In the test trial, the time percentage spent in exploring novel object by CR mice is more than that by KO mice ( $t(25) = 2.80, P < 0.01$ ).

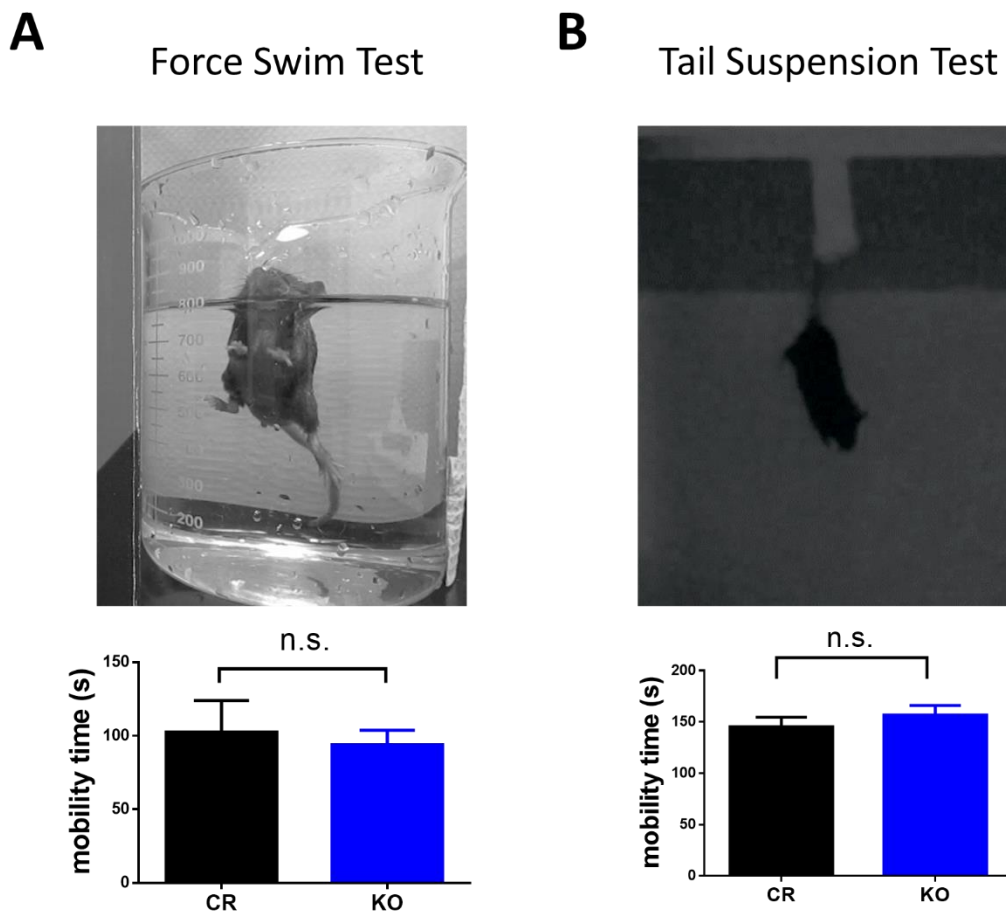


**Figure 3.11.** No significant difference in mobility time in 5-minute force swim test (A,  $P=0.70$ ) and 5-minute tail suspension test (B,  $P=0.40$ ) between CR mice and KO mice.

### **3.4 *Shox2* KO altered intrinsic properties of thalamic neurons and induced cell death.**

The appropriate function of the thalamus depends on the properly working thalamic neurons. Thus, we investigated the role of *Shox2* in the firing and intrinsic properties of thalamic neurons and thalamic cell survival. We conducted electrophysiological recording experiments to determine the change of physiological properties of individual neuron caused by *Shox2* KO. To best identify a single thalamic nucleus and the same neuron group inside a nucleus, we chose anterior paraventricular thalamus (PVA), the most rostral and dorsal midline nucleus, as the target region for recording. To confirm that we always recorded from the same group of neurons from each mouse, we only collected the first 350  $\mu$ M coronal brain slices when we are able to identify the third ventricle and PVA nuclei surrounded by third ventricle and stria medullaris.

To study whether PVA neurons spike spontaneous action potentials, we conducted cell-attached voltage clamp recording to record the action potential currents of the neurons without rupturing the cell membrane (Figure 3.12). Our results indicated that 36% of the cells fired spontaneous action potentials in the CR neurons while only 14% cells fired spontaneous action potentials in *Shox2*

KO neurons ( $\chi^2$  test,  $\chi_2 = 3.84$ ,  $P = 0.05$ ).

To further investigate cell excitability difference, we conducted whole-cell current clamp recordings. Cells were held at resting membrane potential in current clamp  $I=0$  conditions to test whether cells were spontaneously firing potentials (Figure 3.12 B). Our recording data showed a consistent result that there were significantly more active neurons with spontaneous action potentials in CR mice (47%, 18 out of 38) than that in *Shox2* KO mice (18%, 7 out of 39,  $\chi^2$  test,  $\chi_2 = 7.60$ ,  $P < 0.01$ ). The resting membrane potentials were not significantly different between CR and KO neurons, so the decreased cell excitability in PVA neurons of KO mice was not because of resting membrane potential difference (Table 2). Both experiments revealed that *Shox2* KO decreased the spontaneous cell excitability in PVA neurons.

In order to determine the mechanisms of these spiking differences, we investigated intrinsic properties of PVA neurons in CR and *Shox2* KO mice. We injected 10pA and 20pA current to evoke action potential at resting potential and -70mV, and we found evoked action potential frequency in *Shox2* KO neurons was less than that in CR neurons (Figure 3.13). Rebound fast sodium/potassium spikes and slow calcium spikes were induced by injection of

-50pA/-100pA/-150pA current at -70mV (Llinas & Steriade, 2006)(Figure 3.14).

The sag size and total number of rebound spikes were not different between CR and *Shox2* KO neurons. The potential and time of peaks of rebound calcium spikes were not different between CR and *Shox2* KO neurons but *Shox2* KO neurons have a slower decay phase, and therefore, a longer duration and a larger area under voltage trace.

To determine whether *Shox2* is important for cell survival in the thalamus, we utilized the *Gbx2*CreERT mice, in which CreERT was specifically expressed in the midline of the thalamus around P25 days old (Figure 3.15 A). We injected tamoxifen to *Gbx2*CreERT/+, *Shox2*<sup>f/f</sup> mice to specifically knock out *Shox2* in the midline thalamus, but not other areas of the thalamus, such as VB labeled in Figure 3.15 A. We found *Shox2*-inducible KO in the midline thalamus caused significantly increased cell death in the *Gbx2*-expressing PVT according to TUNEL staining (Figure 3.15 B and C,  $P < 0.01$ ) but not in the *Gbx2*-non-expressing VB of the thalamus. Our results indicated *Shox2* KO specifically increased local cell death in the thalamus, and suggested that *Shox2* is important for cell survival.

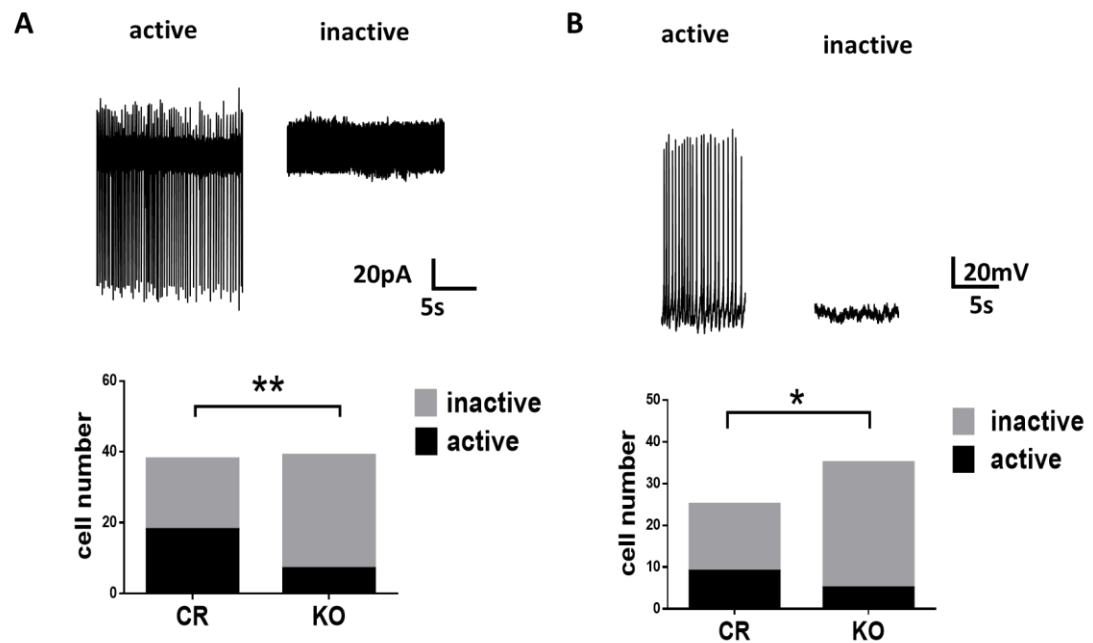


**Figure 3.12. Shox2 KO decreased the ratio of cells with spontaneous action potentials in the anterior paraventricular thalamus (PVA).** A. Top, the examples of attached-cell recording currents of cells with spontaneous action potentials (active) and no action potentials (inactive). Bot, the ratio of active cells recorded via attach-cell recording in PVA from KO mice is significantly smaller than that in CR mice ( $\chi^2$  test,  $\chi^2=7.60$ ,  $P<0.01$ ). B. Top, the examples of whole cell patch-clamp recordings of cells with spontaneous action potentials (active) and no action potentials (inactive). Bot, the ratio of active cells recorded via whole cell recording in PVA from KO mice is significantly smaller than that in CR mice ( $\chi^2$  test,  $\chi^2=3.84$ ,  $P=0.05$ ).

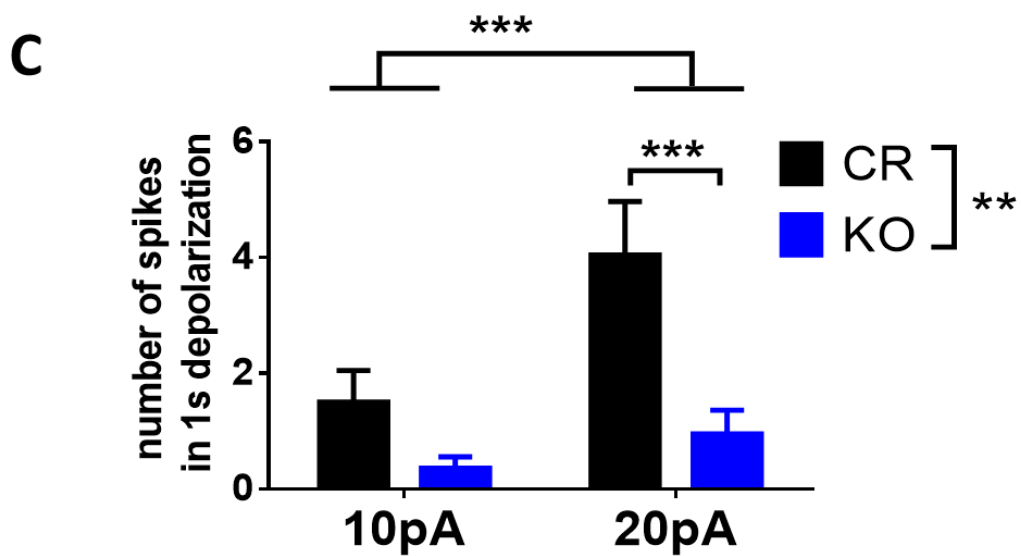
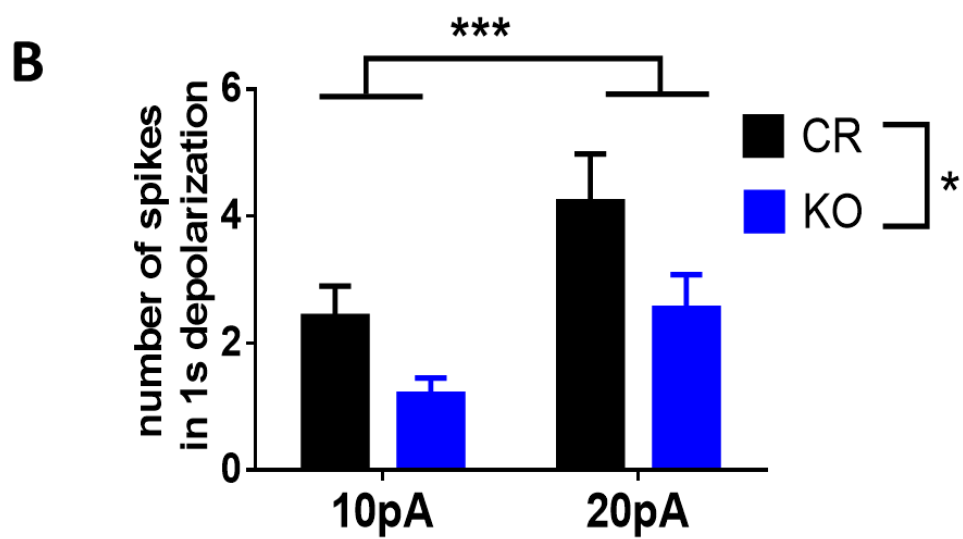
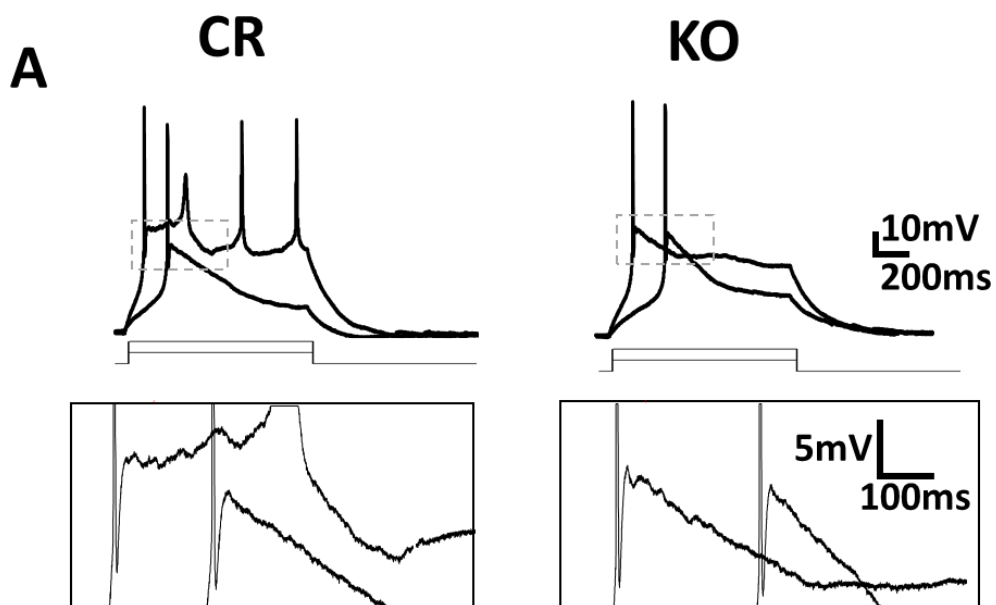




**Figure 3.13. Current injection evoked fewer action potentials in PVA neurons of *Shox2* KO mice compared to that of CR mice.** A. Examples of action potential traces induced by 10pA/20pA current injection when holding membrane potential at -70mV. The dashed boxes in the top two figures are enlarged in the bot boxes. B. The number of spikes induced by 10pA/20pA current injection at -70mV. Two way repeated measures ANOVA indicated significant main effect of genotypes (CR vs KO,  $F(1, 60) = 4.212, P=0.04$ ) and current injection (10pA vs 20pA,  $F(1, 60) = 36.60, P<0.001$ ) in the number of evoked spikes in 1s depolarization from -70mV. C. The number of spikes induced by 10pA/20pA current injection at the membrane resting potential. Two way repeated measures ANOVA indicated significant main effect of genotypes (CR vs KO,  $F(1, 44) = 7.380, P<0.01$ ) and current injection (10pA vs 20pA,  $F(1, 44) = 19.88, P<0.001$ ) in the number of evoked spikes in 1s depolarization. Post-hoc Bonferroni's test revealed significant difference between CR and KO in the number of evoked action potential by 20pA current injection from resting potentials ( $P<0.001$ ).

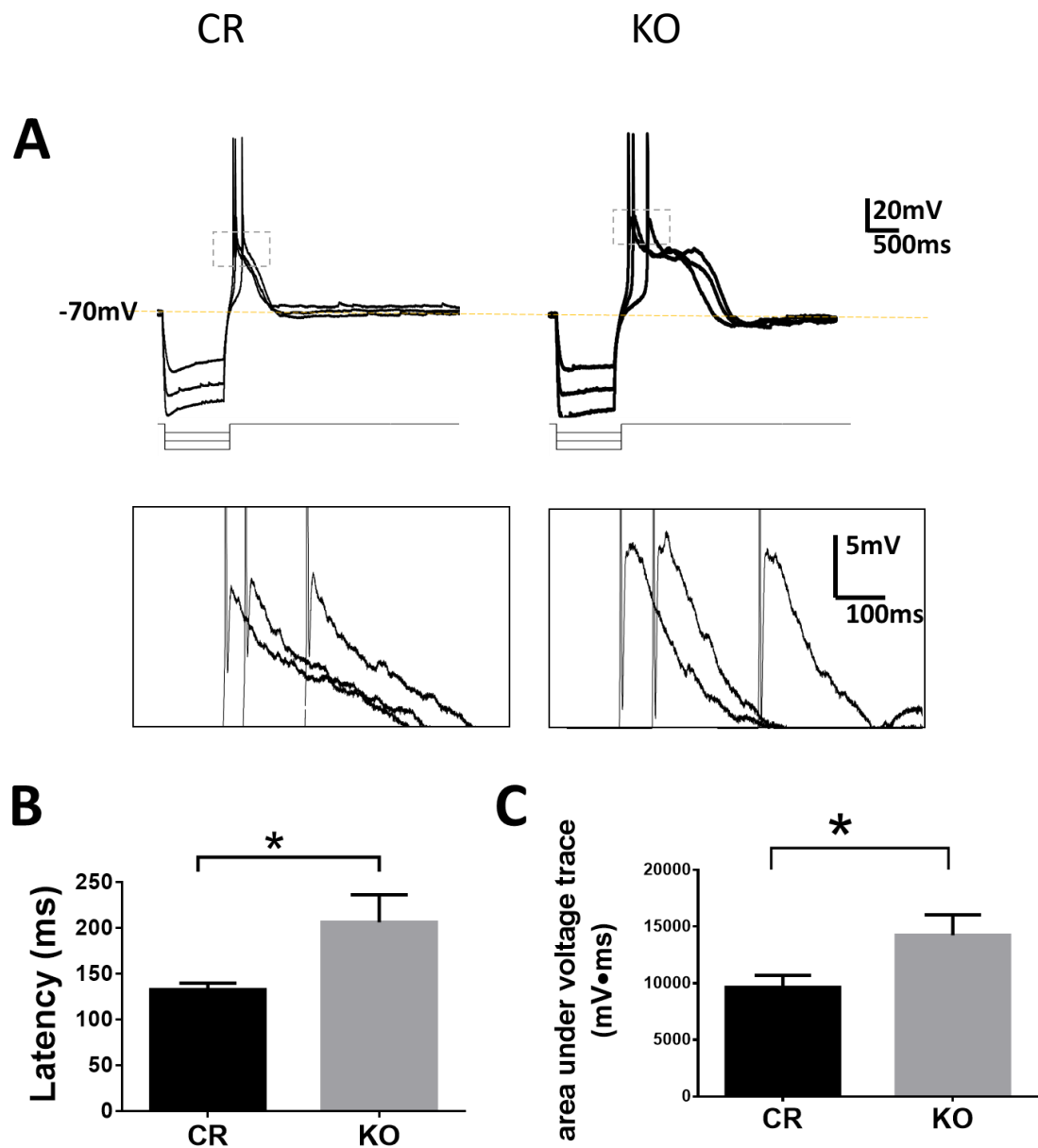


**Figure 3.14** The time to the peak of rebound calcium spike induced by  $-150\text{pA}$  hyperpolarization and the areas under spike traces at  $-70\text{mV}$  in PVA neurons are different between CR and KO. **A.** Examples of rebound spikes by negative current injection  $-50\text{pA}/-100\text{pA}/-150\text{pA}$  from a holding potential at  $-70\text{mV}$ . The top boxed regions are amplified in bot boxes. **B.** The latency to the peak of calcium spike after current injection is significantly longer in *Shox2* KO neurons than that in CR neurons (Student's t-test,  $t(21)=2.29$ ,  $P=0.03$ ). **C.** The areas under voltage trace (between spike traces and  $-70\text{mV}$ ) are significantly larger in *Shox2* KO neurons than that in CR neurons (Student's t-test,  $t(24)=2.11$ ,  $P=0.05$ ).

		CR	KO	P	
Resting Potential (mV)		-55.51±1.66 (n=35)	-54.45±1.68 (n=35)	0.99	
Input Resistance (MΩ)		993.4±52.86 (n=30)	850.3±40.73 (n=29) *	0.04	
Depolarization from -70mV	10pA	Na+ spike time (ms)	201.44±9.97 (n=18)	184.73±15.71(n=13)	0.37
		Ca2+ spike voltage (mV)	-32.14±1.44 (n=18)	-28.72±1.70 (n=13)	0.13
		Ca2+ spike time (ms)	227.66±10.26(n=18)	213.30±16.62(n=13)	0.44
	20pA	Na+ spike time (ms)	102.10±7.95 (n=21)	115.81±10.94 (n=18)	0.32
		Ca2+ spike voltage (mV)	-27.93±1.11 (n=21)	-28.09±1.56 (n=18)	0.93
		Ca2+ spike time (ms)	124.29±8.90 (n=21)	153.98±17.97(n=18)	0.13
Hyperpolarization from -70mV	Rebound spike number		1.78±0.26 (27)	1.46±0.26 (28)	0.4
	-150pA	rebound calcium spike peak potential (mV)	-25.62±1.20 (13)	-27.22±1.59 (15)	0.45
		half rise time (ms)	21.15±1.65 (13)	22.53±1.41 (15)	0.53
		half decay time (ms)	175.3±22.23 (12)	321.6±51.94 (15) *	0.03
		voltage(mV)	-129.24±4.11 (n=27)	-126.00±3.37 (n=28)	0.55
		sag size(mV)	6.47±1.69 (n=27)	6.85±1.98 (n=28)	0.89
	-100pA	voltage(mV)	-114.70±2.66 (n=27)	-112.26±2.33 (n=28)	0.50
		sag size(mV)	4.39±1.28 (n=27)	4.24±1.47 (n=28)	0.94
	-50pA	voltage(mV)	-99.92±1.27 (n=27)	-98.38±1.36 (n=28)	0.42
		sag size(mV)	2.26±0.53 (n=27)	2.41±0.71 (n=28)	0.87
	Hyperpolarization from RP	rebound spike number		2.44±0.26 (n=18)	2.37±0.26 (n=19)
-150pA		rebound calcium spike peak potential (mV)	-25.12±0.95 (n=15)	-27.30±1.21 (n=17)	0.19
		rebound calcium spike peak time (ms)	104.06±10.13(n=14)	104.49±10.59(n=16)	0.95
		voltage(mV)	-129.67±4.73 (n=18)	-125.72±4.73 (n=19)	0.57
		sag size(mV)	10.96±2.53 (n=18)	11.24±3.37 (n=19)	0.89
-100pA		voltage(mV)	-113.85±2.87 (n=18)	-114.49±2.88 (n=19)	0.45
		sag size(mV)	7.68±1.87 (n=18)	6.93±2.34 (n=19)	0.81
-50pA		voltage(mV)	-97.16±1.21 (n=18)	-92.05±3.19 (n=19)	0.16
		sag size(mV)	4.68±1.08 (n=18)	2.93±1.32 (n=19)	0.87

**Table 2. Some insignificant intrinsic properties of PVA neurons of CR and *Shox2* KO mice.** Na<sup>+</sup> spike and Ca<sup>2+</sup> spike time is the time delay of spike peak following current injection; Voltage(mV) under hyperpolarization is the maximum negative voltage at the beginning of each hyperpolarization trace. Sag (mV) is the voltage difference between the beginning and the end of one second negative current injection. Rebound spike numbers are the average number of Na<sup>+</sup> spikes caused by -50pA/-100pA/-150pA current injection.

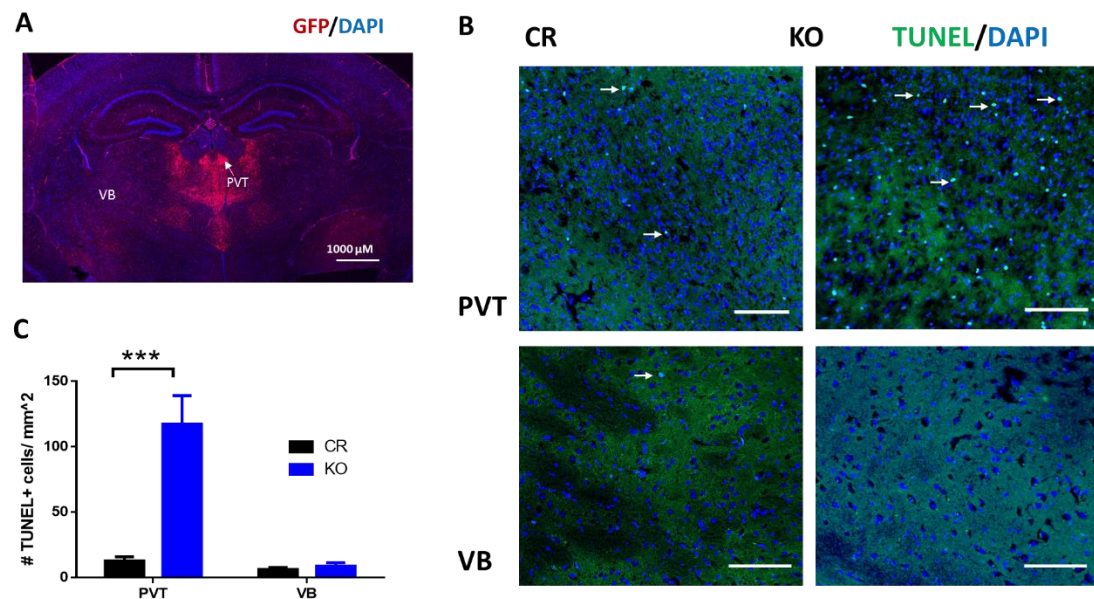


**Figure 3.15. *Shox2* KO-induced cell death in adult mouse brain.** A. GFP staining (red color) represented the expression pattern of *Gbx2* in P25 mouse brain, showing *Gbx2* only expressed in the midline of the thalamus (arrow shows PVT in midline thalamus) but not lateral thalamus. B. TUNEL staining showed *Shox2* KO in *Gbx2* cells induced cell death in PVT (*Gbx2* expression region) but not in VB (non-*Gbx2* expression region). Arrows show examples of TUNEL positive cells. Scale bar= 120  $\mu$ M. C. Two-way ANOVA indicated significant main effect of genotypes (CR vs KO) and regions (PVT vs VB), and significant interaction between genotypes and regions on the number of TUNEL+ cells every squared millimeters (genotypes:  $F(1,29) = 29.11$ ,  $P < 0.01$ ; regions:  $F(1,29) = 37.12$ ,  $P < 0.01$ ; interaction:  $F(1,29) = 32.07$ ,  $P < 0.01$ ). Post-hoc Bonferroni's comparison test showed *Shox2* KO induced more cell death in PVT ( $P < 0.01$ ) but not VB ( $P > 0.99$ ).

### **3.5 *Shox2* KO affected T-type calcium and HCN current in the PVA.**

The decrease in cell excitability and intrinsic properties changes in PVA neurons of *Shox2* KO mice suggested *Shox2* KO impairs ion current in PVA neurons. The important role of *Shox2* in the heart pacemakers suggests *Shox2* may affect pacemaker-related currents, including T-type calcium current and HCN current, in adult thalamus. Therefore, we tested the physiological properties of T-type calcium currents in CR and *Shox2* KO mice. We isolated T-type calcium current in the PVA neurons of CR and *Shox2* KO mice (Figure 3.16 C) with a typical subtraction protocol (C. Zhang, Bosch, Rick, Kelly, & Ronnekleiv, 2009). The T-type  $\text{Ca}^{2+}$  currents induced at -50mV by step voltages ranging from -90mV to 0 mV (Figure 3.16 B) were subtracted from those induced by the same step voltages held at -100mV for a second to remove the inactivation of T-type calcium current (Figure 3.16 A). The isolated current was blocked after application of 2mM  $\text{NiCl}_2$  for 10 minutes (Figure 3.16 D), confirming the isolated current was T-type calcium current (Bhattacharjee, Whitehurst, Zhang, Wang, & Li, 1997; Lee, Gomora, Cribbs, & Perez-Reyes, 1999). We found that the activation voltage range for both CR and KO neurons

was -70mV to -10mV with a peak current at -50mV (Figure 3.16 G H). The activated current density was significantly smaller in the PVA neurons from KO mice compared to CR mice (Figure 3.16 F, two-way repeated measures ANOVA, main effect of genotype:  $F(1, 20) = 8.70$ ,  $P < 0.01$ ; main effect of voltage:  $F(9, 180) = 63.98$ ,  $P < 0.001$ ; interaction:  $F(9, 180) = 6.38$ ,  $P < 0.001$ ). Post-hoc Bonferroni's multiple comparisons test revealed that the current density elicited at -50mV and -60mV in CR neurons was larger than that in KO neurons (Figure 3.16 G,  $P < 0.01$ ). Interestingly, two-way repeated measures ANOVA of normalized T-type calcium activation curve revealed a significant interaction between genotype and voltage ( $F(9, 180) = 3.27$ ,  $P < 0.01$ ) and post-hoc Bonferroni's test showed that normalized T-type calcium current ( $I/I_{max}$ ) was larger at -60mV in CR mice compared KO mice (Figure 3.16 H, 0.36 vs 0.08,  $P < 0.01$ ). It suggests T-type calcium current is activated at a relatively hyperpolarized potential in CR neurons than that in KO neurons. We measured the time to the peak of T-type calcium current evoked at -50 mV. The results indicated that *Shox2* KO neurons have a slower time to peak than that in CR neurons (Figure 3.16 F I, student's t-test,  $t(20) = 2.57$ ,  $P = 0.02$ ). Moreover, the slower kinetic properties of T-type calcium current elicited at -50mV occurred in

activation phase (Figure 3.16 F I,  $P=0.08$ ) but not inactivation phase (Figure 3.16 F I,  $P=0.97$ ).



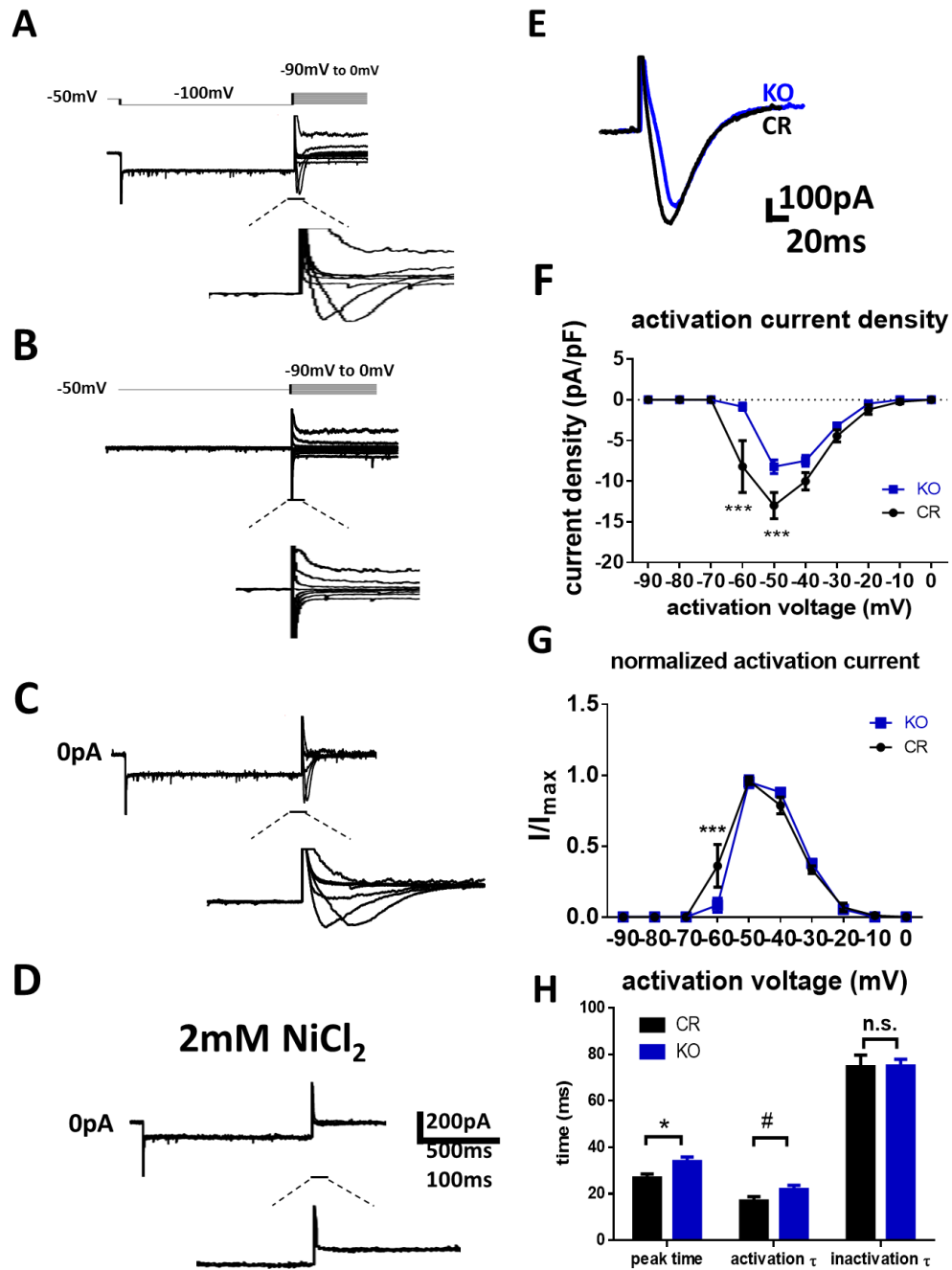


**Figure 3.16. The activation properties of T-type calcium current in PVA neurons of CR and *Shox2* KO mice.** A-D. The T-type calcium current were isolated at voltage-clamp with TTX applied in bath aCSF. A. The membrane potential was hyperpolarized to -100mV for 1s from holding potential -50mV to remove inactivation of the T-type calcium current. Then T-type calcium currents were elicited by stepping from -100mV to a series of incremental depolarizations ranging from -90mV to 0mV. B. The same series of stepping voltages was applied to the same neurons without hyperpolarization to -100mV, instead, the membrane potential was held at -50mV in that time range. C.

The neat T-type calcium currents were isolated by subtracting currents evoked in B from currents evoked in A. D. The isolated current was blocked by 2mM NiCl<sub>2</sub>, confirming the isolated current is T-type calcium current. E. An example of T-type calcium currents recorded from PVA neurons of CR and *Shox2* KO mice. T-type calcium currents in *Shox2* KO mice were smaller and slower than that in CR mice. F. The current density curve of T-type calcium current activation indicated that T-type calcium current density was smaller in PVA neurons of KO mice compared to CR mice (two way repeated measures ANOVA, main effect of genotypes (CR vs KO):  $F(1, 20) = 8.704$ ,  $P < 0.01$ ). Post-hoc Bonferroni's multiple comparisons tests indicated significant differences in T-type calcium current density at -60mV ( $P < 0.01$ ) and -50mV ( $P < 0.01$ ) between CR and KO. G. The normalized activation curves indicated that normalized T-type calcium ( $I/I_{max}$ ) is larger at -60mV in CR mice than that in KO mice (two-way ANOVA test indicated interaction between voltage and genotypes,  $P < 0.01$ ; Post-hoc Bonferroni's multiple comparisons test: at -60mV voltage,  $P < 0.01$ ). H. The time to peak showed that T-type calcium current at -50mV in PVA neurons of KO mice was significantly slower than that of CR mice (Student's t-test,  $t(20) = 2.568$ ,  $P = 0.02$ ). The slower activation kinetics of T-type calcium current elicited at -50mV only occurred in

Further, we tested the inactivation properties of the T-type calcium current by eliciting inactivation T-type calcium currents at -50mV after a 1-second preholding potential ranging from -90mV to -40mV (Figure 3.17 A left). The current was confirmed as T-type calcium current by application of 2mM NiCl<sub>2</sub> for 20 minutes to block it (Figure 3.17 A right). The inactivation curve of T-type calcium current density showed that the current density in KO neurons was decreased compared to CR neurons (Figure 3.17 B C, two-way ANOVA, the main effect of genotypes,  $F(1, 21) = 8.41, P < 0.01$ ). However, the normalized inactivation curves of T-type calcium current from CR neurons and KO neurons overlapped (Figure 3.17 D). It suggested the same inactivation kinetics between CR and KO neurons. The kinetics analysis found a consistent result as that in the activation study that *Shox2* KO neurons have a slower time to peak and activation time constant but not inactivation time constant than that in CR neurons (Figure 3.17 E F).

To summarize, our results indicate that: 1) T-type calcium current density was decreased in PVA neurons of *Shox2* KO mice; 2) The activation of T-type calcium current was slower in PVA neurons of *Shox2* KO mice compared to CR mice; 3) The activation threshold of T-type calcium current was shifted to a

depolarized potential in PVA neurons of *Shox2* KO mice.

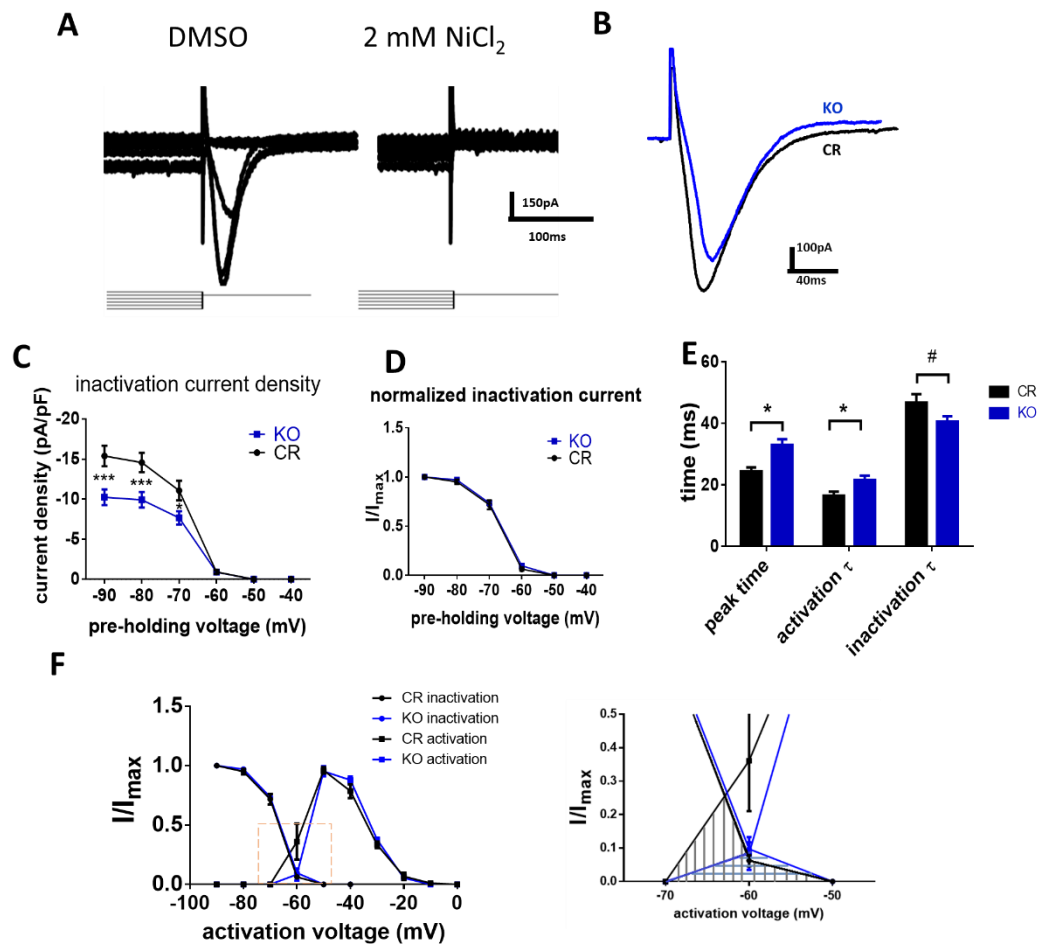


**Figure 3.17. The inactivation properties of T-type calcium current in PVA neurons of CR and *Shox2* KO mice.** A. The T-type calcium currents were elicited at -50mV after recovery from 1s pre-holding step voltage ranging from -90mV to -40mV. The elicited T-type calcium current is confirmed by application of 2mM NiCl<sub>2</sub> to block it. B. The example T-type calcium current isolated from KO neuron and CR neuron evoked at -50mV from -90mV. C. The curve of T-type calcium current inactivation current density at different pre-holding voltage from CR neurons and KO neurons. Two-way repeated measures ANOVA indicated significant main effect of genotypes (CR vs KO,  $F(1,21) = 8.41$ ,  $P < 0.01$ ) and voltage ( $F(5,105) = 218.7$ ,  $P < 0.001$ ) and significant interaction ( $F(5,105) = 8.58$ ,  $P < 0.001$ ). Post-hoc Bonferroni's multiple test indicated that current density of CR neurons is significantly bigger than that of KO neurons at -90mV ( $P < 0.001$ ), -80mV ( $P < 0.001$ ), and -70mV ( $P = 0.01$ ). D. The normalized inactivation current curves of CR and KO neurons are overlapped with each other. (E. The peak time of T-type calcium current at -50mV from the pre-holding potential of -90mV, -80mV and -70mV. Two-way repeated measures ANOVA indicated significant main effect of genotypes ( $F(1,21) = 7.31$ ,  $P = 0.01$ ) and pre-holding voltage ( $F(2,42) = 39.24$ ,  $P < 0.01$ ).

Post-hoc Bonferroni's multiple test indicated that peak time of CR neurons is significantly shorter than that of KO neurons at -90mV ( $P=0.02$ ) and -80mV ( $P=0.03$ ). )

F. The time to the peak of T-type calcium current (peak time) and activation time constant  $\tau$  of T-type calcium current of CR neurons is significantly shorter than that of KO mice at -50mV depolarized from pre-holding one-second -90mV in PVA neurons (activation  $\tau$ , student's t-test,  $t(21)=2.456$ ,  $P=0.02$ ) but not the inactivation time constant  $\tau$  (student's t-test,  $t(21)=2.008$ ,  $P=0.06$ ).

In addition, since HCN2 and HCN4 are highly expressed in the thalamus, we measured HCN current in PVA neurons of CR and *Shox2* KO mice. A previous study demonstrated that the HCN current in PVA neurons is small when recorded during the day, possibly because of low levels of cAMP during the daytime which is the sleep cycle for mice (Kolaj, Zhang, Ronnekleiv, & Renaud, 2012). The goal of our experimental design was to compare the amplitude of HCN currents in control and KO mice. The HCN currents were elicited by hyperpolarizing the cell membrane to -100mV and -150mV from -50 mV. The amplitude of HCN current was measured as the difference between the end current of one second hyperpolarization and the beginning instantaneous current at -150mV hyperpolarization (Figure 3.18 A). Our results showed that the HCN current density in *Shox2* KO neurons was significantly smaller than that in CR neurons (Figure 3.18 B). This result is consistent with our T-type calcium current investigation, demonstrating that *Shox2* KO impaired pace-making related ion currents including T-type calcium current and HCN current.

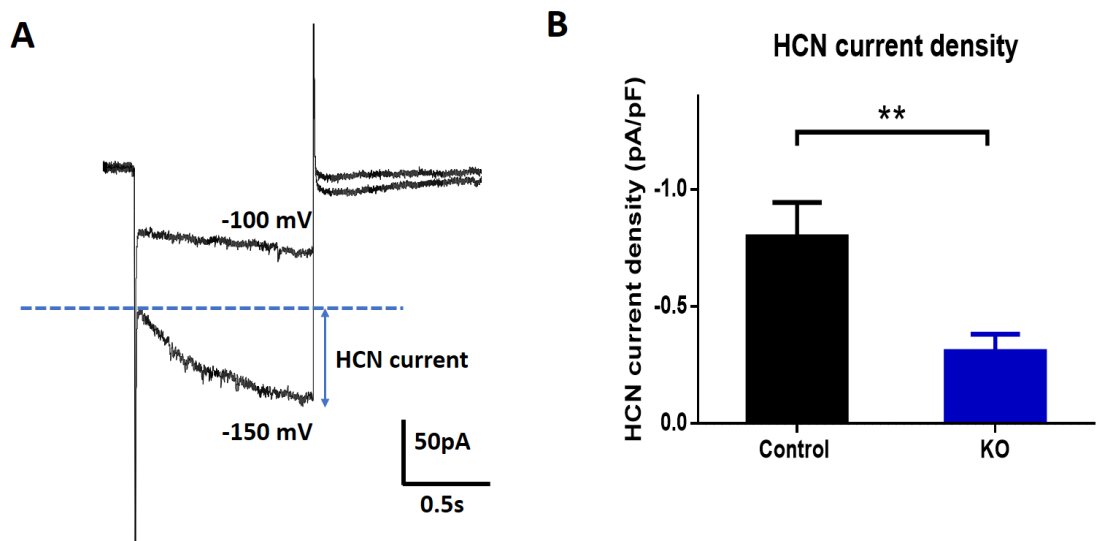


**Figure 3.18. *Shox2* inducible KO decreased HCN current in PVA of neurons.** A. An example of HCN current elicited by hyperpolarizing cell membrane from -50mV to -100mV and -150mV. HCN current is defined as the current difference between the current at the end of 1s hyperpolarization and the current peak at the beginning of hyperpolarization as shown in the figure. B. *Shox2* KO decreased HCN current density in PVA of neurons (student's t-test,  $t(15) = 3.10$ ,  $P < 0.01$ ).



### **3.6 *Shox2* KO decreased the mRNA and protein expression of Cav3.1 and HCN2/4 channel in the thalamus.**

The electrophysiological data indicated reduced T-type calcium currents and HCN currents in *Shox2* KO neurons. We investigated whether T-type calcium channels and HCN channels are downstream regulation targets of *Shox2*. We first tested expression of the channel genes in the thalamus in CR and KO mice.

We conducted RT-qPCR experiments with RNA extracted from the thalamus tissues of 8-10-week-old CR and KO mice. The expression of all the genes tested in the RT-qPCR experiments were normalized to the reference gene  $\beta$ -actin (*Actb*) and *TATA-box binding protein* (*Tbp*) where are widely used as housekeeping reference genes for RT-qPCR experiment (*B. Li et al., 2014; Valente et al., 2009*). All primers were designed and tested, and conditions were optimized to have an efficiency between 95% and 105%. Both the melt curves and gel investigations were used to confirm the RT-qPCR products.

We tested the mRNA expression of genes for T-type calcium channels. Previous studies showed that  $Ca_v3.1$  subunits are highly expressed in the thalamus, and the main T-type calcium channel proteins expressed in the

thalamus (Chen, Parker, & Wang, 2014), with Cav3.2 proteins expressed at lower levels. The genes that code for Cav3.1 and Cav3.2 are *Cacna1g* and *Cacna1h*, respectively. The results showed that the expression of *Cacna1h* was very little in our sample (Figure 3.19 A, less than 1/1000 of *Cacna1g* expression) and not significantly different between CR and KO (Figure 3.19 C). With respect to the expression of *Cacna1g*, our results indicated that *Shox2* KO significantly decreased the mRNA expression of *Cacna1g* (Figure 3.19 B).

Next, we tested the mRNA expression of HCN channels in CR and KO mice. Previous studies have already reported that mice brains express low levels of HCN3 (Moosmang, Biel, Hofmann, & Ludwig, 1999); therefore, we investigated the expression of mRNA for HCN1, HCN2 and HCN4. Our results showed that *Hcn2* mRNA had the highest expression in our thalamus tissue (Figure 3.19 D). *Hcn4* also had a prominent expression while the expression of *Hcn1* was only about 5% of *Hcn2* expression. This result is consistent with previous research indicating HCN2/4 channels are the main HCN channels in the thalamus and provided precise relative expression data of HCN channels in mouse thalamus. *Hcn1* mRNA was demonstrated to have the dominant expression in the neighboring brain regions of the thalamus, such as the cortex

and hippocampus (Moosmang et al., 1999). The low *Hcn1* mRNA level in our results demonstrated the reliability of our thalamic tissue collection. *Hcn2* and *Hcn4* mRNA were significantly reduced in the *Shox2* KO thalamus compared to that in CR mice (*Hcn2*: Student's t-test,  $t(9) = 3.92$ ,  $P < 0.01$ ) and *Hcn4*: Student's t-test,  $t(9) = 4.02$ ,  $P < 0.01$ ). *Hcn1* mRNA expression level was not significantly affected (student's t-test,  $t(9) = 1.85$ ,  $P = 0.10$ ).

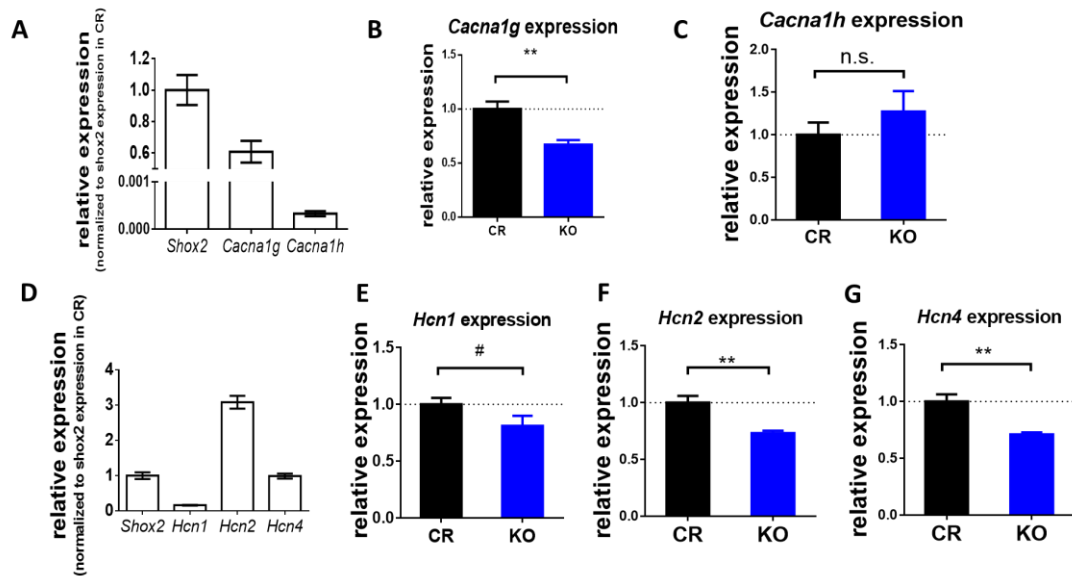


**Figure 3.19. *Shox2* KO decreased the mRNA expression of CACNA1G, HCN2 and HCN4.**

A. We tested the mRNA level of two main T-type calcium channels CACNA1G and CACNA1H. The mRNA level of CACNA1H is very low compared to *SHOX2* and CACNA1G expression. *Shox2* KO significantly decreased mRNA level of CACNA1G (B,  $t(9) = 3.85$ ,  $P < 0.01$ ) but not CACNA1H (C,  $t(9) = 1.02$ ,  $P = 0.34$ ) in adult thalamus. D. We tested the mRNA level of three main HCN channels HCN1, HCN2 and HCN4. The results showed relatively high level of HCN2 and HCN4, but low level of HCN1. *Shox2* KO significantly decreased mRNA level of HCN2 (F,  $t(9) = 3.92$ ,  $P < 0.01$ ) and HCN4 (G,  $t(9) = 4.02$ ,  $P < 0.01$ ), but no HCN1 (E,  $t(9) = 1.85$ ,  $P = 0.10$ ).

Previous studies revealed that *Shox2* KO mice have more cell apoptosis in *Shox2* expression regions including heart (Sun et al., 2015) and brain (Rosin, Kurrasch, et al., 2015; Rosin, McAllister, et al., 2015) during development and our results indicated that *Shox2* KO increased cell death in adult thalamus. Therefore, we tested whether *Shox2* affected cell apoptosis-related genes in the adult thalamus. We picked two important anti-apoptotic members, *Bcl-2* and *Bcl-xl*, from *Bcl-2* family, the apoptosis regulator proteins family. Our results showed a trend of downregulation of low-expressed *Bcl-2* mRNA level (Figure 3.20B,  $P=0.05$ ) and no significant difference in *Bcl-xl* mRNA level (Figure 3.20C,  $P=0.57$ ) in the thalamus from *Shox* KO mice compared to that from CR thalamus.

Besides these genes, we also tested *Glutamate Ionotropic Receptor AMPA Type Subunit 2 (Gria2)* and *Neurotrophic Receptor Tyrosine Kinase 2 (TrkB)* (Figure 3.20 D E F). They were found to be regulated by *Shox2* in the embryonic limbs and DRG, respectively (Abdo et al., 2011) (Ye et al., 2016). Our results confirmed the expression of *Gria2* (Figure 3.20 E,  $P=0.41$ ) and *TrkB* in the thalamus (Figure 3.20 F,  $P=0.21$ ) and found no significant difference in their expression levels between CR and KO.

According to the RT-qPCR results, *Hcn2*, *Hcn4* and *Cacna1g* mRNA expression levels were down-regulated by *Shox2* KO. To investigate that the expression of the protein products of these genes were also downregulated by *Shox2* KO, we conducted western blot staining experiments to test the protein level of the HCN2, HCN4 and Ca<sub>v</sub>3.1 channels. Our results indicated that the expression levels of HCN2 and HCN4 were significantly decreased and a trend toward decreased expression of Ca<sub>v</sub>3.1 proteins mice were significantly in the thalamus from *Shox2* KO mice compared to that from CR mice (Figure 3.21). These Western staining results were consistent with RT-qPCR results and confirmed that HCN2, HCN4 and Ca<sub>v</sub>3.1 are under regulation of *Shox2* in the adult thalamus.

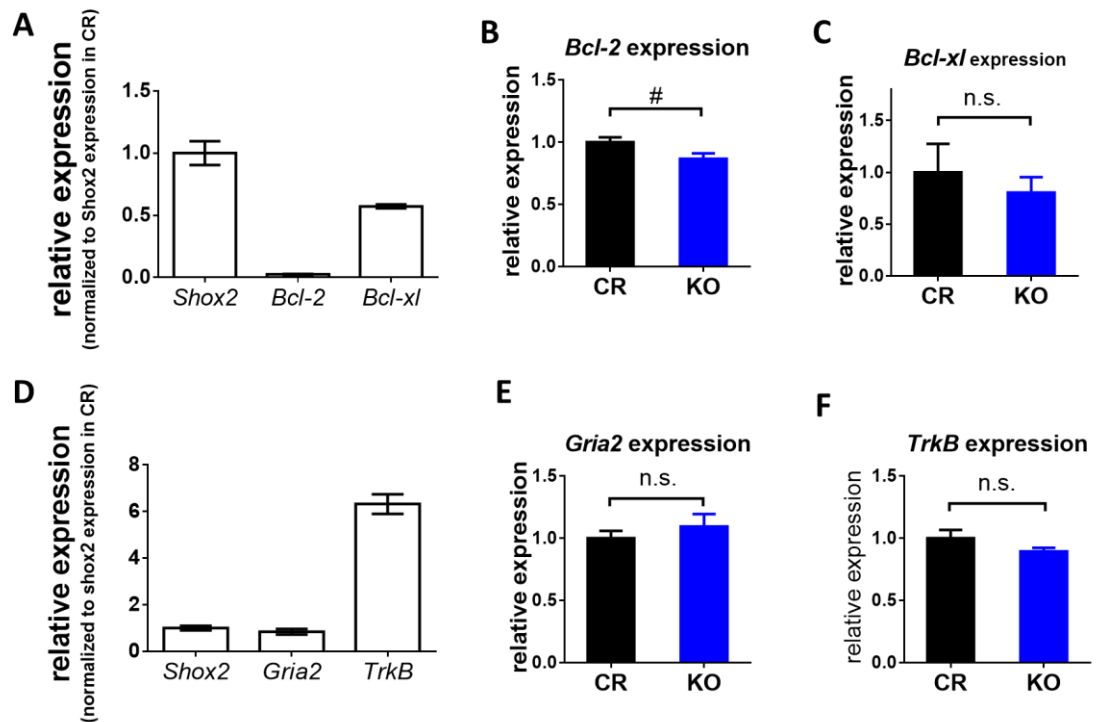


**Figure 3.20. The mRNA expression of several genes in the PVA of CR and *Shox2* KO mice.** A. The relative mRNA expression of *Bcl-2* and *Bcl-xl* gene in the PVA of CR mice. *Shox2* KO showed a trend to decrease *Bcl-2* expression (B, student's t-test,  $t(9) = 2.25$ ,  $P = 0.05$ ) and had no significant effect on *Bcl-xl* expression (C, student's t-test,  $t(9) = 0.59$ ,  $P = 0.57$ ). D. The relative mRNA expression of *Gria* and *TrkB* gene in the PVA of CR mice. *Shox2* KO did not significantly affect the mRNA expression of *Gria* (E, student's t-test,  $t(9) = 0.86$ ,  $P = 0.41$ ) and *TrkB* (F, student's t-test,  $t(9) = 1.35$ ,  $P = 0.21$ ).

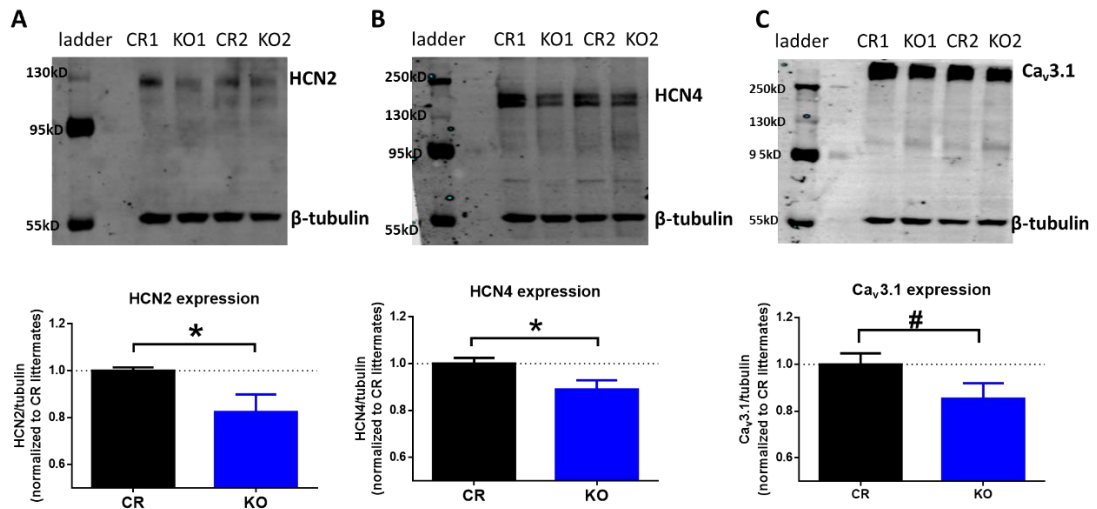


**Figure 3.21. *Shox2* KO decreased the protein expression of HCN2, HCN4 and Ca<sub>v</sub>3.1 expression.** The bands around ~120kD, ~150kD, >250kD at the top of each gel stained by anti-mouse secondary antibody are recognized as HCN2 (A), HCN4 (B) and Ca<sub>v</sub>3.1(C), and the bands around ~55-60kD stained by anti-rabbit secondary antibody are recognized as  $\beta$ -tubulin. Student's t-test indicated *Shox2* KO induced significant decrease of HCN2 ( $t(16) = 2.30, P = 0.04$ ) and HCN4 ( $t(14) = 2.37, P = 0.03$ ) proteins, and a trend to significant decrease of Ca<sub>v</sub>3.1 proteins ( $t(14) = 1.86, P = 0.08$ ).



### **3.7 mRNA sequencing results revealed that *Shox2* is essential for maintenance of thalamic neuron identity and survival.**

Our results indicated *Shox2* specifically expresses in neurons of the thalamus and is important for cell survival, neuronal excitability and ion channel expression. To better understand the regulation targets of *Shox2* within the entire genome, we conducted mRNA sequencing experiments with mRNA samples from midline thalamus. We used the Cre mouse line, *Gbx2*<sup>CreERT</sup>, which has been demonstrated to have good expression in the midline thalamus (Figure 3.15 A). We extracted mRNA from the midline thalamus of 5 KO and 5 littermates CR mice. The mRNA sequencing and a preliminary analysis are done by BGI Americas Corporation, and we used the results of detailed reads, post probability of equally expressed (PPEE) and fragment reads per kilobase per million mapped reads (FPKM) they provided for further analysis.

The mRNA sequencing results showed that the expression of *Shox2* in KO tissue is ~35% of CR mice (FPKM: *Shox2* CR: 48.01±2.76 vs KO: 16.90±0.30), indicating the inducible KO was successfully induced. We set PPEE<0.05 and change more than 10% as the threshold and screened out significantly

regulated genes. We found that 17 genes were downregulated and 18 genes were upregulated in the *Shox2* KO tissue, and all genes are listed in the table 3 and table 4.

The cellular component gene ontology (GO) study found *Shox2* KO regulated 6 genes in GO term of extracellular matrix (17.1% compared to 7.6% genes in the whole genome) and another 4 genes in GO term of neuron projections (11.4% compared to 3.3% genes in the whole genome. Figure 3.22, cellular component), indicated that *Shox2* may be implicated in thalamic neurons identity. Besides, in biological process GO study found *Shox2* KO regulated 2 genes in GO term of neuron projection development (5.7% compared to 0.9% genes in the whole genome), 3 genes in GO term of cell death (8.6% compared to 5.9% genes in the whole genome), 15 genes in GO term of response to stimulus (42.9% compared to 25.4% genes in the whole genome), suggesting the *Shox2* is implicated in cell survival and differentiation in response to stimulus. The GO analysis supports our hypothesis that *Shox2* is involved in the maintenance of thalamic neurons survival and identity and provided us with more information about possible downstream targets. We did not conduct enrichment pathway study because of the limited number of DEGs, but we can

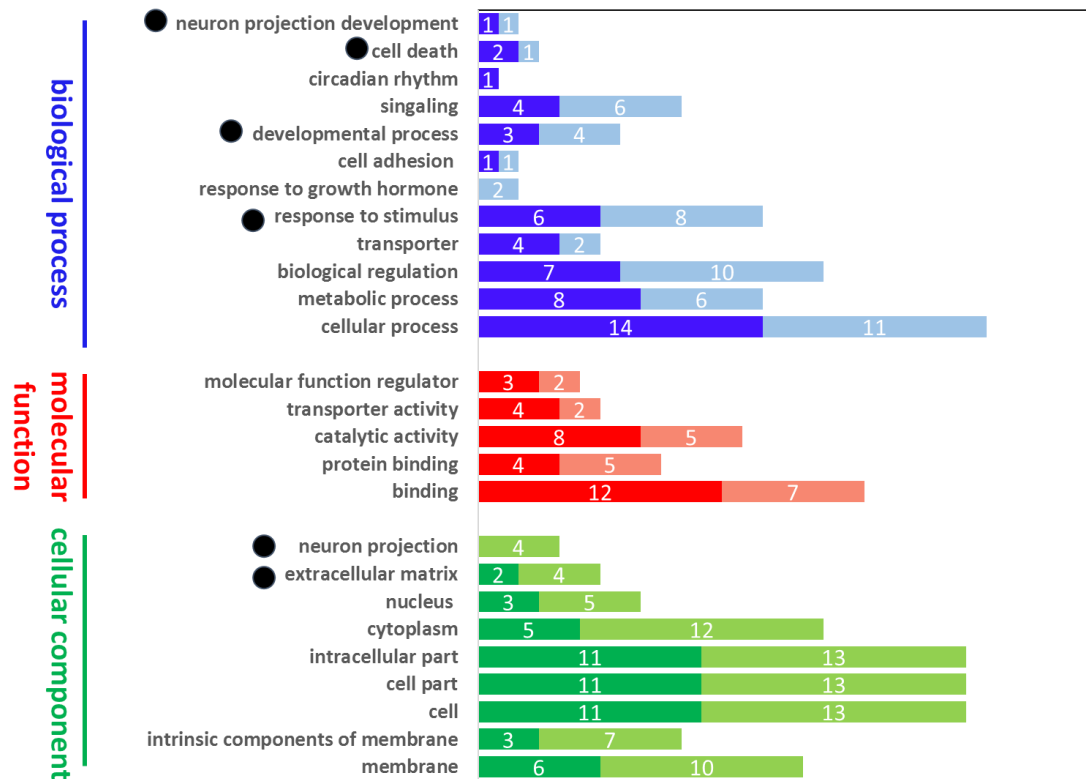
investigate all DEGs one by one in the further study.

For better understanding whether *Shox2* KO affects thalamus cell identity, we investigated the expression of thalamus-specific enriched genes in CR and *Shox2* KO mice. The list of thalamus-specific enriched genes in adult mouse is according to a study of genome-wide gene expression in the adult mouse brain by Allen Brain Atlas based on *in situ* gene expression studies in adult C57Bl/6J mouse (Lein et al., 2007; Ng et al., 2009). To describe how these genes are regulated by *Shox2* KO, we used P value of Student's t-test of gene expression level (FPKM values provided by *BGI*) between 5 CR and 5 KO mouse. Although P value from Student's t-test is not accurate to describe whether a gene is significantly regulated or not because of unadjusted Type I error, our P values from an unpaired comparison of 5 CR samples and 5 KO samples described the relative possibility of differences in each gene. The results showed that thalamus-specific enriched genes are highly regulated by *Shox2* (Figure 3.23 A).  $\chi^2$  test showed that more thalamus-specific enriched genes were likely to be regulated by *Shox2* in the whole genome (Figure 3.23 B).

Interestingly, potassium channels and potassium channels-related proteins are highly regulated by *Shox2* KO especially axon-enriched voltage-gated

*Kcnc4* and *Kcna2*,  $K_v\beta$  subunit *Kcnab1* and *Kcnab3*, BK channels  $\beta$  subunit *Kcnmb4*, inward rectifying channels *Kcnj10*,  $K^+$  channels tetramerization domain protein *Kctd12*, and potassium-interacting protein *Kchip3* have high expression levels in the thalamus and are likely to be regulated by *Shox2* KO, while other ion channels such as sodium channels, calcium channels and chloride channels and their related proteins are not according to Student's t-test of FPKM values of CR and *Shox2* (Figure 3.24,  $\chi^2$  test,  $\chi^2=8.03$ ,  $P=0.02$ ).

## Gene Ontology Analysis of DEGs



Number of downregulation/upregulation genes by *Shox2* KO

**Figure 3.22. Gene ontology (GO) study of significantly regulated gene by *Shox2* KO.**

The black dots indicated enriched genes in GO terms of neuron projection development, cell death, development process, response to stimulus, neuron projection and extracellular matrix.

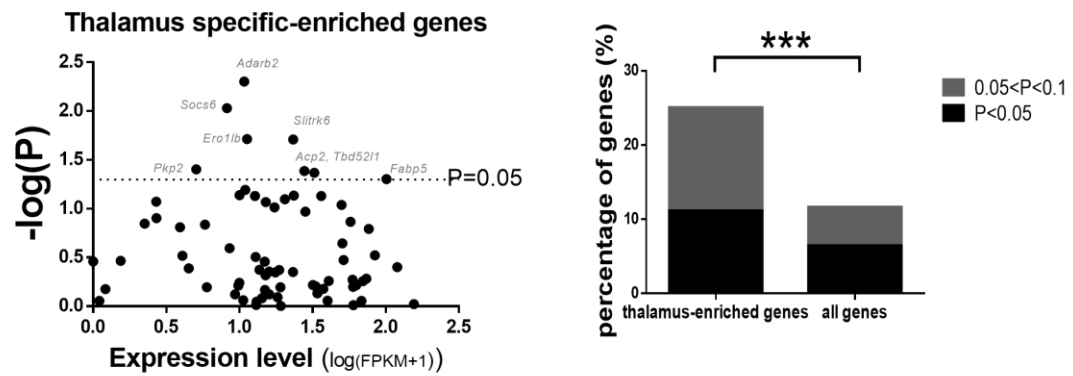


**Figure 3.23. The gene expression profiles in thalamus are highly regulated by *Shox2*.** Left. The thalamus specially enriched genes are highly regulated by *Shox2*. Y-axis shows the P value of Student's t-test of FPKM level between 5 CR and 5 KO samples. The name of genes with P value less than 0.05 ( $-\log(P) > 1.30$ ) are label in the figure. X-axis shows the expression value of genes. Right.  $\chi^2$  tests shows that thalamus-enriched genes are more possible to be significantly or marginally significantly regulated by *Shox2* among all genes detected in our mRNA experiments ( $\chi^2$  test,  $\chi^2=14.15$ ,  $P < 0.001$ ).

**Table 3 The list of upregulated gene by *Shox2* KO**

Symbol	Description	geneLength	Means-CR	Means-KO	change %	PPEE
<b>Pdyn</b>	prodynorphin	747	24.09	43.49	81%	2.00E-02
<b>Pmch</b>	pro-melanin-concentrating hormone	748	1158.20	1898.42	64%	2.92E-05
<b>Parpbbp</b>	PARP1 binding protein	3628	399.99	657.59	64%	1.16E-02
<b>Krt12</b>	keratin 12	1854	48.49	77.17	59%	3.59E-02
<b>Th</b>	tyrosine hydroxylase	1757	65.25	99.68	53%	2.92E-02
<b>Ap1s2</b>	adaptor-related protein complex 1, sigma 2 subunit	3204	198.26	290.51	47%	7.03E-03
<b>Plxdc1</b>	plexin domain containing 1	2901	388.26	560.11	44%	1.51E-03
<b>Rnf152</b>	ring finger protein 152	8466.74	802.54	1010.28	26%	0.00E+00
<b>Kcnc4</b>	potassium voltage gated channel, Shaw-related subfamily, member 4	3013	407.98	506.25	24%	4.73E-07
<b>Cdr2</b>	cerebellar degeneration-related 2	2525	322.88	392.32	22%	5.32E-03
<b>Rgs4</b>	regulator of G-protein signaling 4	2952	6090.26	7293.50	20%	2.26E-02
<b>4933409K07Rik</b>	RIKEN cDNA 4933409K07 gene	4551	2033.09	2408.09	18%	1.72E-10
<b>Spon1</b>	spondin 1, (f-spondin) extracellular matrix protein	6166	1985.77	2324.53	17%	3.64E-14
<b>Fam19a2</b>	family with sequence similarity 19, member A2	4355.24	481.08	561.29	17%	1.54E-02
<b>Sap130</b>	Sin3A associated protein	4015	756.81	864.97	14%	5.42E-03
<b>Pdia6</b>	protein disulfide isomerase associated 6	2125	850.46	957.66	13%	3.75E-02
<b>Stmn2</b>	stathmin-like 2	1904	6276.07	6875.44	10%	2.45E-07

**Table 3. The list of genes upregulated in the midline thalamus of *Shox2* KO mice.** Means-CR and Means-KO showed the mean of reads in CR samples and KO samples.

**Table 4 The list of downregulated gene by *Shox2* KO**

Symbol	Description	geneLength	Means-CR	Means-KO	change %	PPEE
<b>Gm15772</b>	ribosomal protein L26 pseudogene	539	790.56	502%	-99%	1.53E-09
<b>Lrat</b>	lecithin-retinol acyltransferase (phosphatidylcholine-retinol-O-acyltransferase)	5349	24.07	3.92	-84%	4.20E-05
<b>Hbb-b2</b>	hemoglobin, beta adult minor chain	632	36.47	9.94	-73%	1.29E-02
<b>Endou</b>	endonuclease, polyU-specific	2404.97	160.41	49.48	-69%	2.40E-03
<b>Shox2</b>	short stature homeobox 2	1603	834.27	295.12	-65%	0.00E+00
<b>Fcrls</b>	Fc receptor-like 5, scavenger receptor	1991	100.45	48.94	-51%	7.98E-08
<b>Hapln2</b>	hyaluronan and proteoglycan link protein 2	2055	281.99	188.83	-33%	1.92E-12
<b>Tmem144</b>	transmembrane protein 144	2292	170.63	122.88	-28%	6.57E-04
<b>Rsrc1</b>	arginine/serine-rich coiled-coil 1	3232	1425.08	1116.26	-22%	2.30E-11
<b>Stac2</b>	SH3 and cysteine rich domain 2	3049	329.20	256.09	-22%	1.82E-03
<b>Atf5</b>	activating transcription factor 5	1795.75	369.30	297.59	-19%	2.40E-02
<b>Ppp1r16b</b>	protein phosphatase 1, regulatory (inhibitor) subunit 16B	6388.46	1181.46	967.52	-18%	2.17E-02
<b>Gucy1a2</b>	guanylate cyclase 1, soluble, alpha 2	13727	1213.57	1003.92	-17%	1.32E-03
<b>Iqsec3</b>	IQ motif and Sec7 domain 3	6840	2241.57	1893.12	-16%	1.35E-03
<b>Pacsin2</b>	protein kinase C and casein kinase substrate in neurons 2	3693.52	1259.72	1087.93	-14%	8.74E-03
<b>Phactr1</b>	phosphatase and actin regulator 1	5376.32	1534.38	1330.77	-13%	8.36E-04
<b>Cnp</b>	2',3'-cyclic nucleotide 3' phosphodiesterase	2424.23	4807.37	4214.96	-12%	6.67E-04
<b>Otud7b</b>	OTU domain containing 7B	8050.34	1130.73	1003.96	-11%	8.64E-03
<b>Ubc</b>	ubiquitin C	2424	10617.89	9582.93	-10%	9.60E-04

**Table 4. The list of genes downregulated in the midline thalamus of *Shox2* KO mice.**



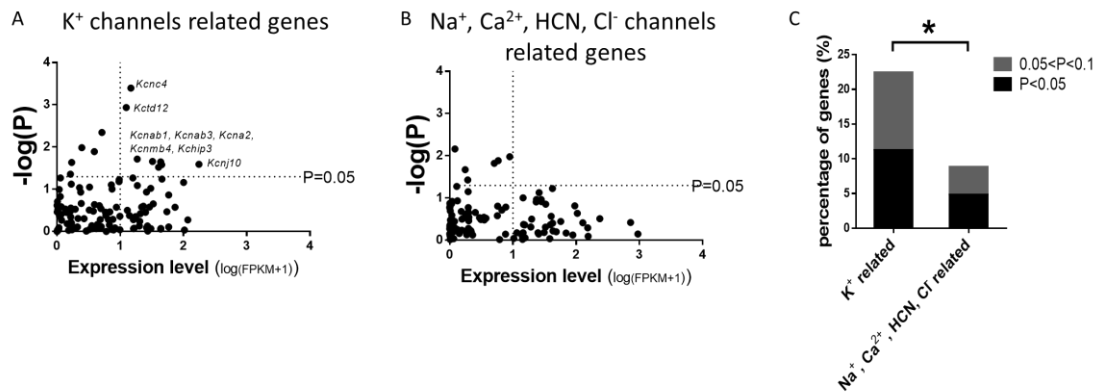


**Figure 3.24. Potassium channels are involved in *Shox2* regulation pathway.** Left figure shows the expression level and Student's t-test P values of all potassium channels and potassium channels related protein such as Kchip protein caused by *Shox2* KO. Right figure shows the expression level and P values of all sodium, calcium, HCN and chloride channels and related proteins including calmodulin caused by *Shox2* KO. The results indicate that potassium channels are largely involved in *Shox2* regulation pathway. The dash line in the figures showed the gene with P value less than 0.05 and with *FPKM*+1 more than 10. All genes in the right top corner of each figure are enriched expressed and significantly affected by *Shox2* KO. The results indicated potassium channels (A) are highly regulated by *Shox2* compared to other ion channels (B) ( $\chi^2$  test,  $\chi^2=8.03$ ,  $P=0.02$ ).

## Chapter IV: DISCUSSION

### 4.1 Summary of results

In this dissertation, I first described the expression pattern of *Shox2* in the forebrain of young adult mouse. *Shox2* expression is strictly limited to the whole thalamus among the forebrain of young adult mouse. With Cre reporter mouse line in which LacZ expression indicating cells that had expressed *Shox2* at some point during development, we found that *Shox2* expression expanded to epithalamus and some midbrain regions such as SC during development, but not to other forebrain regions including prethalamus, cortex, hippocampus, amygdala, hypothalamus, or subcortical nuclei in the forebrain, such as striatum and basal ganglia. Staining results indicated that *Shox2* is only expressed in the neurons that are labeled by NeuN staining (Mullen, Buck, & Smith, 1992) in the thalamus and *Shox2* did not express in glia cells that were labeled by GFAP (Eng, 1985).

To test the role of *Shox2* in thalamus-related behaviors, we established tamoxifen-inducible CreERT-loxP system to knock out *Shox2* in young adult mice. *Shox2* mRNA levels were decreased by more than 60% in *Shox2* KO

mice (Figure 3.8 left) and the body weights of *Shox2* KO mice were significantly decreased compared to CR mice (Figure 3.8 right). We can not exclude peripheral reasons, such as heart-related diseases, for body weight change in *Shox2* KO mice. We tested mice behavior in open field test, paw sensation test (Figure 3.9), novel object recognition test (Figure 3.10), forced swim test and tail suspension test (Figure 3.11). Our results indicated that the total activity in open field was significantly decreased in *Shox2* KO mice (Figure 3.9). This is consistent with a previous finding that *Shox2*-inducible KO in En2-CreERT2 mouse line showed reduced total activity in open field task (Rosin, McAllister, et al., 2015). En2-CreERT2 is dominantly expressed in the cerebellum, and the cerebellar development defects induced by cerebellum *Shox2* KO were believed to underlie the activity deficit. However, several studies have shown that En2 is also expressed in the thalamus (Brielmaier et al., 2012; Tripathi et al., 2009). Moreover, *Shox2* is not expressed in the cerebellum of adult mouse according to our X-gal staining results (Figure 3.1). Therefore, the activity deficit in our *Shox2*-inducible KO mice is likely not directly related to cerebellum but the consequence of thalamus function impairment. In addition, our open field test results indicated that the anxiety levels of *Shox2* KO mice were significantly

decreased. We saw no significant differences in subsequent force swim test and tail suspension between CR and *Shox2* KO mice. Paw sensation test result showed a longer latency for *Shox2* KO to react to the sticky tapes on their paws, suggesting a deficit of somatosensory or sensorimotor functions, the main relay function of the thalamus. Novel object recognition test results showed *Shox2* KO mice spent significantly less percentage of time around the novel object compared to CR mice, suggesting a deficit of learning and memory functions, the main cognitive function of the thalamus. In total, our behavioral experiments indicated that *Shox2* inducible KO in adult mice impaired thalamus-related sensory, motor and cognitive functions.

To further investigate the cellular and molecular mechanisms underlying the regulation of thalamus function by *Shox2*, we used electrophysiological approaches to test the physiological properties of PVA neurons in young adult mice. Our cell-attached patch-clamp recording and whole-cell patch-clamp recording revealed that the percentage of PVA neurons with spontaneous action potential decreased in *Shox2* KO mice (Figure 3.12). In addition, small depolarizing current injections (10pA/20pA) caused more spikes in PVA neurons from CR mice compared to *Shox2* KO mice, both at resting potential

of each neuron or at a holding potential of -70mV (Figure 3.13). This is possibly related to the decreased membrane resistance in KO neurons in Table 2. Big hyperpolarizing current injections (-50pA/-100pA/-150pA) at a holding potential of -70mV induced rebounded Na<sup>+</sup> spikes followed by Ca<sup>2+</sup> spikes (C. Zhang et al., 2009) in PVA neurons from both CR and *Shox2* KO mice (Figure 3.14). The latency to the peak of Ca<sup>2+</sup> spike is longer in *Shox2* KO mice, suggesting a slower rebound slope, which is highly related to T-type calcium and HCN current (Perez-Reyes, 2003; Putrenko & Schwarz, 2011). In addition, our data showed that the areas under spike traces at -70mV are larger in *Shox2* KO neurons. Following investigation revealed a prolonged decay time (Table 2), suggesting that a potassium channels-related regulation is involved in *Shox2* KO.

Besides the physiological properties of PVA neurons, we used TUNEL staining to investigate cell death in midline thalamus of tamoxifen-injected *Gbx2*<sup>CreERT/+</sup>, *Shox2*<sup>ff</sup> mice (KO) and their littermates control mice (CR). *Gbx2* is specifically expressed in the midline thalamus, such as PVT (Figure 3.15), but not VB, therefore tamoxifen injection induced *Shox2* KO in PVT but not in VB nucleus. Therefore, the VB served as an internal control. Our results showed

increased TUNEL staining in the PVT of KO mice but not in the VB (Figure 3.15). These results suggest that the *Shox2* KO induced region-specific cell deaths, which is consistent with the previous studies showing *Shox2* KO induced cell apoptosis during development in both heart and brain (Rosin, Kurrasch, et al., 2015; Rosin, McAllister, et al., 2015; Sun et al., 2015). In adult mouse, neuron death occurs during pathological conditions such as neurodegenerative diseases (Mattson, 2000) and ischemic brain injury (Cao et al., 2002). We investigated cell apoptosis related gene expression and found a decreased trend in an anti-apoptotic gene Bcl-2, which might contribute to increased cell apoptosis in the PVT of *Shox2* KO mice (Figure 3.20). The increased cell death induced by *Shox2*-inducible KO in adult PVT of the thalamus suggested a possible role of *Shox2* in pro-survival or anti-apoptosis in young adult stage.

The change in physiological properties and cell survival in PVA neurons of *Shox2* KO mice, combined with previous pacemaker cells studies in heart, suggest that *Shox2* KO affected T-type calcium current and HCN current. To investigate the change of specific currents in *Shox2* KO neurons, we isolated T-type calcium current and found that the current density was significantly decreased, and the activation time was significantly delayed in PVA neurons of

*Shox2* KO mice (Figure 3.16). The decreased activation time constant but non-affected inactivation time constant suggested the change is not caused by membrane resistance-capacity (RC) circuit property change but because of some intrinsic property changes in T-type calcium channels. The study of activation and inactivation curve of T-type calcium current showed that the area of window current in PVA neurons of CR mice was significantly larger, especially at a voltage of -60mV~-70mV (Figure 3.17). In addition, the current density of isolated HCN current was significantly decreased in PVA neurons of *Shox2* KO mice (Figure 3.18). The impairment of T-type calcium current and HCN currents in PVA neurons of *Shox2* KO mice suggests T-type calcium and HCN currents are under regulation of *Shox2* and mediate *Shox2* KO-induced impairment in thalamic neurons' physiological properties, thalamic cell survival and thalamus-related behaviors.

To investigate the underlying mechanism of changes of T-type calcium current and HCN current, we further used RT-qPCR and Westernblot experiments to test the mRNA and protein levels of T-type calcium genes and HCN genes. Our results showed that *Cacna1g* was the dominate T-type calcium gene in the thalamus. The mRNA level and protein product  $Ca_v3.1$  was

downregulated in the thalamus of *Shox2* KO mice (Figure 3.19 and Figure 3.21). *Hcn2* and *Hcn4* were the dominant HCN genes in the thalamus. The mRNA levels and protein products of *Hcn2* and *Hcn4* genes were downregulated in the thalamus of *Shox2* KO mice (Figure 3.19 and Figure 3.21). Our results suggested thalamus enriched  $Ca_v3.1$ , HCN2 and HCN4 were under regulation of *Shox2* and mediated *Shox2* KO-induced impairment in T-type calcium current and HCN current.

Our mRNA sequencing results further showed *Shox2*-inducible KO in mouse with  $Gbx2^{CreERT}$  affected a series of gene expression in the midline thalamus. DEGs study screened out 17 upregulated and 18 downregulated genes induced by *Shox2* KO. Especially, GO study revealed enriched genes in terms of neuron projections, extracellular matrix, neuron projection development, cell death and response to stimulus, suggesting the *Shox2* is implicated in cell survival and differentiation in response to stimulus and signaling (detailed information shown in Figure 3.22, Table 3 and Table 4). In addition, our results showed that thalamus-specific enriched genes are highly regulated by *Shox2* KO (Figure 3.23). These results suggested *Shox2* is essential in maintenance of thalamic neurons gene expression profile. Besides,



our analysis showed that K<sup>+</sup> channels related genes are more regulated by *Shox2* KO compared to genes related to other channels including Na<sup>+</sup>, Ca<sup>2+</sup> and Cl<sup>-</sup> channels (Figure 3.24).

#### **4.2 *Shox2* KO impairs thalamus-related functions and thalamic physiological properties in young adult mice.**

Our results showed that *Shox2* is specifically expressed in the thalamic neurons and *Shox2* KO impairs thalamic-related behavior functions, thalamic neurons physiological properties and thalamic cell survival. The following study indicated that Cav3.1-mediated T-type calcium and HCN2/HCN4-mediated HCN current are under regulation of *Shox2* and this regulation is the underlying mechanism for thalamic neurons properties and function impairment in young adult *Shox2* KO mice.

The cellular physiological properties and cell survival studies suggested two possible underlying mechanism for behavioral changes in *Shox2* KO mice. The first possibility is that the thalamus-related behavior deficits are a consequence that *Shox2* KO changed the physiological properties of thalamic neurons such as reduced cell excitability. The physiological properties of

thalamic neurons determine thalamus functions, thereby the *Shox2* KO-induced cell excitability decrease resulted in thalamus-related behavior impairments. The second possibility is that the behavioral deficits resulted from *Shox2* KO-induced cell death in the thalamus. The physiological properties deficits resulted from a lack of supporting glia in *Shox2* KO mice or recording from unhealthy neurons. However, we cannot rule out that *Shox2* also plays a role in other important cellular functions of the thalamus. *Shox2* KO may also affect other vital functions of the thalamus, such as impairment of sleep function, and the observed functional effects are a direct consequence of sleep impairments. Further research is necessary to determine the specific roles of *Shox2* in thalamus function.

Our recordings of spontaneous action potentials and depolarization-evoked action potentials showed that action potentials are mostly fired in a tonic way. Although the depolarization or hyperpolarization -induced action potentials at -70mV showed  $\text{Ca}^{2+}$ -like spikes which usually mediated burst spikes, but no stable burst firing pattern was founded. This is consistent with a previous study indicating the lack of stable burst action potential pattern both in the spontaneous and evoked conditions in PVA of the thalamus due to limited T-

type calcium current and HCN current activity at daytime (Kolaj et al., 2012). In the future, nighttime recording may be conducted for the role of *Shox2* in burst spikes pattern and sleep regulation.

Our results suggested that the decreased mRNA level (Figure 3.19) and protein level of  $Ca_v3.1$  (Figure 3.21) underlie the decreased T-type calcium current density after *Shox2* KO (Figure 3.17). However, the reason for the change in activation curve and delayed activation time was not determined. It is not likely caused by the change of  $Ca_v3.1/Ca_v3.2$  ratio since the  $Ca_v3.2$  expression was still very low and not significantly increased after *Shox2* KO (Figure 3.19). In addition, the T-type window current is dramatically larger in PVA neurons of CR mice a voltage of  $-60\text{mV}\sim-70\text{mV}$  (Figure 3.17), a relative hyperpolarized range (compared to our resting membrane potential shown in Table 2) at which thalamic neurons are more likely to fire action potentials in burst patterns. The results suggested that *Shox2* KO-induced T-type calcium window current change may have big effects at relatively hyperpolarized potentials and affect burst action potential patterns. The future nighttime recording will be applied to study the importance of T-type calcium current in burst spikes pattern.

Our RT-qPCR results indicated that Cav3.1 gene is the dominate T-type calcium channels in the thalamus, and HCN2 and HCN4 are the dominate T-type calcium channels as reported before (Aguado et al., 2016; Cheong & Shin, 2013; Ludwig et al., 2003; Notomi & Shigemoto, 2004) (Figure 3.19). All subtypes of HCN channels mediate a similar hyperpolarization-activated non-selective-ion-mediated depolarization current and all of them are involved in the brain rhythms and oscillation. However, the difference in their physiological properties determines their different role in physiological functions. HCN1 channels are the most highly-expressed HCN channels in the brain with fast activation time depolarized activation threshold; thus they participate more in responses to integrate synaptic singles (Magee, 2000), and suppress low-frequency (< 4Hz) membrane activity (Nolan, Dudman, Dodson, & Santoro, 2007). However, HCN2 and HCN4 are relatively less studied in the brain because of their relatively lower expression, but well-studied as the main HCN channels in the SAN of the heart. HCN2 and HCN4 channels are more slowly activated compared to HCN1, and they have a more hyperpolarized threshold, thus they are activated at hyperpolarized membrane potentials. At hyperpolarized potentials, HCN2 and HCN4 caused a slower but longer HCN

current because of slower kinetics. More importantly, the inactivation of T-type calcium channels is removed at hyperpolarization and ready to cause a salient calcium spike. In this way, the slow HCN2 and HCN4 channels are not activated until the membrane is totally hyperpolarized and contribute to the pace generation in the cells. So HCN2 and HCN4 are important channels in low-frequency (<4Hz) automaticity than HCN1. HCN2 and HCN4 channels were shown to be associated with each other and co-assemble and form functional heteromeric channels in SAN node of hearts and rat thalamus (Much et al., 2003; Whitaker, Angoli, Nazzari, Shigemoto, & Accili, 2007; Q. Zhang, Huang, Lin, & Yu, 2009). Our results showing both HCN2 and HCN4 were highly expressed in the thalamus and decreased of HCN2 and HCN4 expression by *Shox2*-inducible KO confirmed the associated expression between HCN2 and HCN4. This suggests the possible mechanism that *Shox2* works as an upstream gene controlling both the expression of HCN2 and HCN4. Our results confirmed the high mRNA expression of  $Ca_v3.1$ , HCN2 and HCN4 channels and indicated *Shox2* KO decreased the expression of the proteins for these three channels. This expression pattern is very different from other parts of forebrains but very similar with nodal-like pacemaker cells in hearts (Cribbs,

2010; Ludwig et al., 2003; Ludwig et al., 1999; Mangoni et al., 2006; Whitaker et al., 2007), suggesting the expression of these channels in the thalamus and SA nodes in hearts are under a similar regulation pathway by *Shox2*.

### **4.3. The expression of *Shox2* in thalamic neurons provided new information for brain development study.**

*Shox2* has been reported to be expressed in the facial nucleus in the hindbrain (Rosin, Kurrasch, et al., 2015), cerebellum (Rosin, McAllister, et al., 2015), spinal cord (Dougherty et al., 2013), and dorsal root ganglia (DRG) (Abdo et al., 2011) in the nervous system. Our staining results indicated the expression of *Shox2* in the forebrain, the region involved in high-level cognitive functions. The restricted expression of *Shox2* to the whole thalamus but not in any other forebrain regions in adult mouse makes *Shox2* an effective specific marker for the thalamus. The *Shox2* promoter and our *Shox2*<sup>Cre</sup> mouse line provide a good tool for thalamus functional studies because of better specificity in neurons of the whole thalamus, while the widely used ‘thalamus-specific’ *Gbx2* promoter is only expressed in the medial part of thalamus in adult mouse (Figure 3.15 A).

Our expression results are consistent with and provide more evidence for the diencephalon regionalization proposed by Berquist in 1932 (Ishikawa et al., 2007). In early pre-natal development, the brain of vertebrates consists of three main parts: prosencephalon which develops into forebrain, mesencephalon which develops into midbrain, and rhombencephalon which develops into hindbrain (Ericson et al., 1995). Further development and differentiation of prosencephalon into telencephalon and diencephalon has been explained by different models. The Berquist (1932) model is revised continuously according to new discoveries, proposing that the telencephalon and hypothalamus are the dorsal and ventral derivatives of the secondary prosencephalon, respectively. The remaining caudal part is diencephalon which divides into three parts: prethalamus (p3), thalamus/epithalamus (p2) and pretectum (p1) (Wilson & Houart, 2004).

The main evidence for this model is from the expression of homeobox genes, which are a family of genes with the same homeobox sequence to determine the formation and position of many body structures, including development of brain structures (P. Holland, 1992; P. W. Holland, 2013). For example, *Gbx2* is the typical homeobox gene specifically expressed in the p2

of the diencephalon from the embryonic stage and is found to be important for the thalamus formation, thalamic nuclei differentiation and thalamocortical projection (Chatterjee et al., 2012; K. Li, Zhang, & Li, 2012). Paired box gene 6 (Pax6) is specifically expressed in the p3 and p1 of the diencephalon, and embryonic mice with Pax6 mutation have undeveloped p1, less-defined boundaries of p1/p2 and p2/p3, and other development deficits in the diencephalon (Grindley, Hargett, Hill, Ross, & Hogan, 1997; Mastick, Davis, Andrew, & Easter, 1997). Distal-less homeobox 2 (Dlx2) expresses in the p1 of the diencephalon and determines the fate of GABAergic neurons in the prethalamus. Deletion of Dlx2 in p1 alters the prethalamus formation, and forced expression of Dlx2 in p2 switches glutamatergic thalamic neurons into GABAergic neurons like prethalamus (Sellers, Zyka, Lumsden, & Delogu, 2014), suggesting Dlx2 has a role in interneuron fate determination. These examples demonstrate the importance of homeobox genes in the diencephalon development, and regionalization and expression of these homeobox genes demonstrate the sub-region identification in the diencephalon in turn. Our results indicate that *Shox2* is expressed in the thalamus and epithalamus, the p2 region of diencephalon, and limited to the ventral part of p2, specifically the



thalamus, in adult stage. Especially, the distinct border shown by *Shox2* expression between the thalamus and RT supported that prethalamus, including RT, develops from a distinct sub-region (p1) within the thalamus. The expression of *Shox2* in habenula decreases during development, and suggests epithalamus including, habenula, originates from the same sub-region with the thalamus (p2). The disappearance of *Shox2* in the epithalamus during development suggests *Shox2* may be under regulation of some dorsoventral signals, such as sonic hedgehog (SHH), during development. Our data showing *Shox2* expression in neurons has variable ratios in different nuclei, relatively higher in midline thalamus, AV, VB and MGN but lower in AD (Figure 3.5 A C) and LD (Figure 2.1 D), are consistent with dorsoventral axis of thalamus during development (Martinez-Ferre & Martinez, 2012). This expression pattern suggests the involvement of *Shox2* in dorsoventral-related differentiation of the thalamus.

In the previous studies, *Shox2* has been considered as the typical downstream target of *Arx*, according to mRNA assay study and chromatin immunoprecipitation (ChIP) study (Fulp et al., 2008; Poeta et al., 2013; Shoubridge et al., 2012). *ARX* mutation in human has been found to cause a

series of brain development diseases including infantile spasm, autism, and mental retardation (Olivetti et al., 2014; Sherr, 2003). More interestingly, different types of *ARX* mutation caused different types of brain development diseases, suggesting the phenotypes of *ARX* mutation does not just result from changed expression level of *ARX* but also from impaired functional domains. Studies in mouse have demonstrated that *Arx* is specifically expressed in interneurons including ventral thalamus (Colombo et al., 2004; Poirier et al., 2004; Vogt et al., 2014), and *Shox2* expression level is repressed by *Arx* and is an important indicator of *Arx* function (Colombo et al., 2004; Olivetti et al., 2014). These results suggest that *Shox2* may be important for at least some of the phenotypical effects observed in some of the *ARX*-related disorders. Surprisingly, our results indicated that *Shox2* was not expressed in any neurons of ventral thalamus nor in PV+ inhibitory interneurons. Further research will be critical for understanding the *Arx/Shox2* regulation pathway in early brain development. One possibility is that *Arx*, as a homeobox gene, may be secreted and transferred to neighboring cells. Previous research has found that homeodomains in all homeobox genes contain secretion and internalization sequences which allow homeobox proteins to be secreted and transferred to

neighboring cells (Brunet et al., 2005; Joliot & Prochiantz, 2004). For example, mRNA of the homeobox gene, *Otx2*, is only expressed in a small group of interneurons in LGN and retina, but homeobox protein of *Otx2* exists in interneurons among the visual cortex, LGN and retina (Sugiyama, Prochiantz, & Hensch, 2009). The regulation of *Shox2* by *Arx* may be a consequence that ARX protein is secreted by ventral thalamus and taken up by thalamic neurons, thereby regulating *Shox2* expression in thalamic neurons. Another possibility is ARX protein binds the *Shox2* promoter and totally inhibits *Shox2* expression in ventral thalamus and inhibitory interneurons. In this way, ARX did not regulate *Shox2* expression directly. The regulation of *Shox2* expression detected in *Arx*-mutation mice (Fulp et al., 2008; Olivetti et al., 2014) is not the direct phenotype but may be caused by interrupted ratio of thalamic neurons in the whole brain. *Arx* mutation impaired brain development and morphology including thalamus development (Colombo et al., 2007; Kitamura et al., 2002) and the results of mRNA study showed that *Shox2* is repressed by *Arx*. More research is needed in the future for the possible mechanisms.

The NeuN co-expression result indicated that *Shox2* is only expressed in neurons (Figure 3.5). It suggests there are two or more sources or types of

neurons in the thalamus. It has been proposed before that thalamus of vertebrate, especially primate, consists of calbindin-immunoreactive 'matrix' neurons which project into superficial layers or cortex over wide areas and PV-immunoreactive 'core' neurons which project into layer IV of cortex in an area-specific manner (E. G. Jones, 1998, 2001). Our results (Figure 3.3), are consistent with previous studies that showed the mouse thalamus lacks PV-immuno-reactive neurons (Arcelli et al., 1997; Bodor et al., 2008). However, there still is the fact that multiple types of neurons with different projection profiles exist in rodents thalamus (Theyel, Lee, & Sherman, 2010). Thus, calbindin/PV system may not be the essential marker for the different types of neurons in rodents' thalamus. Our finding that *Shox2* is expressed in a portion of thalamic neurons in a nucleus-specific manner, combined with the role of *Shox2* as a member of homeobox genes which have been found to be important in thalamocortical projections (Chatterjee et al., 2012), suggests that *Shox2* might determine the thalamic generation and differentiation. Together, these results suggest that *Shox2* is a possible marker to label an important type of neurons. The further study will be applied for the specific physiological role of *Shox2* expressing neurons.

In this dissertation, the study of *Shox2* expression with *Shox2<sup>cre</sup>* or *Shox2<sup>LacZ</sup>* mice only labeled the neurons with *Shox2* mRNA expression. But *Shox2* protein may be secreted and taken up by all thalamic neurons and even glia. GFAP co-expression result indicated that the limited expression level of GFAP in the thalamus and confirmed that *Shox2* was not expressed in the GFAP positive glia (Figure 3.6 3.7). The negative relationship between *Shox2* and GFAP and lack of GFAP staining in the thalamus is interesting and might be studied in the future.

#### **4.4. *Shox2* is essential to maintain the thalamic neurons physiological properties and functions.**

Our mRNA sequencing results indicated enriched genes found in GO terms of neuron projection, extracellular matrix, neuron projection development and cell death. Genes in these terms are related to the thalamic neurons' physiological properties and survival. Especially, enriched genes in terms of neuron projection development suggested a possible activation of development related process, which has been demonstrated to be related to neurodegenerative diseases in central nervous system (Lull & Block, 2010;

Papageorgiou, Fetani, Lewen, Heinemann, & Kann, 2015; Pitter et al., 2014).

It provided another possibility to the effects of cell death we detected in *Shox2* KO mice. In addition, *Shox2* is involved in the regulation of genes specifically enriched in the thalamus, which represented thalamic identity and specific properties. Our results suggest a general transcriptome change related to the maintenance of thalamic neurons identity and survival.

The reason and importance of the involvement of potassium channels under *Shox2* regulation needs to be determined in the future. Previous studies have shown that traumatic brain injury or stroke increased potassium channels expression, which is considered as a protective regulation because of increased potassium channel function usually leads to decreased cell excitability (Bierbower, Choveau, Lechleiter, & Shapiro, 2015; Jiang, Huang, Lin, Gao, & Fei, 2013; Lei, Deng, Li, & Xu, 2012). Accordingly, the general regulation of potassium channels may be a protective process after *Shox2* KO, especially the increase of high-level inward rectifying channels, *Kcnj10*. Regulation of this channel may underlie the decreased input resistance and the decreased spontaneous and evoked action potential frequency recorded in our electrophysiological experiments.

The previous study from cardiac tissue demonstrated that *Shox2* is important for the fate determination and differentiation of pacemaker cells in hearts and pulmonary vein because conditional KO of *Shox2* impaired the pacemaker-like action potentials in nodal-like cells. However, the expression of *Shox2* in SAN of the heart continues into adulthood when cells in SAN always have pace-maker properties, but is suppressed in pulmonary vein and coronary sinus to the adult when cells have lost their automaticity and pacemaker properties during development (Kofler et al., 2017; J. Wang et al., 2010). It suggests a role for *Shox2* in maintenance of pacemaker properties up to adulthood in addition to the involvement of pacemaker cells differentiation in embryonic stage. In this study, we inducibly knocked-out *Shox2* in adult mouse by tamoxifen injection and confirmed the role of *Shox2* in maintenance of pacemaker-related physiological properties in the young adult thalamus. With the inducible KO method, the embryonic lethality is avoided. These experiments revealed that the role of *Shox2* in thalamic neurons identity and survival in young adult stage.

Overall, we made several important observations. First, we found *Shox2* is specifically expressed in the thalamic neurons of young adult mouse with

outstanding high-level expression of Cav3.1, HCN2 and HCN4 channels. The co-expression pattern of *Shox2* with Cav3.1, HCN2 and HCN4, and the pace-making properties of thalamic neurons suggested *Shox2* determines thalamic neurons pace-making related properties. Besides, our results indicated comprehensive thalamus properties and function deficits in *Shox2*-inducible-KO young adult mice, including thalamus-related behavior deficit, thalamic neurons intrinsic properties change, increased cell death in the thalamus, thalamic pacemaking-related T-type calcium and HCN current and channel expression impairment, and transcriptome change. Combined, all these results suggest *Shox2* is essential to maintain the thalamic neurons physiological properties and functions in young-adult mice.

In addition, some preliminary data showing that *Shox2* in the thalamus may be downregulated by aging or pilocarpine-induced seizure (preliminary data not shown). The abnormal *Shox2* expression may be related to changes in thalamic neuron properties and neurodegeneration under aging or other pathological conditions. More importantly, the *Shox2* studies in young adult mouse provided a possible way to manipulate thalamic neurons physiological properties and survival, and thus provided a better possibility of medical interference for



thalamus-related diseases including epilepsy, autism and schizophrenia and cognitive deficits caused by *Shox2* insufficient syndromes such as Turner Syndromes.

## Reference:

- Abbas, S. Y., Ying, S. W., & Goldstein, P. A. (2006). Compartmental distribution of hyperpolarization-activated cyclic-nucleotide-gated channel 2 and hyperpolarization-activated cyclic-nucleotide-gated channel 4 in thalamic reticular and thalamocortical relay neurons. *Neuroscience*, *141*(4), 1811-1825. doi: 10.1016/j.neuroscience.2006.05.034
- Abdo, H., Li, L., Lallemand, F., Bachy, I., Xu, X. J., Rice, F. L., & Ernfors, P. (2011). Dependence on the transcription factor Shox2 for specification of sensory neurons conveying discriminative touch. *Eur J Neurosci*, *34*(10), 1529-1541. doi: 10.1111/j.1460-9568.2011.07883.x
- Abe-Higuchi, N., Uchida, S., Yamagata, H., Higuchi, F., Hobara, T., Hara, K., . . . Watanabe, Y. (2016). Hippocampal Sirtuin 1 Signaling Mediates Depression-like Behavior. *Biol Psychiatry*, *80*(11), 815-826. doi: 10.1016/j.biopsych.2016.01.009
- Aguado, C., Garcia-Madrona, S., Gil-Minguez, M., & Lujan, R. (2016). Ontogenic Changes and Differential Localization of T-type Ca(2+) Channel Subunits Cav3.1 and Cav3.2 in Mouse Hippocampus and Cerebellum. *Front Neuroanat*, *10*, 83. doi: 10.3389/fnana.2016.00083
- Allen, A. E., Procyk, C. A., Howarth, M., Walmsley, L., & Brown, T. M. (2016). Visual input to the mouse lateral posterior and posterior thalamic nuclei: photoreceptive origins and retinotopic order. *J Physiol*, *594*(7), 1911-1929. doi: 10.1113/JP271707
- Altomare, C., Terragni, B., Brioschi, C., Milanese, R., Pagliuca, C., Viscomi, C., . . . DiFrancesco, D. (2003). Heteromeric HCN1-HCN4 channels: a comparison with native pacemaker channels from the rabbit sinoatrial node. *J Physiol*, *549*(Pt 2), 347-359. doi: 10.1113/jphysiol.2002.027698
- Antunes, M., & Biala, G. (2012). The novel object recognition memory: neurobiology, test procedure, and its modifications. *Cogn Process*, *13*(2), 93-110. doi: 10.1007/s10339-011-0430-z
- Arakawa, H., Suzuki, A., Zhao, S., Tsytsarev, V., Lo, F. S., Hayashi, Y., . . . Erzurumlu, R. S. (2014). Thalamic NMDA receptor function is necessary for patterning of the thalamocortical somatosensory map and for sensorimotor behaviors. *J Neurosci*, *34*(36), 12001-12014. doi: 10.1523/JNEUROSCI.1663-14.2014
- Arcelli, P., Frassoni, C., Regondi, M. C., De Biasi, S., & Spreafico, R. (1997). GABAergic neurons in mammalian thalamus: a marker of thalamic complexity? *Brain Res Bull*, *42*(1), 27-37.
- Avanzini, G., de Curtis, M., Marescaux, C., Panzica, F., Spreafico, R., & Vergnes, M. (1992). Role of the thalamic reticular nucleus in the generation of rhythmic thalamo-cortical activities subserving spike and waves. *J Neural Transm Suppl*, *35*, 85-95.
- Aza-Carmona, M., Barca-Tierno, V., Hisado-Oliva, A., Belinchon, A., Gorbenko-del Blanco, D., Rodriguez, J. I., . . . Heath, K. E. (2014). NPPB and ACAN, two novel SHOX2 transcription

- targets implicated in skeletal development. *PLoS One*, *9*(1), e83104. doi: 10.1371/journal.pone.0083104
- Bai, W., & Zhang, X. (2016). Nucleus or cytoplasm? The mysterious case of SIRT1's subcellular localization. *Cell Cycle*, *15*(24), 3337-3338. doi: 10.1080/15384101.2016.1237170
- Barca-Tierno, V., Aza-Carmona, M., Barroso, E., Heine-Suner, D., Azmanov, D., Rosell, J., . . . Heath, K. E. (2011). Identification of a Gypsy SHOX mutation (p.A170P) in Leri-Weill dyschondrosteosis and Langer mesomelic dysplasia. *Eur J Hum Genet*, *19*(12), 1218-1225. doi: 10.1038/ejhg.2011.128
- Basso, M. A., Uhlrich, D., & Bickford, M. E. (2005). Cortical function: a view from the thalamus. *Neuron*, *45*(4), 485-488.
- Belin, V., Cusin, V., Viot, G., Girlich, D., Toutain, A., Moncla, A., . . . Cormier-Daire, V. (1998). SHOX mutations in dyschondrosteosis (Leri-Weill syndrome). *Nat Genet*, *19*(1), 67-69. doi: 10.1038/ng0198-67
- Bhatnagar, S., Huber, R., Nowak, N., & Trotter, P. (2002). Lesions of the posterior paraventricular thalamus block habituation of hypothalamic-pituitary-adrenal responses to repeated restraint. *J Neuroendocrinol*, *14*(5), 403-410.
- Bhattacharjee, A., Whitehurst, R. M., Jr., Zhang, M., Wang, L., & Li, M. (1997). T-type calcium channels facilitate insulin secretion by enhancing general excitability in the insulin-secreting beta-cell line, INS-1. *Endocrinology*, *138*(9), 3735-3740. doi: 10.1210/endo.138.9.5390
- Bierbower, S. M., Choveau, F. S., Lechleiter, J. D., & Shapiro, M. S. (2015). Augmentation of M-type (KCNQ) potassium channels as a novel strategy to reduce stroke-induced brain injury. *J Neurosci*, *35*(5), 2101-2111. doi: 10.1523/JNEUROSCI.3805-14.2015
- Bobick, B. E., & Cobb, J. (2012). Shox2 regulates progression through chondrogenesis in the mouse proximal limb. *J Cell Sci*, *125*(Pt 24), 6071-6083. doi: 10.1242/jcs.111997
- Bodor, A. L., Giber, K., Rovo, Z., Ulbert, I., & Acsady, L. (2008). Structural correlates of efficient GABAergic transmission in the basal ganglia-thalamus pathway. *J Neurosci*, *28*(12), 3090-3102. doi: 10.1523/JNEUROSCI.5266-07.2008
- Bouet, V., Boulouard, M., Toutain, J., Divoux, D., Bernaudin, M., Schumann-Bard, P., & Freret, T. (2009). The adhesive removal test: a sensitive method to assess sensorimotor deficits in mice. *Nat Protoc*, *4*(10), 1560-1564. doi: 10.1038/nprot.2009.125
- Boyault, C., Sadoul, K., Pabion, M., & Khochbin, S. (2007). HDAC6, at the crossroads between cytoskeleton and cell signaling by acetylation and ubiquitination. *Oncogene*, *26*(37), 5468-5476. doi: 10.1038/sj.onc.1210614
- Brenner, R., Chen, Q. H., Vilaythong, A., Toney, G. M., Noebels, J. L., & Aldrich, R. W. (2005). BK channel beta4 subunit reduces dentate gyrus excitability and protects against temporal

- lobe seizures. *Nat Neurosci*, 8(12), 1752-1759. doi: 10.1038/nn1573
- Brielmaier, J., Matteson, P. G., Silverman, J. L., Senerth, J. M., Kelly, S., Genestine, M., . . . Crawley, J. N. (2012). Autism-relevant social abnormalities and cognitive deficits in engrailed-2 knockout mice. *PLoS One*, 7(7), e40914. doi: 10.1371/journal.pone.0040914
- Brunet, I., Weinl, C., Piper, M., Trembleau, A., Volovitch, M., Harris, W., . . . Holt, C. (2005). The transcription factor Engrailed-2 guides retinal axons. *Nature*, 438(7064), 94-98. doi: 10.1038/nature04110
- Butler, P. L., Staruschenko, A., & Snyder, P. M. (2015). Acetylation stimulates the epithelial sodium channel by reducing its ubiquitination and degradation. *J Biol Chem*, 290(20), 12497-12503. doi: 10.1074/jbc.M114.635540
- Can, A., Dao, D. T., Arad, M., Terrillion, C. E., Piantadosi, S. C., & Gould, T. D. (2012). The mouse forced swim test. *J Vis Exp*(59), e3638. doi: 10.3791/3638
- Can, A., Dao, D. T., Terrillion, C. E., Piantadosi, S. C., Bhat, S., & Gould, T. D. (2012). The tail suspension test. *J Vis Exp*(59), e3769. doi: 10.3791/3769
- Canto, C., Menzies, K. J., & Auwerx, J. (2015). NAD(+) Metabolism and the Control of Energy Homeostasis: A Balancing Act between Mitochondria and the Nucleus. *Cell Metab*, 22(1), 31-53. doi: 10.1016/j.cmet.2015.05.023
- Cao, G., Pei, W., Ge, H., Liang, Q., Luo, Y., Sharp, F. R., . . . Chen, J. (2002). In Vivo Delivery of a Bcl-xL Fusion Protein Containing the TAT Protein Transduction Domain Protects against Ischemic Brain Injury and Neuronal Apoptosis. *J Neurosci*, 22(13), 5423-5431. doi: 20026550
- Cardoso-Cruz, H., Sousa, M., Vieira, J. B., Lima, D., & Galhardo, V. (2013). Prefrontal cortex and mediodorsal thalamus reduced connectivity is associated with spatial working memory impairment in rats with inflammatory pain. *Pain*, 154(11), 2397-2406. doi: 10.1016/j.pain.2013.07.020
- Caron, C., Boyault, C., & Khochbin, S. (2005). Regulatory cross-talk between lysine acetylation and ubiquitination: role in the control of protein stability. *Bioessays*, 27(4), 408-415. doi: 10.1002/bies.20210
- Catarino, T., Ribeiro, L., Santos, S. D., & Carvalho, A. L. (2013). Regulation of synapse composition by protein acetylation: the role of acetylated cortactin. *J Cell Sci*, 126(Pt 1), 149-162. doi: 10.1242/jcs.110742
- Cechetto, D. F., & Saper, C. B. (1987). Evidence for a viscerotopic sensory representation in the cortex and thalamus in the rat. *J Comp Neurol*, 262(1), 27-45. doi: 10.1002/cne.902620104
- Chatterjee, M., Li, K., Chen, L., Maisano, X., Guo, Q., Gan, L., & Li, J. Y. (2012). Gbx2 regulates thalamocortical axon guidance by modifying the LIM and Robo codes. *Development*, 139(24), 4633-4643. doi: 10.1242/dev.086991
- Chen, Y., Parker, W. D., & Wang, K. (2014). The role of T-type calcium channel genes in absence

- seizures. *Front Neurol*, 5, 45. doi: 10.3389/fneur.2014.00045
- Cheong, E., & Shin, H. S. (2013). T-type Ca<sup>2+</sup> channels in normal and abnormal brain functions. *Physiol Rev*, 93(3), 961-992. doi: 10.1152/physrev.00010.2012
- Choi, D. L., Davis, J. F., Magrisso, I. J., Fitzgerald, M. E., Lipton, J. W., & Benoit, S. C. (2012). Orexin signaling in the paraventricular thalamic nucleus modulates mesolimbic dopamine and hedonic feeding in the rat. *Neuroscience*, 210, 243-248. doi: 10.1016/j.neuroscience.2012.02.036
- Cholvin, T., Loureiro, M., Cassel, R., Cosquer, B., Geiger, K., De Sa Nogueira, D., . . . Cassel, J. C. (2013). The ventral midline thalamus contributes to strategy shifting in a memory task requiring both prefrontal cortical and hippocampal functions. *J Neurosci*, 33(20), 8772-8783. doi: 10.1523/JNEUROSCI.0771-13.2013
- Clark, B. J., & Taube, J. S. (2012). Vestibular and attractor network basis of the head direction cell signal in subcortical circuits. *Front Neural Circuits*, 6, 7. doi: 10.3389/fncir.2012.00007
- Cobb, J., Dierich, A., Huss-Garcia, Y., & Duboule, D. (2006). A mouse model for human short-stature syndromes identifies Shox2 as an upstream regulator of Runx2 during long-bone development. *Proc Natl Acad Sci U S A*, 103(12), 4511-4515. doi: 10.1073/pnas.0510544103
- Colombo, E., Collombat, P., Colasante, G., Bianchi, M., Long, J., Mansouri, A., . . . Broccoli, V. (2007). Inactivation of Arx, the murine ortholog of the X-linked lissencephaly with ambiguous genitalia gene, leads to severe disorganization of the ventral telencephalon with impaired neuronal migration and differentiation. *J Neurosci*, 27(17), 4786-4798. doi: 10.1523/JNEUROSCI.0417-07.2007
- Colombo, E., Galli, R., Cossu, G., Gecz, J., & Broccoli, V. (2004). Mouse orthologue of ARX, a gene mutated in several X-linked forms of mental retardation and epilepsy, is a marker of adult neural stem cells and forebrain GABAergic neurons. *Dev Dyn*, 231(3), 631-639. doi: 10.1002/dvdy.20164
- Concha, M. L., & Wilson, S. W. (2001). Asymmetry in the epithalamus of vertebrates. *J Anat*, 199(Pt 1-2), 63-84.
- Cribbs, L. (2010). T-type calcium channel expression and function in the diseased heart. *Channels (Austin)*, 4(6), 447-452.
- Cruikshank, S. J., Ahmed, O. J., Stevens, T. R., Patrick, S. L., Gonzalez, A. N., Elmaleh, M., & Connors, B. W. (2012). Thalamic control of layer 1 circuits in prefrontal cortex. *J Neurosci*, 32(49), 17813-17823. doi: 10.1523/JNEUROSCI.3231-12.2012
- Dan, Y., Alonso, J. M., Usrey, W. M., & Reid, R. C. (1998). Coding of visual information by precisely correlated spikes in the lateral geniculate nucleus. *Nat Neurosci*, 1(6), 501-507. doi: 10.1038/2217
- De Baere, E., Speleman, F., Van Roy, N., De Paepe, A., & Messiaen, L. (1998). Assignment of SHOX2

- (alias OG12X and SHOT) to human chromosome bands 3q25-->q26.1 by in situ hybridization. *Cytogenet Cell Genet*, *82*(3-4), 228-229.
- Dougherty, K. J., Zagoraïou, L., Satoh, D., Rozani, I., Doobar, S., Arber, S., . . . Kiehn, O. (2013). Locomotor rhythm generation linked to the output of spinal *shox2* excitatory interneurons. *Neuron*, *80*(4), 920-933. doi: 10.1016/j.neuron.2013.08.015
- Eng, L. F. (1985). Glial fibrillary acidic protein (GFAP): the major protein of glial intermediate filaments in differentiated astrocytes. *J Neuroimmunol*, *8*(4-6), 203-214.
- Engin, E., Smith, K. S., Gao, Y., Nagy, D., Foster, R. A., Tsvetkov, E., . . . Rudolph, U. (2016). Modulation of anxiety and fear via distinct intrahippocampal circuits. *Elife*, *5*, e14120. doi: 10.7554/eLife.14120
- Ericson, J., Muhr, J., Placzek, M., Lints, T., Jessell, T. M., & Edlund, T. (1995). Sonic hedgehog induces the differentiation of ventral forebrain neurons: a common signal for ventral patterning within the neural tube. *Cell*, *81*(5), 747-756.
- Espinoza-Lewis, R. A., Yu, L., He, F., Liu, H., Tang, R., Shi, J., . . . Chen, Y. (2009). *Shox2* is essential for the differentiation of cardiac pacemaker cells by repressing *Nkx2-5*. *Dev Biol*, *327*(2), 376-385. doi: 10.1016/j.ydbio.2008.12.028
- Fabrizio, P., Gattazzo, C., Battistella, L., Wei, M., Cheng, C., McGrew, K., & Longo, V. D. (2005). Sir2 blocks extreme life-span extension. *Cell*, *123*(4), 655-667. doi: 10.1016/j.cell.2005.08.042
- Ferland, C. L., Hawley, W. R., Puckett, R. E., Wineberg, K., Lubin, F. D., Dohanich, G. P., & Schrader, L. A. (2013). Sirtuin activity in dentate gyrus contributes to chronic stress-induced behavior and extracellular signal-regulated protein kinases 1 and 2 cascade changes in the hippocampus. *Biol Psychiatry*, *74*(12), 927-935. doi: 10.1016/j.biopsych.2013.07.029
- Ferland, C. L., & Schrader, L. A. (2011). Regulation of histone acetylation in the hippocampus of chronically stressed rats: a potential role of sirtuins. *Neuroscience*, *174*, 104-114. doi: 10.1016/j.neuroscience.2010.10.077
- Fraschini, F., Mess, B., & Martini, L. (1968). Pineal gland, melatonin and the control of luteinizing hormone secretion. *Endocrinology*, *82*(5), 919-924. doi: 10.1210/endo-82-5-919
- Frints, S. G., Froyen, G., Marynen, P., Willekens, D., Legius, E., & Fryns, J. P. (2002). Re-evaluation of MRX36 family after discovery of an ARX gene mutation reveals mild neurological features of Partington syndrome. *Am J Med Genet*, *112*(4), 427-428. doi: 10.1002/ajmg.10628
- Fulp, C. T., Cho, G., Marsh, E. D., Nasrallah, I. M., Labosky, P. A., & Golden, J. A. (2008). Identification of Arx transcriptional targets in the developing basal forebrain. *Hum Mol Genet*, *17*(23), 3740-3760. doi: 10.1093/hmg/ddn271
- Gervasini, C., Grati, F. R., Lalatta, F., Tabano, S., Gentilin, B., Colapietro, P., . . . Miozzo, M. (2010). SHOX duplications found in some cases with type I Mayer-Rokitansky-Kuster-Hauser syndrome. *Genet Med*, *12*(10), 634-640. doi: 10.1097/GIM.0b013e3181ed6185

- Giordano, G., Foppiani, E., Minuto, F., Marugo, M., & Barreca, T. (1973). [Sleep-wakefulness rhythm of the somatotropin secretion in the man under the influence of alpha-methyl dopa and disulfiram]. *Arch Maragliano Patol Clin*, 29(1), 7-14.
- Glaser, A., Arora, R., Hoffmann, S., Li, L., Gretz, N., Papaioannou, V. E., & Rappold, G. A. (2014). Tbx4 interacts with the short stature homeobox gene Shox2 in limb development. *Dev Dyn*, 243(5), 629-639. doi: 10.1002/dvdy.24104
- Greisas, A., & Zlochiver, S. (2016). Modulation of cardiac pacemaker inter beat intervals by sinoatrial fibroblasts -a numerical study. *Conf Proc IEEE Eng Med Biol Soc*, 2016, 165-168. doi: 10.1109/EMBC.2016.7590666
- Grindley, J. C., Hargett, L. K., Hill, R. E., Ross, A., & Hogan, B. L. (1997). Disruption of PAX6 function in mice homozygous for the Pax6<sup>Sey-1</sup>Neu mutation produces abnormalities in the early development and regionalization of the diencephalon. *Mech Dev*, 64(1-2), 111-126.
- Gronskov, K., Diness, B., Stahlhut, M., Zilmer, M., Tumer, Z., Bisgaard, A. M., & Brondum-Nielsen, K. (2014). Mosaicism for c.431\_454dup in ARX causes a mild Partington syndrome phenotype. *Eur J Med Genet*, 57(6), 284-287. doi: 10.1016/j.ejmg.2014.03.009
- Gu, S., Wei, N., Yu, L., Fei, J., & Chen, Y. (2008). Shox2-deficiency leads to dysplasia and ankylosis of the temporomandibular joint in mice. *Mech Dev*, 125(8), 729-742. doi: 10.1016/j.mod.2008.04.003
- Guerrini, R., Moro, F., Kato, M., Barkovich, A. J., Shiihara, T., McShane, M. A., . . . Dobyns, W. B. (2007). Expansion of the first PolyA tract of ARX causes infantile spasms and status dystonicus. *Neurology*, 69(5), 427-433. doi: 10.1212/01.wnl.0000266594.16202.c1
- Guillery, R. W. (1995). Anatomical evidence concerning the role of the thalamus in corticocortical communication: a brief review. *J Anat*, 187 ( Pt 3), 583-592.
- Gusel'nikova, V. V., & Korzhevskiy, D. E. (2015). NeuN As a Neuronal Nuclear Antigen and Neuron Differentiation Marker. *Acta Naturae*, 7(2), 42-47.
- Haigis, M. C., & Sinclair, D. A. (2010). Mammalian sirtuins: biological insights and disease relevance. *Annu Rev Pathol*, 5, 253-295. doi: 10.1146/annurev.pathol.4.110807.092250
- Hallock, H. L., Wang, A., & Griffin, A. L. (2016). Ventral Midline Thalamus Is Critical for Hippocampal-Prefrontal Synchrony and Spatial Working Memory. *J Neurosci*, 36(32), 8372-8389. doi: 10.1523/JNEUROSCI.0991-16.2016
- Harris, J. J., Jolivet, R., & Attwell, D. (2012). Synaptic energy use and supply. *Neuron*, 75(5), 762-777. doi: 10.1016/j.neuron.2012.08.019
- He, J. H., Cui, Y., Song, M., Yang, Y., Dang, Y. Y., Jiang, T. Z., & Xu, R. X. (2015). Decreased functional connectivity between the mediodorsal thalamus and default mode network in patients with disorders of consciousness. *Acta Neurol Scand*, 131(3), 145-151. doi: 10.1111/ane.12299

- Herculano-Houzel, S., & Lent, R. (2005). Isotropic fractionator: a simple, rapid method for the quantification of total cell and neuron numbers in the brain. *J Neurosci*, *25*(10), 2518-2521. doi: 10.1523/JNEUROSCI.4526-04.2005
- Herrero, M. T., Barcia, C., & Navarro, J. M. (2002). Functional anatomy of thalamus and basal ganglia. *Childs Nerv Syst*, *18*(8), 386-404. doi: 10.1007/s00381-002-0604-1
- Hikosaka, O. (2010). The habenula: from stress evasion to value-based decision-making. *Nat Rev Neurosci*, *11*(7), 503-513. doi: 10.1038/nrn2866
- Hirsch, J. C., Fourment, A., & Marc, M. E. (1983). Sleep-related variations of membrane potential in the lateral geniculate body relay neurons of the cat. *Brain Res*, *259*(2), 308-312.
- Hirschfeldova, K., & Solc, R. (2017). Comparison of SHOX and associated elements duplications distribution between patients (Leri-Weill dyschondrosteosis/idiopathic short stature) and population sample. *Gene*, *627*, 164-168. doi: 10.1016/j.gene.2017.06.034
- Holland, P. (1992). Homeobox genes in vertebrate evolution. *Bioessays*, *14*(4), 267-273. doi: 10.1002/bies.950140412
- Holland, P. W. (2013). Evolution of homeobox genes. *Wiley Interdiscip Rev Dev Biol*, *2*(1), 31-45. doi: 10.1002/wdev.78
- Iftinca, M. C. (2011). Neuronal T-type calcium channels: what's new? Iftinca: T-type channel regulation. *J Med Life*, *4*(2), 126-138.
- Imai, S., Armstrong, C. M., Kaeberlein, M., & Guarente, L. (2000). Transcriptional silencing and longevity protein Sir2 is an NAD-dependent histone deacetylase. *Nature*, *403*(6771), 795-800. doi: 10.1038/35001622
- Imai, S., & Guarente, L. (2010). Ten years of NAD-dependent SIR2 family deacetylases: implications for metabolic diseases. *Trends Pharmacol Sci*, *31*(5), 212-220. doi: 10.1016/j.tips.2010.02.003
- Ionta, V., Liang, W., Kim, E. H., Rafie, R., Giacomello, A., Marban, E., & Cho, H. C. (2015). SHOX2 overexpression favors differentiation of embryonic stem cells into cardiac pacemaker cells, improving biological pacing ability. *Stem Cell Reports*, *4*(1), 129-142. doi: 10.1016/j.stemcr.2014.11.004
- Irle, E., & Markowitsch, H. J. (1982). Connections of the hippocampal formation, mamillary bodies, anterior thalamus and cingulate cortex. A retrograde study using horseradish peroxidase in the cat. *Exp Brain Res*, *47*(1), 79-94.
- Ishii, T. M., Takano, M., & Ohmori, H. (2001). Determinants of activation kinetics in mammalian hyperpolarization-activated cation channels. *J Physiol*, *537*(Pt 1), 93-100.
- Ishikawa, Y., Yamamoto, N., Yoshimoto, M., Yasuda, T., Maruyama, K., Kage, T., . . . Ito, H. (2007). Developmental origin of diencephalic sensory relay nuclei in teleosts. *Brain Behav Evol*, *69*(2), 87-95. doi: 10.1159/000095197



- Jankowski, M. M., Ronnqvist, K. C., Tsanov, M., Vann, S. D., Wright, N. F., Erichsen, J. T., . . . O'Mara, S. M. (2013). The anterior thalamus provides a subcortical circuit supporting memory and spatial navigation. *Front Syst Neurosci*, *7*, 45. doi: 10.3389/fnsys.2013.00045
- Jeong, J. K., Moon, M. H., Bae, B. C., Lee, Y. J., Seol, J. W., Kang, H. S., . . . Park, S. Y. (2012). Autophagy induced by resveratrol prevents human prion protein-mediated neurotoxicity. *Neurosci Res*, *73*(2), 99-105. doi: 10.1016/j.neures.2012.03.005
- Jiang, X., Huang, Y., Lin, W., Gao, D., & Fei, Z. (2013). Protective effects of hydrogen sulfide in a rat model of traumatic brain injury via activation of mitochondrial adenosine triphosphate-sensitive potassium channels and reduction of oxidative stress. *J Surg Res*, *184*(2), e27-35. doi: 10.1016/j.jss.2013.03.067
- Joels, M., Krugers, H., & Karst, H. (2008). Stress-induced changes in hippocampal function. *Prog Brain Res*, *167*, 3-15. doi: 10.1016/S0079-6123(07)67001-0
- Joliot, A., & Prochiantz, A. (2004). Transduction peptides: from technology to physiology. *Nat Cell Biol*, *6*(3), 189-196. doi: 10.1038/ncb0304-189
- Jones, E. G. (1998). Viewpoint: the core and matrix of thalamic organization. *Neuroscience*, *85*(2), 331-345.
- Jones, E. G. (2001). The thalamic matrix and thalamocortical synchrony. *Trends Neurosci*, *24*(10), 595-601.
- Jones, E. G. (2012). *The thalamus*: Springer Science & Business Media.
- Jones, E. G., & Friedman, D. P. (1982). Projection pattern of functional components of thalamic ventrobasal complex on monkey somatosensory cortex. *J Neurophysiol*, *48*(2), 521-544.
- Kaeberlein, M., McVey, M., & Guarente, L. (1999). The SIR2/3/4 complex and SIR2 alone promote longevity in *Saccharomyces cerevisiae* by two different mechanisms. *Genes Dev*, *13*(19), 2570-2580.
- Kakefuda, K., Fujita, Y., Oyagi, A., Hyakkoku, K., Kojima, T., Umemura, K., . . . Hara, H. (2009). Sirtuin 1 overexpression mice show a reference memory deficit, but not neuroprotection. *Biochem Biophys Res Commun*, *387*(4), 784-788. doi: 10.1016/j.bbrc.2009.07.119
- Karst, H., & Joels, M. (2003). Effect of chronic stress on synaptic currents in rat hippocampal dentate gyrus neurons. *J Neurophysiol*, *89*(1), 625-633. doi: 10.1152/jn.00691.2002
- Kato, M., Saitoh, S., Kamei, A., Shiraishi, H., Ueda, Y., Akasaka, M., . . . Hayasaka, K. (2007). A longer polyalanine expansion mutation in the ARX gene causes early infantile epileptic encephalopathy with suppression-burst pattern (Ohtahara syndrome). *Am J Hum Genet*, *81*(2), 361-366. doi: 10.1086/518903
- Kayama, Y., & Koyama, Y. (2003). Control of sleep and wakefulness by brainstem monoaminergic and cholinergic neurons. *Acta Neurochir Suppl*, *87*, 3-6.
- Kheirbek, M. A., Drew, L. J., Burghardt, N. S., Costantini, D. O., Tannenholz, L., Ahmari, S. E., . . . Hen,

- R. (2013). Differential control of learning and anxiety along the dorsoventral axis of the dentate gyrus. *Neuron*, *77*(5), 955-968. doi: 10.1016/j.neuron.2012.12.038
- Kheirbek, M. A., Klemenhagen, K. C., Sahay, A., & Hen, R. (2012). Neurogenesis and generalization: a new approach to stratify and treat anxiety disorders. *Nat Neurosci*, *15*(12), 1613-1620. doi: 10.1038/nn.3262
- Kim, E. Y., Ridgway, L. D., & Dryer, S. E. (2007). Interactions with filamin A stimulate surface expression of large-conductance Ca<sup>2+</sup>-activated K<sup>+</sup> channels in the absence of direct actin binding. *Mol Pharmacol*, *72*(3), 622-630. doi: 10.1124/mol.107.038026
- Kim, S. J., Ao, Z., Warnock, G., & McIntosh, C. H. (2013). Incretin-stimulated interaction between beta-cell Kv1.5 and Kvbeta2 channel proteins involves acetylation/deacetylation by CBP/Sirt1. *Biochem J*, *451*(2), 227-234. doi: 10.1042/BJ20121669
- Kinomura, S., Larsson, J., Gulyas, B., & Roland, P. E. (1996). Activation by attention of the human reticular formation and thalamic intralaminar nuclei. *Science*, *271*(5248), 512-515.
- Kishi, T., Yoshimura, R., Kitajima, T., Okochi, T., Okumura, T., Tsunoka, T., . . . Iwata, N. (2010). SIRT1 gene is associated with major depressive disorder in the Japanese population. *J Affect Disord*, *126*(1-2), 167-173. doi: 10.1016/j.jad.2010.04.003
- Kitamura, K., Yanazawa, M., Sugiyama, N., Miura, H., Iizuka-Kogo, A., Kusaka, M., . . . Morohashi, K. (2002). Mutation of ARX causes abnormal development of forebrain and testes in mice and X-linked lissencephaly with abnormal genitalia in humans. *Nat Genet*, *32*(3), 359-369. doi: 10.1038/ng1009
- Kloc, M., & Maffei, A. (2014). Target-specific properties of thalamocortical synapses onto layer 4 of mouse primary visual cortex. *J Neurosci*, *34*(46), 15455-15465. doi: 10.1523/JNEUROSCI.2595-14.2014
- Koch, C. (1995). Visual awareness and the thalamic intralaminar nuclei. *Conscious Cogn*, *4*(2), 163-166.
- Kofler, T., Theriault, S., Bossard, M., Aeschbacher, S., Bernet, S., Krisai, P., . . . Conen, D. (2017). Relationships of Measured and Genetically Determined Height With the Cardiac Conduction System in Healthy Adults. *Circ Arrhythm Electrophysiol*, *10*(1). doi: 10.1161/CIRCEP.116.004735
- Kolaj, M., Zhang, L., Ronnekleiv, O. K., & Renaud, L. P. (2012). Midline thalamic paraventricular nucleus neurons display diurnal variation in resting membrane potentials, conductances, and firing patterns in vitro. *J Neurophysiol*, *107*(7), 1835-1844. doi: 10.1152/jn.00974.2011
- Kosho, T., Muroya, K., Nagai, T., Fujimoto, M., Yokoya, S., Sakamoto, H., . . . Ogata, T. (1999). Skeletal features and growth patterns in 14 patients with haploinsufficiency of SHOX: implications for the development of Turner syndrome. *J Clin Endocrinol Metab*, *84*(12), 4613-4621. doi: 10.1210/jcem.84.12.6289

- Lecourtier, L., Neijt, H. C., & Kelly, P. H. (2004). Habenula lesions cause impaired cognitive performance in rats: implications for schizophrenia. *Eur J Neurosci*, *19*(9), 2551-2560. doi: 10.1111/j.0953-816X.2004.03356.x
- Lee, J. H., Gomora, J. C., Cribbs, L. L., & Perez-Reyes, E. (1999). Nickel block of three cloned T-type calcium channels: low concentrations selectively block alpha1H. *Biophys J*, *77*(6), 3034-3042. doi: 10.1016/S0006-3495(99)77134-1
- Lei, Z., Deng, P., Li, J., & Xu, Z. C. (2012). Alterations of A-type potassium channels in hippocampal neurons after traumatic brain injury. *J Neurotrauma*, *29*(2), 235-245. doi: 10.1089/neu.2010.1537
- Lein, E. S., Hawrylycz, M. J., Ao, N., Ayres, M., Bensinger, A., Bernard, A., . . . Jones, A. R. (2007). Genome-wide atlas of gene expression in the adult mouse brain. *Nature*, *445*(7124), 168-176. doi: 10.1038/nature05453
- Leo, M. D., Bulley, S., Bannister, J. P., Kuruvilla, K. P., Narayanan, D., & Jaggar, J. H. (2015). Angiotensin II stimulates internalization and degradation of arterial myocyte plasma membrane BK channels to induce vasoconstriction. *Am J Physiol Cell Physiol*, *309*(6), C392-402. doi: 10.1152/ajpcell.00127.2015
- Li, B., Matter, E. K., Hoppert, H. T., Grayson, B. E., Seeley, R. J., & Sandoval, D. A. (2014). Identification of optimal reference genes for RT-qPCR in the rat hypothalamus and intestine for the study of obesity. *Int J Obes (Lond)*, *38*(2), 192-197. doi: 10.1038/ijo.2013.86
- Li, J., Li, Y., Zhang, B., Shen, X., & Zhao, H. (2016). Why depression and pain often coexist and mutually reinforce: Role of the lateral habenula. *Exp Neurol*, *284*(Pt A), 106-113. doi: 10.1016/j.expneurol.2016.08.010
- Li, K., Zhang, J., & Li, J. Y. (2012). Gbx2 plays an essential but transient role in the formation of thalamic nuclei. *PLoS One*, *7*(10), e47111. doi: 10.1371/journal.pone.0047111
- Li, M., Long, C., & Yang, L. (2015). Hippocampal-prefrontal circuit and disrupted functional connectivity in psychiatric and neurodegenerative disorders. *Biomed Res Int*, *2015*, 810548. doi: 10.1155/2015/810548
- Li, M., Luo, J., Brooks, C. L., & Gu, W. (2002). Acetylation of p53 inhibits its ubiquitination by Mdm2. *J Biol Chem*, *277*(52), 50607-50611. doi: 10.1074/jbc.C200578200
- Li, T., Diner, B. A., Chen, J., & Cristea, I. M. (2012). Acetylation modulates cellular distribution and DNA sensing ability of interferon-inducible protein IFI16. *Proc Natl Acad Sci U S A*, *109*(26), 10558-10563. doi: 10.1073/pnas.1203447109
- Li, Y., Xu, W., McBurney, M. W., & Longo, V. D. (2008). SirT1 inhibition reduces IGF-I/IRS-2/Ras/ERK1/2 signaling and protects neurons. *Cell Metab*, *8*(1), 38-48. doi: 10.1016/j.cmet.2008.05.004
- Libert, S., Pointer, K., Bell, E. L., Das, A., Cohen, D. E., Asara, J. M., . . . Guarente, L. (2011). SIRT1

- activates MAO-A in the brain to mediate anxiety and exploratory drive. *Cell*, *147*(7), 1459-1472. doi: 10.1016/j.cell.2011.10.054
- Lippe, B. (1991). Turner syndrome. *Endocrinol Metab Clin North Am*, *20*(1), 121-152.
- Liu, H., Chen, C. H., Espinoza-Lewis, R. A., Jiao, Z., Sheu, I., Hu, X., . . . Chen, Y. (2011). Functional redundancy between human SHOX and mouse Shox2 genes in the regulation of sinoatrial node formation and pacemaking function. *J Biol Chem*, *286*(19), 17029-17038. doi: 10.1074/jbc.M111.234252
- Llinas, R. R., & Steriade, M. (2006). Bursting of thalamic neurons and states of vigilance. *J Neurophysiol*, *95*(6), 3297-3308. doi: 10.1152/jn.00166.2006
- Loureiro, M., Cholvin, T., Lopez, J., Merienne, N., Latreche, A., Cosquer, B., . . . Pereira de Vasconcelos, A. (2012). The ventral midline thalamus (reuniens and rhomboid nuclei) contributes to the persistence of spatial memory in rats. *J Neurosci*, *32*(29), 9947-9959. doi: 10.1523/JNEUROSCI.0410-12.2012
- Ludwig, A., Budde, T., Stieber, J., Moosmang, S., Wahl, C., Holthoff, K., . . . Hofmann, F. (2003). Absence epilepsy and sinus dysrhythmia in mice lacking the pacemaker channel HCN2. *EMBO J*, *22*(2), 216-224. doi: 10.1093/emboj/cdg032
- Ludwig, A., Zong, X., Stieber, J., Hullin, R., Hofmann, F., & Biel, M. (1999). Two pacemaker channels from human heart with profoundly different activation kinetics. *EMBO J*, *18*(9), 2323-2329. doi: 10.1093/emboj/18.9.2323
- Lull, M. E., & Block, M. L. (2010). Microglial activation and chronic neurodegeneration. *Neurotherapeutics*, *7*(4), 354-365. doi: 10.1016/j.nurt.2010.05.014
- Luthi, A., & McCormick, D. A. (1998). H-current: properties of a neuronal and network pacemaker. *Neuron*, *21*(1), 9-12.
- Magee, J. C. (2000). Dendritic integration of excitatory synaptic input. *Nat Rev Neurosci*, *1*(3), 181-190. doi: 10.1038/35044552
- Mangoni, M. E., Couette, B., Marger, L., Bourinet, E., Striessnig, J., & Nargeot, J. (2006). Voltage-dependent calcium channels and cardiac pacemaker activity: from ionic currents to genes. *Prog Biophys Mol Biol*, *90*(1-3), 38-63. doi: 10.1016/j.pbiomolbio.2005.05.003
- Marsh, E. D., Nasrallah, M. P., Walsh, C., Murray, K. A., Nicole Sunnen, C., McCoy, A., & Golden, J. A. (2016). Developmental interneuron subtype deficits after targeted loss of Arx. *BMC Neurosci*, *17*(1), 35. doi: 10.1186/s12868-016-0265-8
- Martinez-Ferre, A., & Martinez, S. (2012). Molecular regionalization of the diencephalon. *Front Neurosci*, *6*, 73. doi: 10.3389/fnins.2012.00073
- Mashour, G. A., & Alkire, M. T. (2013). Consciousness, anesthesia, and the thalamocortical system. *Anesthesiology*, *118*(1), 13-15. doi: 10.1097/ALN.0b013e318277a9c6
- Mastick, G. S., Davis, N. M., Andrew, G. L., & Easter, S. S., Jr. (1997). Pax-6 functions in boundary

- formation and axon guidance in the embryonic mouse forebrain. *Development*, **124**(10), 1985-1997.
- Mathis, V., & Lecourtier, L. (2017). Role of the lateral habenula in memory through online processing of information. *Pharmacol Biochem Behav.* doi: 10.1016/j.pbb.2017.07.004
- Mattson, M. P. (2000). Apoptosis in neurodegenerative disorders. *Nat Rev Mol Cell Biol*, **1**(2), 120-129. doi: 10.1038/35040009
- McCormick, D. A., & Bal, T. (1997). Sleep and arousal: thalamocortical mechanisms. *Annu Rev Neurosci*, **20**, 185-215. doi: 10.1146/annurev.neuro.20.1.185
- McCormick, D. A., & Pape, H. C. (1990). Properties of a hyperpolarization-activated cation current and its role in rhythmic oscillation in thalamic relay neurones. *J Physiol*, **431**, 291-318.
- McCormick, D. A., & Prince, D. A. (1987). Actions of acetylcholine in the guinea-pig and cat medial and lateral geniculate nuclei, in vitro. *J Physiol*, **392**, 147-165.
- McDermott, C. M., & Schrader, L. A. (2011). Activation of kappa opioid receptors increases intrinsic excitability of dentate gyrus granule cells. *J Physiol*, **589**(Pt 14), 3517-3532. doi: 10.1113/jphysiol.2011.211623
- Mishra, S., & Mishra, R. C. (2012). The transylvian trans-insular approach to lateral thalamic lesions. *Neurol India*, **60**(4), 385-389. doi: 10.4103/0028-3886.100725
- Mitchell, A. S. (2015). The mediodorsal thalamus as a higher order thalamic relay nucleus important for learning and decision-making. *Neurosci Biobehav Rev*, **54**, 76-88. doi: 10.1016/j.neubiorev.2015.03.001
- Moosmang, S., Biel, M., Hofmann, F., & Ludwig, A. (1999). Differential distribution of four hyperpolarization-activated cation channels in mouse brain. *Biol Chem*, **380**(7-8), 975-980. doi: 10.1515/BC.1999.121
- Much, B., Wahl-Schott, C., Zong, X., Schneider, A., Baumann, L., Moosmang, S., . . . Biel, M. (2003). Role of subunit heteromerization and N-linked glycosylation in the formation of functional hyperpolarization-activated cyclic nucleotide-gated channels. *J Biol Chem*, **278**(44), 43781-43786. doi: 10.1074/jbc.M306958200
- Mullen, R. J., Buck, C. R., & Smith, A. M. (1992). NeuN, a neuronal specific nuclear protein in vertebrates. *Development*, **116**(1), 201-211.
- Nasca, C., Bigio, B., Zelli, D., Nicoletti, F., & McEwen, B. S. (2015). Mind the gap: glucocorticoids modulate hippocampal glutamate tone underlying individual differences in stress susceptibility. *Mol Psychiatry*, **20**(6), 755-763. doi: 10.1038/mp.2014.96
- Nayagam, V. M., Wang, X., Tan, Y. C., Poulsen, A., Goh, K. C., Ng, T., . . . Stunkel, W. (2006). SIRT1 modulating compounds from high-throughput screening as anti-inflammatory and insulin-sensitizing agents. *J Biomol Screen*, **11**(8), 959-967. doi: 10.1177/1087057106294710
- Nerbonne, J. M., & Kass, R. S. (2005). Molecular physiology of cardiac repolarization. *Physiol Rev*,

- 85(4), 1205-1253. doi: 10.1152/physrev.00002.2005
- Newman, L. A., & Burk, J. A. (2005). Effects of excitotoxic thalamic intralaminar nuclei lesions on attention and working memory. *Behav Brain Res*, 162(2), 264-271. doi: 10.1016/j.bbr.2005.03.018
- Ng, L., Bernard, A., Lau, C., Overly, C. C., Dong, H. W., Kuan, C., . . . Hawrylycz, M. (2009). An anatomic gene expression atlas of the adult mouse brain. *Nat Neurosci*, 12(3), 356-362. doi: 10.1038/nn.2281
- Nolan, M. F., Dudman, J. T., Dodson, P. D., & Santoro, B. (2007). HCN1 channels control resting and active integrative properties of stellate cells from layer II of the entorhinal cortex. *J Neurosci*, 27(46), 12440-12451. doi: 10.1523/JNEUROSCI.2358-07.2007
- Nolan, M. F., Malleret, G., Dudman, J. T., Buhl, D. L., Santoro, B., Gibbs, E., . . . Morozov, A. (2004). A behavioral role for dendritic integration: HCN1 channels constrain spatial memory and plasticity at inputs to distal dendrites of CA1 pyramidal neurons. *Cell*, 119(5), 719-732. doi: 10.1016/j.cell.2004.11.020
- Nolan, M. F., Malleret, G., Lee, K. H., Gibbs, E., Dudman, J. T., Santoro, B., . . . Morozov, A. (2003). The hyperpolarization-activated HCN1 channel is important for motor learning and neuronal integration by cerebellar Purkinje cells. *Cell*, 115(5), 551-564.
- Notomi, T., & Shigemoto, R. (2004). Immunohistochemical localization of Ih channel subunits, HCN1-4, in the rat brain. *J Comp Neurol*, 471(3), 241-276. doi: 10.1002/cne.11039
- Olivetti, P. R., Maheshwari, A., & Noebels, J. L. (2014). Neonatal estradiol stimulation prevents epilepsy in Arx model of X-linked infantile spasms syndrome. *Sci Transl Med*, 6(220), 220ra212. doi: 10.1126/scitranslmed.3007231
- Papageorgiou, I. E., Fetani, A. F., Lewen, A., Heinemann, U., & Kann, O. (2015). Widespread activation of microglial cells in the hippocampus of chronic epileptic rats correlates only partially with neurodegeneration. *Brain Struct Funct*, 220(4), 2423-2439. doi: 10.1007/s00429-014-0802-0
- Parnaudeau, S., O'Neill, P. K., Bolkan, S. S., Ward, R. D., Abbas, A. I., Roth, B. L., . . . Kellendonk, C. (2013). Inhibition of mediodorsal thalamus disrupts thalamofrontal connectivity and cognition. *Neuron*, 77(6), 1151-1162. doi: 10.1016/j.neuron.2013.01.038
- Perez-Reyes, E. (2003). Molecular physiology of low-voltage-activated t-type calcium channels. *Physiol Rev*, 83(1), 117-161. doi: 10.1152/physrev.00018.2002
- Petrik, D., Wang, B., & Brenner, R. (2011). Modulation by the BK accessory beta4 subunit of phosphorylation-dependent changes in excitability of dentate gyrus granule neurons. *Eur J Neurosci*, 34(5), 695-704. doi: 10.1111/j.1460-9568.2011.07799.x
- Pinault, D. (2004). The thalamic reticular nucleus: structure, function and concept. *Brain Res Brain Res Rev*, 46(1), 1-31. doi: 10.1016/j.brainresrev.2004.04.008

- Pitter, K. L., Tamagno, I., Feng, X., Ghosal, K., Amankulor, N., Holland, E. C., & Hambardzumyan, D. (2014). The SHH/Gli pathway is reactivated in reactive glia and drives proliferation in response to neurodegeneration-induced lesions. *Glia*, *62*(10), 1595-1607. doi: 10.1002/glia.22702
- Poeta, L., Fusco, F., Drongitis, D., Shoubridge, C., Manganelli, G., Filosa, S., . . . Miano, M. G. (2013). A regulatory path associated with X-linked intellectual disability and epilepsy links KDM5C to the polyalanine expansions in ARX. *Am J Hum Genet*, *92*(1), 114-125. doi: 10.1016/j.ajhg.2012.11.008
- Poirier, K., Van Esch, H., Friocourt, G., Saillour, Y., Bahi, N., Backer, S., . . . Chelly, J. (2004). Neuroanatomical distribution of ARX in brain and its localisation in GABAergic neurons. *Brain Res Mol Brain Res*, *122*(1), 35-46. doi: 10.1016/j.molbrainres.2003.11.021
- Porcu, M., & Chiarugi, A. (2005). The emerging therapeutic potential of sirtuin-interacting drugs: from cell death to lifespan extension. *Trends Pharmacol Sci*, *26*(2), 94-103. doi: 10.1016/j.tips.2004.12.009
- Proulx, C. D., Hikosaka, O., & Malinow, R. (2014). Reward processing by the lateral habenula in normal and depressive behaviors. *Nat Neurosci*, *17*(9), 1146-1152. doi: 10.1038/nn.3779
- Puskarić, S., Schmitteckert, S., Mori, A. D., Glaser, A., Schneider, K. U., Bruneau, B. G., . . . Rappold, G. (2010). Shox2 mediates Tbx5 activity by regulating Bmp4 in the pacemaker region of the developing heart. *Hum Mol Genet*, *19*(23), 4625-4633. doi: 10.1093/hmg/ddq393
- Putrenko, I., & Schwarz, S. K. (2011). Lidocaine blocks the hyperpolarization-activated mixed cation current, I(h), in rat thalamocortical neurons. *Anesthesiology*, *115*(4), 822-835. doi: 10.1097/ALN.0b013e31822ddf08
- Reinagel, P., Godwin, D., Sherman, S. M., & Koch, C. (1999). Encoding of visual information by LGN bursts. *J Neurophysiol*, *81*(5), 2558-2569.
- Robertson, S. P., Shears, D. J., Oei, P., Winter, R. M., Scambler, P. J., Aftimos, S., & Savarirayan, R. (2000). Homozygous deletion of SHOX in a mentally retarded male with Langer mesomelic dysplasia. *J Med Genet*, *37*(12), 959-964.
- Rodgers, J. T., Lerin, C., Haas, W., Gygi, S. P., Spiegelman, B. M., & Puigserver, P. (2005). Nutrient control of glucose homeostasis through a complex of PGC-1alpha and SIRT1. *Nature*, *434*(7029), 113-118. doi: 10.1038/nature03354
- Rogina, B., & Helfand, S. L. (2004). Sir2 mediates longevity in the fly through a pathway related to calorie restriction. *Proc Natl Acad Sci U S A*, *101*(45), 15998-16003. doi: 10.1073/pnas.0404184101
- Rosin, J. M., Abassah-Oppong, S., & Cobb, J. (2013). Comparative transgenic analysis of enhancers from the human SHOX and mouse Shox2 genomic regions. *Hum Mol Genet*, *22*(15), 3063-3076. doi: 10.1093/hmg/ddt163

- Rosin, J. M., Kurrasch, D. M., & Cobb, J. (2015). Shox2 is required for the proper development of the facial motor nucleus and the establishment of the facial nerves. *BMC Neurosci*, *16*, 39. doi: 10.1186/s12868-015-0176-0
- Rosin, J. M., McAllister, B. B., Dyck, R. H., Percival, C. J., Kurrasch, D. M., & Cobb, J. (2015). Mice lacking the transcription factor SHOX2 display impaired cerebellar development and deficits in motor coordination. *Dev Biol*, *399*(1), 54-67. doi: 10.1016/j.ydbio.2014.12.013
- Saalman, Y. B. (2014). Intralaminar and medial thalamic influence on cortical synchrony, information transmission and cognition. *Front Syst Neurosci*, *8*, 83. doi: 10.3389/fnsys.2014.00083
- Sadoul, K., Wang, J., Diagouraga, B., & Khochbin, S. (2011). The tale of protein lysine acetylation in the cytoplasm. *J Biomed Biotechnol*, *2011*, 970382. doi: 10.1155/2011/970382
- Salazar-Juarez, A., Escobar, C., & Aguilar-Roblero, R. (2002). Anterior paraventricular thalamus modulates light-induced phase shifts in circadian rhythmicity in rats. *Am J Physiol Regul Integr Comp Physiol*, *283*(4), R897-904. doi: 10.1152/ajpregu.00259.2002
- Satoh, A., Imai, S. I., & Guarente, L. (2017). The brain, sirtuins, and ageing. *Nat Rev Neurosci*, *18*(6), 362-374. doi: 10.1038/nrn.2017.42
- Seki, M., & Zyo, K. (1984). Anterior thalamic afferents from the mamillary body and the limbic cortex in the rat. *J Comp Neurol*, *229*(2), 242-256. doi: 10.1002/cne.902290209
- Sellers, K., Zyka, V., Lumsden, A. G., & Delogu, A. (2014). Transcriptional control of GABAergic neuronal subtype identity in the thalamus. *Neural Dev*, *9*, 14. doi: 10.1186/1749-8104-9-14
- Seo, G. H., Kang, E., Cho, J. H., Lee, B. H., Choi, J. H., Kim, G. H., . . . Yoo, H. W. (2015). Turner syndrome presented with tall stature due to overdosage of the SHOX gene. *Ann Pediatr Endocrinol Metab*, *20*(2), 110-113. doi: 10.6065/apem.2015.20.2.110
- Sheline, C. T., Behrens, M. M., & Choi, D. W. (2000). Zinc-induced cortical neuronal death: contribution of energy failure attributable to loss of NAD(+) and inhibition of glycolysis. *J Neurosci*, *20*(9), 3139-3146.
- Sherman, S. M. (2007). The thalamus is more than just a relay. *Curr Opin Neurobiol*, *17*(4), 417-422. doi: 10.1016/j.conb.2007.07.003
- Sherman, S. M. (2016). Thalamus plays a central role in ongoing cortical functioning. *Nat Neurosci*, *19*(4), 533-541. doi: 10.1038/nn.4269
- Sherr, E. H. (2003). The ARX story (epilepsy, mental retardation, autism, and cerebral malformations): one gene leads to many phenotypes. *Curr Opin Pediatr*, *15*(6), 567-571.
- Shipp, S. (2005). The importance of being agranular: a comparative account of visual and motor cortex. *Philos Trans R Soc Lond B Biol Sci*, *360*(1456), 797-814. doi: 10.1098/rstb.2005.1630
- Shosaku, A., Kayama, Y., & Sumitomo, I. (1984). Somatotopic organization in the rat thalamic reticular nucleus. *Brain Res*, *311*(1), 57-63.



- Shoubridge, C., Tan, M. H., Seiboth, G., & Gecz, J. (2012). ARX homeodomain mutations abolish DNA binding and lead to a loss of transcriptional repression. *Hum Mol Genet*, *21*(7), 1639-1647. doi: 10.1093/hmg/ddr601
- Snyder, J. S., Soumier, A., Brewer, M., Pickel, J., & Cameron, H. A. (2011). Adult hippocampal neurogenesis buffers stress responses and depressive behaviour. *Nature*, *476*(7361), 458-461. doi: 10.1038/nature10287
- Song, J., & Kim, J. (2016). Role of Sirtuins in Linking Metabolic Syndrome with Depression. *Front Cell Neurosci*, *10*, 86. doi: 10.3389/fncel.2016.00086
- Song, N. Y., & Surh, Y. J. (2012). Janus-faced role of SIRT1 in tumorigenesis. *Ann N Y Acad Sci*, *1271*, 10-19. doi: 10.1111/j.1749-6632.2012.06762.x
- Soriano, P. (1999). Generalized lacZ expression with the ROSA26 Cre reporter strain. *Nat Genet*, *21*(1), 70-71. doi: 10.1038/5007
- Sparse whole-genome sequencing identifies two loci for major depressive disorder. (2015). *Nature*, *523*(7562), 588-591. doi: 10.1038/nature14659
- Sugiyama, S., Prochiantz, A., & Hensch, T. K. (2009). From brain formation to plasticity: insights on Otx2 homeoprotein. *Dev Growth Differ*, *51*(3), 369-377. doi: 10.1111/j.1440-169X.2009.01093.x
- Sun, C., Yu, D., Ye, W., Liu, C., Gu, S., Sinsheimer, N. R., . . . Chen, Y. (2015). The short stature homeobox 2 (Shox2)-bone morphogenetic protein (BMP) pathway regulates dorsal mesenchymal protrusion development and its temporary function as a pacemaker during cardiogenesis. *J Biol Chem*, *290*(4), 2007-2023. doi: 10.1074/jbc.M114.619007
- Sun, C., Zhang, T., Liu, C., Gu, S., & Chen, Y. (2013). Generation of Shox2-Cre allele for tissue specific manipulation of genes in the developing heart, palate, and limb. *Genesis*, *51*(7), 515-522. doi: 10.1002/dvg.22397
- Takahashi, T. (1985). The organization of the lateral thalamus of the hooded rat. *J Comp Neurol*, *231*(3), 281-309. doi: 10.1002/cne.902310302
- Tang, B. L. (2009). Sirt1's complex roles in neuroprotection. *Cell Mol Neurobiol*, *29*(8), 1093-1103. doi: 10.1007/s10571-009-9414-2
- Tanno, M., Sakamoto, J., Miura, T., Shimamoto, K., & Horio, Y. (2007). Nucleocytoplasmic shuttling of the NAD<sup>+</sup>-dependent histone deacetylase SIRT1. *J Biol Chem*, *282*(9), 6823-6832. doi: 10.1074/jbc.M609554200
- Taube, J. S. (1995). Head direction cells recorded in the anterior thalamic nuclei of freely moving rats. *J Neurosci*, *15*(1 Pt 1), 70-86.
- Theyel, B. B., Lee, C. C., & Sherman, S. M. (2010). Specific and nonspecific thalamocortical connectivity in the auditory and somatosensory thalamocortical slices. *Neuroreport*, *21*(13), 861-864. doi: 10.1097/WNR.0b013e32833d7cec

- Theyel, B. B., Llano, D. A., & Sherman, S. M. (2010). The corticothalamocortical circuit drives higher-order cortex in the mouse. *Nat Neurosci*, *13*(1), 84-88. doi: 10.1038/nn.2449
- Tissenbaum, H. A., & Guarente, L. (2001). Increased dosage of a sir-2 gene extends lifespan in *Caenorhabditis elegans*. *Nature*, *410*(6825), 227-230. doi: 10.1038/35065638
- Tomaiuolo, M., Gonzalez, C., Medina, J. H., & Piriz, J. (2014). Lateral Habenula determines long-term storage of aversive memories. *Front Behav Neurosci*, *8*, 170. doi: 10.3389/fnbeh.2014.00170
- Tripathi, P. P., Sgado, P., Scali, M., Viaggi, C., Casarosa, S., Simon, H. H., . . . Bozzi, Y. (2009). Increased susceptibility to kainic acid-induced seizures in Engrailed-2 knockout mice. *Neuroscience*, *159*(2), 842-849. doi: 10.1016/j.neuroscience.2009.01.007
- Tsanov, M., Chah, E., Wright, N., Vann, S. D., Reilly, R., Erichsen, J. T., . . . O'Mara, S. M. (2011). Oscillatory entrainment of thalamic neurons by theta rhythm in freely moving rats. *J Neurophysiol*, *105*(1), 4-17. doi: 10.1152/jn.00771.2010
- Turner, G., Partington, M., Kerr, B., Mangelsdorf, M., & Gecz, J. (2002). Variable expression of mental retardation, autism, seizures, and dystonic hand movements in two families with an identical ARX gene mutation. *Am J Med Genet*, *112*(4), 405-411. doi: 10.1002/ajmg.10714
- Valente, V., Teixeira, S. A., Neder, L., Okamoto, O. K., Oba-Shinjo, S. M., Marie, S. K., . . . Carlotti, C. G., Jr. (2009). Selection of suitable housekeeping genes for expression analysis in glioblastoma using quantitative RT-PCR. *BMC Mol Biol*, *10*, 17. doi: 10.1186/1471-2199-10-17
- Van der Werf, Y. D., Witter, M. P., & Groenewegen, H. J. (2002). The intralaminar and midline nuclei of the thalamus. Anatomical and functional evidence for participation in processes of arousal and awareness. *Brain Res Brain Res Rev*, *39*(2-3), 107-140.
- Velazquez-Marrero, C., Burgos, A., Garcia, J. O., Palacio, S., Marrero, H. G., Bernardo, A., . . . Treisman, S. N. (2016). Alcohol Regulates BK Surface Expression via Wnt/beta-Catenin Signaling. *J Neurosci*, *36*(41), 10625-10639. doi: 10.1523/JNEUROSCI.0491-16.2016
- Vertes, R. P., Linley, S. B., & Hoover, W. B. (2015). Limbic circuitry of the midline thalamus. *Neurosci Biobehav Rev*, *54*, 89-107. doi: 10.1016/j.neubiorev.2015.01.014
- Vogt, D., Hunt, R. F., Mandal, S., Sandberg, M., Silberberg, S. N., Nagasawa, T., . . . Rubenstein, J. L. (2014). Lhx6 directly regulates Arx and CXCR7 to determine cortical interneuron fate and laminar position. *Neuron*, *82*(2), 350-364. doi: 10.1016/j.neuron.2014.02.030
- Wahl-Schott, C., & Biel, M. (2009). HCN channels: structure, cellular regulation and physiological function. *Cell Mol Life Sci*, *66*(3), 470-494. doi: 10.1007/s00018-008-8525-0
- Wang, B., Bugay, V., Ling, L., Chuang, H. H., Jaffe, D. B., & Brenner, R. (2016). Knockout of the BK beta4-subunit promotes a functional coupling of BK channels and ryanodine receptors that mediate a fAHP-induced increase in excitability. *J Neurophysiol*, *116*(2), 456-465. doi:

10.1152/jn.00857.2015

- Wang, B., Jaffe, D. B., & Brenner, R. (2014). Current understanding of iberiotoxin-resistant BK channels in the nervous system. *Front Physiol*, *5*, 382. doi: 10.3389/fphys.2014.00382
- Wang, J., Klysik, E., Sood, S., Johnson, R. L., Wehrens, X. H., & Martin, J. F. (2010). Pitx2 prevents susceptibility to atrial arrhythmias by inhibiting left-sided pacemaker specification. *Proc Natl Acad Sci U S A*, *107*(21), 9753-9758. doi: 10.1073/pnas.0912585107
- Watson, C., Janke, A. L., Hamalainen, C., Bagheri, S. M., Paxinos, G., Reutens, D. C., & Ullmann, J. F. P. (2017). An ontologically consistent MRI-based atlas of the mouse diencephalon. *Neuroimage*, *157*, 275-287. doi: 10.1016/j.neuroimage.2017.05.057
- Wehr, M., & Zador, A. M. (2003). Balanced inhibition underlies tuning and sharpens spike timing in auditory cortex. *Nature*, *426*(6965), 442-446. doi: 10.1038/nature02116
- Whitaker, G. M., Angoli, D., Nazzari, H., Shigemoto, R., & Accili, E. A. (2007). HCN2 and HCN4 isoforms self-assemble and co-assemble with equal preference to form functional pacemaker channels. *J Biol Chem*, *282*(31), 22900-22909. doi: 10.1074/jbc.M610978200
- Wilson, S. W., & Houart, C. (2004). Early steps in the development of the forebrain. *Dev Cell*, *6*(2), 167-181.
- Yang, Z., & Wang, K. K. (2015). Glial fibrillary acidic protein: from intermediate filament assembly and gliosis to neurobiomarker. *Trends Neurosci*, *38*(6), 364-374. doi: 10.1016/j.tins.2015.04.003
- Ye, W., Song, Y., Huang, Z., Osterwalder, M., Ljubojevic, A., Xu, J., . . . Chen, Y. (2016). A unique stylopod patterning mechanism by Shox2-controlled osteogenesis. *Development*, *143*(14), 2548-2560. doi: 10.1242/dev.138750
- Ye, W., Wang, J., Song, Y., Yu, D., Sun, C., Liu, C., . . . Chen, Y. (2015). A common Shox2-Nkx2-5 antagonistic mechanism primes the pacemaker cell fate in the pulmonary vein myocardium and sinoatrial node. *Development*, *142*(14), 2521-2532. doi: 10.1242/dev.120220
- Yu, L., Gu, S., Alappat, S., Song, Y., Yan, M., Zhang, X., . . . Chen, Y. (2005). Shox2-deficient mice exhibit a rare type of incomplete clefting of the secondary palate. *Development*, *132*(19), 4397-4406. doi: 10.1242/dev.02013
- Zhang, C., Bosch, M. A., Rick, E. A., Kelly, M. J., & Ronnekleiv, O. K. (2009). 17Beta-estradiol regulation of T-type calcium channels in gonadotropin-releasing hormone neurons. *J Neurosci*, *29*(34), 10552-10562. doi: 10.1523/JNEUROSCI.2962-09.2009
- Zhang, Q., Huang, A., Lin, Y. C., & Yu, H. G. (2009). Associated changes in HCN2 and HCN4 transcripts and I(f) pacemaker current in myocytes. *Biochim Biophys Acta*, *1788*(5), 1138-1147. doi: 10.1016/j.bbame.2009.02.011
- Zhang, Y., Zhang, M., Dong, H., Yong, S., Li, X., Olashaw, N., . . . Zhang, X. (2009). Deacetylation of cortactin by SIRT1 promotes cell migration. *Oncogene*, *28*(3), 445-460. doi:

**10.1038/onc.2008.388**

**Zhou, Z., & January, C. T. (1998). Both T- and L-type Ca<sup>2+</sup> channels can contribute to excitation-contraction coupling in cardiac Purkinje cells. *Biophys J*, 74(4), 1830-1839. doi:**

**10.1016/S0006-3495(98)77893-2**

## Appendix

## **SIRT1 activity rapidly affects synaptic properties in dentate gyrus through BK channel deacetylation and is related to anxiety and the maladaptive response to stress**

Diankun Yu<sup>1</sup>, Damek R. Homiack<sup>1</sup>, Edward J. Sawyer<sup>1</sup>, and Laura A. Schrader<sup>1,2</sup> <sup>1</sup>. Neuroscience Program, Brain Institute <sup>2</sup>. Cell and Molecular Biology Tulane University, New Orleans, LA 70118

### **Abstract**

Previous genomic studies in humans indicated that SIRT1, an NAD<sup>+</sup>-dependent protein deacetylase, is involved in anxiety and depression, but the mechanisms of its role in these and other neuropathologies are unclear. Our lab has used an animal model of chronic stress to elucidate the role of SIRT1 in depression-like behaviors. Several studies have shown that the function of SIRT1 is likely dependent upon its localization within the cell, cytoplasmic or nuclear, as well as the substrates that it targets during a given physiological demand. We previously showed that SIRT1 is highly activated in the nuclear fraction of the chronically stressed animals and SIRT1 functions to inhibit memory formation and increase anhedonic behavior during chronic stress, but specific cytoplasmic SIRT1 function has not been studied. We used electrophysiology, biochemistry and behavioral techniques to demonstrate that SIRT1 activity rapidly modulates intrinsic and synaptic properties in the dentate gyrus granule cells through deacetylation and internalization of BK channel  $\alpha$  subunits in control animals and modulates anxiety behaviors. On the other hand, chronic stress decreases BK  $\alpha$  channel membrane expression, and SIRT1 activity has no rapid effects on synaptic transmission or intrinsic properties in the chronically stressed animal. We propose that the loss of the SIRT1/BK-mediated rapid regulation participates in the maladaptive response to chronic stress in the hippocampus. Together with previous studies, these results suggest that SIRT1 activity rapidly modulates DG physiological properties and function, and this modulation is important to behavioral output during different physiological states.

## Introduction

The sirtuins (SIRT1-7) are a highly-conserved family of nicotinamide adenine dinucleotide (NAD<sup>+</sup>)-dependent protein deacetylases that are expressed in cells throughout an organism, including cells in the nervous system (Imai & Guarente, 2010; Satoh, Imai, & Guarente, 2017). One member of the sirtuin family, SIRT1, the mammalian homologue of yeast Sir2, was first implicated in extension of lifespan by caloric restriction (Imai, Armstrong, Kaeberlein, & Guarente, 2000) and has been linked to cell energy metabolism, oxidative stress (Fabrizio et al., 2005; Kaeberlein, McVey, & Guarente, 1999; Rogina & Helfand, 2004; Tissenbaum & Guarente, 2001) and neurodegenerative disorders in mammals (Haigis & Sinclair, 2010). Recent studies have implicated SIRT1 in mood disorders in humans. Two independent whole genome sequencing studies, including the Cai et al. Converge consortium ("Sparse whole-genome sequencing identifies two loci for major depressive disorder," 2015), found that SIRT1 single nucleotide polymorphisms (SNPs) are associated with major depressive disorder (Kishi et al., 2010). In addition, variations in the SIRT1 gene were shown to be associated with risk of anxiety in human population samples (Libert et al., 2011).

Animal models of anxiety and chronic variable stress (CVS) are used to determine mechanisms involved in development of anxiety- and depression-like behaviors.

Brain-specific SIRT1 KO mice showed reduced anxiety, while SIRT1 overexpressing mice exhibited enhanced anxiety (Libert et al., 2011), suggesting that chronic SIRT1 function also modulates anxiety-like behaviors in mice. Further, previous work from our lab showed that SIRT1 is hyper-activated in the nuclear-enriched fraction from the dentate gyrus (DG) of the hippocampus of rats exposed to CVS (Ferland & Schrader, 2011), and chronic inhibition of SIRT1 with sirtinol infused into the DG reversed CVS-induced memory impairments and anhedonia (Ferland et al., 2013). On the other hand, another study demonstrated reduced SIRT1 activity in the hippocampus of chronic ultra-mild stress-treated mice, and increased SIRT1 activation reversed the stress-induced dendritic atrophy and anhedonia in mice (Abe-Higuchi et al., 2016). While these results are inconsistent with our previous study, they indicate a critical role for SIRT1 activity modulation during stress, but also highlight the need for further identification of the specific roles of SIRT1 and its substrates in hippocampus function during control and chronic stress conditions. Furthermore, taken together with the human genetic studies, these studies define an important relationship between SIRT1-dependent mechanisms and development of anxiety and depressive disorder-related behaviors.

Interestingly, the roles of SIRT1 in many physiological functions can be opposing and are dependent on the cellular localization of SIRT1 and its substrates. While most



studies have demonstrated that SIRT1 is localized to the nucleus and functions in gene transcription (Bai & Zhang, 2016; Tanno, Sakamoto, Miura, Shimamoto, & Horio, 2007), recent research shows that SIRT1 is highly expressed in both the nucleus and cytoplasm of neurons (Y. Li, Xu, McBurney, & Longo, 2008), with two nuclear export and import signals within SIRT1's amino acid sequence (Tanno et al., 2007), suggesting potential for dynamic changes in localization. The cellular localization and targets of SIRT1 function can change rapidly and likely depend on physiological functional demand, for example, in response to metabolic demand or developmental state. Opposing effects of cytosolic and nuclear SIRT1 have been demonstrated in the fields of tumor growth studies (N. Y. Song & Surh, 2012) as well as neuroprotection (Jeong et al., 2012; Kakefuda et al., 2009; Tang, 2009). Furthermore, SIRT1 can affect multiple functions, depending on localization. For example, in pancreatic  $\beta$  cells, cytoplasmic SIRT1 inhibits  $\beta$ -cell survival through Kv1.5 and Kv $\beta$  acetylation while nuclear SIRT1 suppression of the expression of uncoupling protein gene 2 increases insulin secretion (S. J. Kim, Ao, Warnock, & McIntosh, 2013). Therefore, the localization of SIRT1 and its substrates appears to play a decisive role in the overall functional output of cells. However, the involvement of SIRT1 in anxiety and depressive disorder-related behavior regulation was previously studied under chronic SIRT1 activity modulation

such as SIRT1 KO, overexpression or long-term pharmacological modulation. The implication of rapid effects of cytosolic SIRT1 in CVS and anxiety behavior regulation has not yet been studied.

We hypothesized that rapid deacetylation of targets by cytosolic SIRT1 in the granule cells of the DG may mediate differential acute effects compared to chronic modulation of SIRT1 previously described. Thus, dynamic deacetylation of membrane or cytosolic targets may affect neuronal intrinsic properties or synaptic transmission independent of transcription-dependent effects. In this study, we investigated membrane targets of SIRT1 deacetylation that mediate rapid effects in the granule cells of the dentate gyrus in control and chronically stressed animals. Using electrophysiological recordings from granule cells, we found that activation and inhibition of SIRT1 activity rapidly modulated DG granule cell intrinsic properties and excitatory transmission. These effects in control mice were mediated through the large conductance, voltage- and  $\text{Ca}^{2+}$ -gated BK channels, and we found that the primary  $\alpha$  subunit of BK channels is a direct target of SIRT1 activity. Interestingly, no effect of SIRT1 activity was observed in animals previously exposed to chronic stress, and chronic stress decreased BK channel membrane expression levels and currents in the CVS-treated animals, a mechanism which may underlie the stress-induced

impairment of SIRT1 rapid effect. Finally, we show that modulation of SIRT1 activity in the dentate gyrus can rapidly affect anxiety behavior, as SIRT1 inhibition in the dentate gyrus caused a rapid anxiogenic effect, while activation was anxiolytic in mouse open field test.

**Methods:***Animals:*

All animals and procedures were approved by Tulane Institutional Animal Care and Use Committee (IACUC) according to National Institutes of Health (NIH) guidelines. Mice were 4 -10 weeks old C57 male mice ordered from Charles River. All mice were housed on a 12:12 light/dark cycle and received food and water *ad libitum*. Animals were handled daily to avoid acute stress prior to experiments.

*Electrophysiology:*

Hippocampus slices were prepared according to previously described methods (McDermott & Schrader, 2011). Briefly, mice were deeply anesthetized with isoflurane and decapitated, and the brains were rapidly removed. Acute hippocampus brain slices were prepared in ice-cold oxygenated (95% O<sub>2</sub>/5% CO<sub>2</sub>) cutting artificial cerebrospinal fluid (aCSF) with a vibratome. Slices were incubated at 35°C for 30 minutes then held at room temperature in oxygenated standard aCSF until use. In some experiments, 1

$\mu\text{M}$  tetrodotoxin (TTX, Alomone Labs Cat #T-550) or 50  $\mu\text{M}$  paxilline (Sigma Aldrich, Cat #57186-25-1) was applied during the incubation to inhibit voltage-gated sodium or large conductance calcium-dependent potassium channels (BK channels) respectively. Dentate gyrus granule cells were identified under infrared differential interference contrast (DIC) videomicroscopy and only cells from the upper blade of dentate gyrus were targeted for whole-cell patch clamp recordings. Recordings were done at room temperature using a Digidata 1322A digitizer with Multiclamp 700B amplifier. Series resistance was monitored throughout the recording, and any cells with access resistance more than  $20\text{M}\Omega$  or more than 20% change were excluded from further analysis. Spontaneous excitatory postsynaptic current (sEPSC) and miniature EPSC (mEPSC) events were recorded at holding potential of  $-70\text{mV}$  under voltage clamp with pClamp software and analyzed by *Minianalysis*. Action potentials were evoked by small current injection ranging from 10 pA to 60 pA from a holding potential of  $-65\text{mV}$  under current clamp. Fast afterhyperpolarization (fAHP) amplitude was defined as the voltage difference between fAHP and threshold of the first evoked spike at 50pA current injection, and the spike width was defined as the time difference between up- and down-stroke at the threshold voltage. Statistical analysis was done in *Graphpad Prism 6*. Unless otherwise specified, paired t-tests were used to

determine significance between control and drug application. **Solution Recipe:**

Cutting aCSF (mM): 125 NaCl, 2.5 KCl, 26 NaHCO<sub>3</sub>, 1.24 NaH<sub>2</sub>PO<sub>3</sub>, 25 Dextrose, 8

MgSO<sub>4</sub>, 0.25 CaCl<sub>2</sub>; Standard aCSF (mM): 125 NaCl, 2.5 KCl, 26 NaHCO<sub>3</sub>, 1.24

NaH<sub>2</sub>PO<sub>3</sub>, 25 Dextrose, 2 MgSO<sub>4</sub>, 2 CaCl<sub>2</sub>; Pipette solution (mM): 120 Kglu, 20 KCl,

0.2 EGTA, 10 Hepes, 4 NaCl, 4 Mg<sup>2+</sup>ATP, 14 phosphocreatine, 0.3 Tris GTP. pH was

adjusted to 7.2-7.25 by KOH. Osmolarity was adjusted to 305-315 mOsm by sorbitol.

The main SIRT1 inhibitor and activator drugs were made as 1000 x stock solution in

DMSO stored aliquoted at -20 °C, and bath applied at a concentration demonstrated

before (Nayagam et al., 2006; Porcu & Chiarugi, 2005) prior to bath application: SIRT1

inhibitor IV (Calbiochem Cat #566325): 1µM; SIRT1 activator 3 (Santa Cruz

Biotechnology, Inc. sc-222315): 50 µM.

#### *Chronic Variable Stress:*

CVS was conducted using a similar method as previously reported (Ferland et al., 2013;

Ferland & Schrader, 2011). Briefly, the CVS paradigm consisted of randomized stressors

twice a day daily for 21 days, with occasional overnight stressors. Morning and

afternoon stressors consisted of cold swim (8 min at 20°C tap water), cold room (1

hour at 4°C), warm swim (20 min at 35°C tap water), shaking plate (1 hour on shaking

plate), wet bedding (1 hour). Overnight stressors consisted of no bedding, single housing and overcrowding (6 mice in each cage). Daily food consumption and weight gain were monitored and demonstrated the CVS mice were stressed as CVS decreased daily food consumption and weight gain (Supplementary Figure 1). Mice received 21 days of stressors that concluded the day before recordings to avoid the confounds of acute stress. For recordings, all control and CVS mice were handled the same way and sacrificed at the same time of the day (11 am  $\pm$  30 min).

*Immunoprecipitation / Co-Immunoprecipitation (IP/Co-IP):*

Hippocampus tissue was collected from acute mouse brain slices which were prepared in the same way as those in electrophysiological experiments. The brain slices were incubated in either 1:1000 DMSO, 50  $\mu$ M SIRT1 activator 3 or 1  $\mu$ M SIRT1 inhibitor IV before IP procedures. Pierce™ Classic Magnetic IP/Co-IP Kit (Thermo Scientific, 88804) was used for IP/Co-IP experiments. To avoid post-translational modification of proteins, phosphatase inhibitor cocktail (Calbiochem, Cat.# 524627, 1:100), 10mM sodium fluoride, 20mM sodium butyrate and 1mM sodium orthovanadate as well as protease inhibitor (Calbiochem, Cat.# 535142, 1:100) were added to the NP-40 lysis buffer provided in the kit. The protein concentration was determined and all samples

were diluted to the same concentration before IP. The immunocomplex was 2  $\mu$ g antibodies in 200  $\mu$ L lysis buffers with 0.6 mg/mL proteins. All procedures followed the instruction of Pierce™ Classic Magnetic IP/Co-IP Kit. The Western blot analysis protocols were followed to immuno-blot (IB) our target protein.

*Bis(sulfosuccinimidyl) suberate (BS3) crosslinking:*

Hippocampus and surrounding cortical slices were randomly divided into 3 groups and incubated in 1:1000 DMSO, 1  $\mu$ M SIRT1 inhibitor IV, or 50  $\mu$ M SIRT1 activator 3 for 15 minutes. After wash, slices were placed into ice-cold standard aCSF containing 2mM bis(sulfosuccinimidyl) suberate (BS3) (ThermoFisher, 21580) for crosslinking for 30 minutes. The reaction was quenched with 100 mM glycine. Slices were washed with ice-cold standard aCSF. Hippocampi were removed from slices and lysed in the lysis buffer with protease inhibitor and 20mM sodium butyrate, aliquoted and processed with the same western blot analysis protocol, except that proteins were transferred to the membrane overnight at 40 mV in a 4 °C cold room.

*Western blot analysis*

Tissue from rats exposed to CVS or controls was gathered by bilaterally sub-dissecting the hippocampus into DG, CA3, and CA1 sub-regions as previously described before

(Ferland & Schrader, 2011). Dentate gyrus tissue was sub-fractionated using a commercially available kit (Millipore compartmental fractionation kit, 2145) per manufacturer's instructions to generate a membrane enriched fraction. For mouse tissue, the whole hippocampi were collected from acute brain slices prepared in the same way as electrophysiological experiments and lysed with NP-40 lysis buffer with protease inhibitor and 20mM sodium butyrate. The protein concentration was determined by Bio-Rad DC protein assay (BioRad, Hercules, CA, Cat #500) and all samples in the same experiments were diluted to the same concentration before further procedure such as IP or aliquot. To denature and reduce the samples, sample buffer (5x, Thermo-Fisher Scientific, 39001) and dithiothreitol (DTT, final concentration to 50mM) were added to all samples and samples were boiled for 5 minutes before loading. The same amount of protein was loaded into 10% SDS-PAGE gels, separated and transferred to a PVDF membrane. The membranes were blocked in Odyssey® Blocking Buffer (TBS) (LI-COR®, Part No. 927-50000) for 1 hour at room temperature with constant rocking. The membranes were incubated with primary antibodies including anti-BK  $\alpha$  (Neuromab, L6/60, 1:1000), anti-BK  $\beta$ 2 (Neuromab, N53/32 1:1000), anti-BK  $\beta$ 4 (Neuromab, L18A.3, 1:1000), anti-SIRT1 (Santa Cruz, sc-15404, 1:1000), anti-acetylated lysine (Cell Signaling, 9441S, 1:1000) or anti-GAPDH (Cell



Signaling, 1:10,000) primary antibodies at 4 °C overnight with constant rocking. The membranes were washed three times with TTBS and incubated with fluorescence conjugated secondary antibodies (IRDye® 680RD Goat anti-mouse, IRDye® 800CW Goat anti-rabbit, 1: 10,000) for 1 hour at room temperature. Immuno-reactive bands were acquired using Odyssey® imaging system (LI-COR). Results were analyzed by *Image Studio Lite V5.2*.

#### *Surgery and Behavior*

Animals were anesthetized by ketamine/xylazine and maintained on isoflurane and placed in a Kopf stereotaxic instrument with the toothbar set level with the interaural line. Two stainless steel 23-gauge cannula were implanted bilaterally 2.5 mm above the DG of the hippocampus, coordinates: AP - 3.6 (Bregma), L  $\pm$  2.2  $\pm$  0.1, DV - 3.0 (skull). The open-field behavior experiment was conducted two weeks after surgery in a repeated-measures design. 8 mice received three different drug conditions: 1:1000 DMSO, 1  $\mu$ M SIRT1 inhibitor IV and 50  $\mu$ M SIRT1 activator 3 in sterile saline and the sequence of three drug application was randomized with one-week interval between any two conditions to avoid interaction between conditions. Mice were handled regularly and habituated for 3 days before every experiment day. On the experiment day, the drugs were injected at a flow rate of 100 nL/min through the

bilateral cannula (PlasticsOne 1mm C315GA 33GA internal cannula) pumped by Osmotic pump and two 250 $\mu$ L infusion syringe (Hamilton) for two minutes. Fifteen minutes after drug infusion, the 5-minute open field test was conducted. Infrared beams and computer-based software *Fusion* was used to track mice and calculate mice activity and time spent in the center (4x4) of open field (8x8). Matlab R2014a was used to calculate the heat map shown in Figure 9.. After all experiments, all mice were sacrificed and the positions of cannula guides are checked with vibratome dissection.

## RESULTS

To confirm effective manipulation of SIRT1 activity by SIRT1 activator 3 and SIRT1 inhibitor IV in acute brain slices, brain slices were incubated in aCSF with 1:1000 DMSO, 50  $\mu$ M SIRT1 activator 3, or 1  $\mu$ M SIRT1 inhibitor IV for 1 hour at room temperature, and the acetylation levels of the well-established SIRT1 substrate, acetylated p53 were tested. Our results showed that the acetylation level of p53 was modulated by 50  $\mu$ M SIRT1 activator and 1  $\mu$ M SIRT1 inhibitor IV bath application (supplementary Figure 2), indicating the validation of the activation and inhibition effects of these chemicals.

## **SIRT1 activity modulates sEPSC and mEPSC frequency recorded in DG granule cells**

In order to determine rapid effects of SIRT1 activation, we first investigated the role of modulation of SIRT1 activity on excitatory synaptic inputs in DG granule cells. Spontaneous excitatory postsynaptic currents (EPSCs) were recorded from DG granule cells in hippocampus slices from control mice before and 10 minutes after application of 1  $\mu$ M SIRT1 inhibitor IV or 50  $\mu$ M SIRT1 activator 3. SIRT1 inhibition had no significant effect on sEPSC amplitude ( $t_{(9)} = 0.87$ ,  $P = 0.40$ ) but significantly increased sEPSC frequency ( $t_{(9)} = 3.13$ ,  $P = 0.01$ ; Fig. 1A). Another SIRT1 inhibitor, sirtinol (30  $\mu$ M) showed a similar increase of sEPSC frequency (supplementary Fig. 3). SIRT1 activation had no significant effect on sEPSC amplitude ( $t_{(10)} = 1.5$ ,  $P = 0.17$ ) but significantly decreased sEPSC frequency ( $t_{(10)} = 4.14$ ,  $P < 0.01$ ; Fig. 1B). Similar effects were observed with another commonly used SIRT1 activator, resveratrol (200  $\mu$ M), which significantly decreased sEPSC frequency in granule cells (supplementary Figure 3). These rapid effects of SIRT1 manipulation suggest that SIRT1 activity bidirectionally modulated glutamatergic neurotransmission independent of gene transcription.

To determine whether the modulation of sEPSC frequency was action potential-dependent, the effect of SIRT1 activity on mEPSC frequency was investigated by pre-incubation of slices in 1  $\mu$ M TTX, a voltage-gated sodium channel blocker. Similar to the effect on spontaneous activity, inhibition of SIRT1 activity significantly increased mEPSC frequency ( $t_{(8)} = 2.65$ ,  $P = 0.03$ ; Fig. 1C) with no significant effect on amplitude ( $t_{(9)} = 0.48$ ,  $P = 0.65$ ); while activation significantly reduced mEPSC frequency ( $t_{(10)} = 2.34$ ,  $P = 0.04$ ; Fig. 1D) with no significant effect on amplitude ( $t_{(10)} = 1.67$ ,  $P = 0.13$ ). These results suggest that SIRT1 activity affected glutamate release from the presynaptic terminal, but the smaller magnitude of the change in mEPSC frequency (SIRT1 activator 3: -7.61% mEPSC frequency vs -19.35% sEPSC frequency; SIRT1 inhibitor IV: +10.65% mEPSC frequency vs +18.74% sEPSC frequency) suggests that SIRT1 activity also regulated the excitability of presynaptic glutamatergic cells.

### **SIRT1 activity modulates spike width and fast afterhyperpolarization (fAHP) amplitude of evoked action potentials in DG granule cells**

We next investigated the rapid effects of SIRT1 activity on granule cell intrinsic properties by investigating changes in the evoked action potentials 15 minutes after

bath application of SIRT1 activator or inhibitor. Manipulation of SIRT1 activity modulated spike width and fast afterhyperpolarization (fAHP) amplitude (Fig. 2A). SIRT1 inhibition significantly increased spike width ( $t_{(11)} = 4.90$ ,  $P < 0.01$ ) and significantly decreased fAHP amplitude ( $t_{(11)} = 4.10$ ,  $P < 0.01$ ). On the other hand, SIRT1 activation had no significant effect on spike width ( $t_{(8)} = 1.79$ ,  $P = 0.11$ ) but did significantly reduce the fAHP amplitude (Fig. 2B;  $t_{(8)} = 3.1$ ,  $P = 0.02$ ). Input resistance, resting potential, and rise time of action potentials were not affected by SIRT1 inhibition or activation (Table 1). These results suggest that SIRT1 rapidly modulated voltage-gated currents that modulate the repolarization phase of action potentials in DG granule cells.

### **BK channels mediate the rapid effect of SIRT1 activity in the DG.**

The decrease in fAHP amplitude and increase in spike width caused by SIRT1 inhibition, in addition to the effects on glutamate release in response to SIRT1 manipulation, suggested the participation of potassium channels that are critical in the repolarization phase of action potentials, specifically, currents formed by BK channels. To test whether changes in these currents participate in the SIRT1 regulation pathway, acute slices were pre-incubated in aCSF with 5  $\mu$ M paxilline, a specific blocker of BK

channels, and the effects of SIRT1 inhibition on spike width and fAHP amplitude were measured (Fig. 3A). Pre-incubation with paxilline blocked the effects of SIRT1 inhibition, such that SIRT1 inhibition had no further significant effect on spike width ( $t_{(8)}=1.25$ ,  $P=0.25$ ) or fAHP amplitude ( $t_{(8)}=0.57$ ,  $P=0.59$ ). This result suggests that BK channels mediate at least part of the effect of SIRT1 activity on spike width and fAHP amplitude in control animals. In addition, we tested the effect of BK channel blockade on sEPSC frequency. Consistent with the effect of BK channel blockade on spike width and fAHP, pre-incubation of slices in aCSF with 5 $\mu$ M paxilline blocked the effect of SIRT1 inhibitor on sEPSC frequency (Fig. 3B,  $t_{(8)}=2.00$ ,  $P=0.08$ ). These results further confirmed BK channels are a possible regulation target of SIRT1 since the BK channel inhibitor blocked the SIRT1 inhibition effect.

### **BK channels $\alpha$ subunits are potential deacetylation targets of cytosolic SIRT1.**

Typically, SIRT1 acts on proteins to remove the acetyl-groups from lysine residues, which may have important regulatory effects on protein-protein interactions or protein function. Since the experiments described suggested that the BK channels are involved in the effects of SIRT1 activity, we hypothesized that the pore-forming BK channel  $\alpha$  subunits are direct targets of SIRT1 deacetylation, and that the two proteins

directly interact. We investigated protein-protein interactions between BK $\alpha$  and SIRT1 using co-immunoprecipitation (co-IP) of hippocampus tissue. Immunoprecipitation with the anti-SIRT1 antibody and immunoblot with the anti-BK $\alpha$  antibody recognized bands at the ~130 kD level of BK $\alpha$  subunit (Fig. 4A). The co-IP bands indicated a protein-protein interaction between BK $\alpha$  and SIRT1. The reciprocal co-IP experiment of immunoprecipitation with the anti-BK $\alpha$  antibody and immunoblot with the anti-SIRT1 antibody (Fig. 4A) recognized a band at the ~80kD level and confirmed the interaction. These results show that BK $\alpha$  and SIRT1 proteins interact.

BK  $\alpha$  subunits also interact with  $\beta$  subunits which are important for modulation of BK properties (B. Wang, Jaffe, & Brenner, 2014). Specifically,  $\beta$ 2 and  $\beta$ 4 subunits are highly expressed in the hippocampus (Brenner et al., 2005; Petrik, Wang, & Brenner, 2011; B. Wang et al., 2016) and are also possible candidates for SIRT1 targets; therefore, we tested whether  $\beta$ 2 and  $\beta$ 4 subunits may also interact with SIRT1. The BK $\alpha$  and SIRT1 IP samples were immunoblotted with BK $\beta$ 2 and BK $\beta$ 4 antibodies (Fig. 4B). The results showed the BK $\beta$  immunoreactivity was recognized in BK $\alpha$  immunoprecipitation sample but not in SIRT1 immunoprecipitation samples, suggesting an interaction with BK $\alpha$  as expected, but no interaction between SIRT1 and BK $\beta$ 2 or BK $\beta$ 4.

To further determine if BK $\alpha$  is a SIRT1 deacetylase substrate, we tested whether native BK  $\alpha$  subunits have acetylated lysine residues. Proteins were immunoprecipitated from fresh hippocampus lysates with the anti-BK $\alpha$  subunit antibody and immunoblotted with anti-acetylated lysine antibody along with the inverse experiment, proteins were immunoprecipitated with the anti-acetylated antibody and immunoblotted with the BK $\alpha$  antibody (Fig. 4C). The Co-IP bands detected in immunoblotting with both antibodies suggested that the BK $\alpha$  subunit was acetylated in the brain.

Finally, to determine whether SIRT1 deacetylates BK $\alpha$  subunits in the hippocampus, we tested whether the acetylation levels of BK $\alpha$  subunit are modulated by SIRT1 activity (Fig. 4D). We immunoprecipitated hippocampus lysates from acute brain slices that were bathed with vehicle, SIRT1 activator 3 or inhibitor IV for 15 minutes with BK $\alpha$  antibodies and tested the acetylation level by immunoblotting with anti-acetylated lysine antibodies. Our results showed the percentage change from control in the ratios between acetylated lysine band intensity and BK $\alpha$  band intensity were significantly different between decreased and increased SIRT1 activity (Student's t-test,  $t_{(8)} = 5.09$ ,  $P < 0.01$ ). SIRT1 activation decreased BK channel acetylation ( $-8 \pm 5\%$ ,  $n=5$ ), while the SIRT1 inhibition increased BK channel acetylation



( $23.35 \pm 3.6\%$ ,  $n=5$ ; Fig. 4D). These immunoprecipitation and immunoblotting experiments showed that BK $\alpha$  is a potential target of SIRT1 deacetylation. These results suggest this deacetylation of the BK $\alpha$  subunit protein by SIRT1 contributed to the rapid effect of SIRT1 activity on the synaptic activity and intrinsic properties of DG granule cells.

**Surface cross-linking experiments indicate SIRT1 activity modulates BK channel membrane distribution.**

Internalization of BK channels is important for their physiological functions (E. Y. Kim, Ridgway, & Dryer, 2007; Leo et al., 2015; Velazquez-Marrero et al., 2016), and protein acetylation has been shown to inhibit protein ubiquitination and trafficking, thus affecting cellular distribution of proteins (Caron, Boyault, & Khochbin, 2005). Therefore, we hypothesized that deacetylation of BK subunits with SIRT1 will affect BK channel internalization and cellular distribution. To test whether SIRT1 activity rapidly affects BK $\alpha$  surface expression, acute brain slices were incubated with 1:1000 DMSO, 50  $\mu$ M SIRT1 activator 3, or 1  $\mu$ M SIRT1 inhibitor IV for 15 minutes prior to cross-linking all surface proteins in the plasma membranes using BS3, a membrane impermeable amine-to-amine crosslinker. Two bands appeared in our immunoblotting results, the

intracellular BK $\alpha$  band around 130kD and the crosslinked membrane BK $\alpha$  band at the top of gels. The ratios between membrane and intracellular BK $\alpha$  immunoreactive bands were determined in these three drug conditions and used to describe BK $\alpha$  subunit internalization and cellular distribution. Our results suggested SIRT1 activation significantly affected BK $\alpha$  subunit surface distribution (Fig. 5, Student's t-test,  $t_{(10)}=2.67$ ,  $P = 0.02$ ), while SIRT1 inhibition had no significant effect on surface BK $\alpha$  expression ( $P = 0.50$ ). This suggests that SIRT1 activation significantly decreased the membrane BK $\alpha$  ratios and facilitated BK channels internalization in acute brain slices.

**CVS-treated rodents showed impaired BK $\alpha$  membrane expression and altered evoked action potential traces in granule cells in the DG.**

Since the previous results from our lab (Ferland et al., 2013; Ferland & Schrader, 2011) demonstrated increased nuclear SIRT1 activity in the hippocampus of animals exposed to CVS, we tested the rapid effects of SIRT1 activity in CVS-treated mice. Stress has been shown to affect glutamatergic transmission in the hippocampus (Joels, Krugers, & Karst, 2008; Karst & Joels, 2003; Nasca, Bigio, Zelli, Nicoletti, & McEwen, 2015),

therefore, we hypothesized that SIRT1 activity may also play a role in the stress-induced regulation of glutamatergic activity (Fig. 6). Interestingly, sEPSC and mEPSC frequency in granule cells from slices from CVS-treated mice did not change in response to SIRT1 inhibition (sEPSC:  $t_{(8)} = 2.2$ ,  $P = 0.06$ , Fig 6A; mEPSC:  $t_{(9)} = 1.53$ ,  $P = 0.16$ ; Fig. 6C) or SIRT1 activation (sEPSC:  $t_{(8)} = 1.28$ ,  $P = 0.24$ , Fig 6B; mEPSC:  $t_{(9)} = 0.47$ ,  $P = 0.65$ , Fig. 6D). The loss of the rapid sensitivity to SIRT1 activity in granule cells from the DG of CVS mice compared to control mice, combined with the previously reported elevated SIRT1 activity in the nuclear-enriched fraction of the DG after CVS exposure, suggest that chronic stress modulated SIRT1 activity at localized targets, cytoplasmic vs nuclear.

We also investigated the rapid effect of SIRT1 activity on action potential repolarization phase in CVS-treated mice. Spike width and fAHP amplitude recorded from granule cells of CVS mice did not change after SIRT1 inhibition (spike width,  $t_{(9)} = 1.71$ ,  $P = 0.13$ ; fAHP amplitude,  $t_{(8)} = 2.04$ ,  $P = 0.08$ ; Fig.7A) and SIRT1 activation (spike width,  $t_{(8)} = 1.61$ ,  $P = 0.15$ ; fAHP amplitude,  $t_{(8)} = 0.72$ ,  $P = 0.49$ , Fig. 7B).

The electrophysiological results also showed that the spike width in CVS mice ( $4.6 \pm 0.11$  ms) had a similar average value compared to that from control mice with paxilline pre-incubation ( $4.86 \pm 0.2$  ms) (Fig. 8). Therefore, we hypothesized that the

loss of sensitivity to SIRT1 activity in CVS DG granule cells may be due to the loss of SIRT1-mediated changes in BK currents. The membrane expression of BK channels in control and CVS-treated animals was determined by immunoblotting with anti-BK $\alpha$  antibody in DG tissue extract. Membrane BK $\alpha$  immunoreactivity decreased significantly in DG extract from CVS-treated rats compared to controls (Fig. 8A, Student's t-test,  $t_{(17)} = 3.33$ ,  $P < 0.01$ ).

We investigated the frequency of action potentials evoked by a family of current injections in the DG granule cells in hippocampus slices from control mice with DMSO, BK blocker treatment (control mice with paxilline) and CVS treatment (CVS with DMSO) (Fig. 8B). Two-way ANOVA test showed the main effect of current injection and treatment, as well as the interaction between these two main effects were significant (two-way ANOVA, current injection:  $F_{(5,230)} = 142.30$ ,  $P < 0.0001$ , treatment:  $F_{(2, 46)} = 5.78$ ,  $P = 0.006$ ; interaction:  $F_{(10,230)} = 4.66$ ,  $P < 0.0001$ ). The post-hoc Bonferroni's test showed action potential frequency in paxilline and CVS treatments are significantly smaller than no treatment (Fig. 8B bottom). This similarity between paxilline and CVS treatment is consistent with the expression data that CVS caused decreased BK membrane expression in the DG.

**Micro-infusion of SIRT1 inhibitor IV or SIRT1 activator 3 into DG rapidly affect mice anxiety behaviors.**

Previous studies have shown that the DG is involved in modulation of anxiety behavior, and signaling in the DG is also important for anxiety-like behaviors (Kheirbek, Klemenhagen, Sahay, & Hen, 2012). To investigate whether the rapid response to SIRT1 activity is important for DG function, we infused SIRT1 inhibitor IV or SIRT1 activator 3 bilaterally through pre-implanted cannulas investigated mice behaviors in an open field within 15 minutes. The positions of the cannulas were confirmed in every mouse after all behavior experiments (Fig. 9A). There were no significant differences in total distance travelled in the open field between the three groups of mice (Fig. 9C, one-way repeated measures ANOVA test,  $F_{(2,12)} = 1.23$ ,  $P = 0.33$ ). The time spent in the center of the open field was significantly affected by SIRT1 activity (Fig. 9D, one-way repeated measures ANOVA test,  $F_{(2,12)} = 9.94$ ,  $P < 0.01$ ). Mice spend more time in the center of the open field 15 minutes after SIRT1 activator 3 infusion (paired t-test,  $t(6) = 2.13$ ,  $P = 0.07$ ) and less time after SIRT1 inhibitor infusion (paired t-test,  $t(6) = 2.58$ ,  $P = 0.04$ ) compared to that after the same amount DMSO infusion. These results showed that rapid effects of SIRT1 activity in the DG can modulate anxiety behavior in a rapid manner.

**Discussion:**

In this study, we demonstrated that SIRT1 activity rapidly modulated glutamatergic synaptic transmission and intrinsic properties in DG granule cells of the hippocampus. SIRT1 inhibition increased the frequency of excitatory synaptic activity and spike width and decreased fAHP amplitude of DG granule cells in hippocampus slices from control mice, while SIRT1 activation decreased the frequency of excitatory synaptic activity and fAHP amplitude. The increased sEPSC frequency and decreased fAHP amplitude caused by SIRT1 inhibition in control slices was blocked by the BK channel-specific blocker, paxilline. This occlusion of the SIRT1 effect by BK channel blockade suggested a role for changes in BK channel activity in response to SIRT1 inhibition and BK channel complexes as possible SIRT1 targets. To further investigate the BK channel  $\alpha$  subunits as potential targets of SIRT1, we found that SIRT1 interacted with BK channel  $\alpha$  subunits but not the  $\beta$ 2 or  $\beta$ 4 subunits, and the  $\alpha$  subunit acetylation levels were modulated by manipulation of SIRT1 activity in hippocampus slices, suggesting direct deacetylation of the BK channel  $\alpha$  subunit by SIRT1. Furthermore, SIRT1 activity modulated BK $\alpha$  subunit surface expression providing a possible mechanism for SIRT1 modulation of BK channel activity.

The rapid effects of SIRT1 modulation on excitatory synaptic activity and action potentials in the hippocampus were absent after chronic stress. A possible mechanism for this lack of effect in stressed animals is that the BK  $\alpha$  subunit expression was decreased after CVS which resulted in functional changes in cell excitability. These changes were mimicked by the effects of paxilline treatment in slices from control mice, suggesting that CVS decreased the SIRT1/BK channel mechanism of rapid changes in intrinsic excitability. Finally, the behavioral data demonstrated that SIRT1 inhibition in the DG of the hippocampus rapidly decreased the time spent in the center of the open field in mice. This modulation of the behavioral response in the open field links the rapid effects of changes in SIRT1 activity that we observed in the slice preparation to modulation of anxiety behaviors mediated by changes in SIRT1 activity in the behaving animal. Thus, SIRT1 can facilitate rapid physiological effects independent of transcriptional effects.

The data demonstrating direct de-acetylation of BK channels to modulate functional activity and surface expression is consistent with the role of protein acetylation as a mechanism of protection from ubiquitination to stabilize proteins. Ubiquitination occurs at lysine sites within the protein amino acid sequence, and acetylation at those sites competitively inhibits ubiquitination and subsequent protein

degradation. Thus, dynamic modulation of acetylation and deacetylation is important for regulation of cell functions in various contexts (Boyault, Sadoul, Pabion, & Khochbin, 2007; Caron et al., 2005; M. Li, Luo, Brooks, & Gu, 2002; T. Li, Diner, Chen, & Cristea, 2012). For example, our results are consistent with the previous study that the deacetylation of a type of peripheral ion channels, epithelial Na<sup>+</sup> channels (ENaC), increased their ubiquitination and decreased membrane expression (Butler, Staruschenko, & Snyder, 2015). Furthermore, our results are also consistent with several studies indicating the important deacetylation function of cytosolic SIRT1 in the general principal of changes in cell and synapse structure. SIRT1 deacetylation of cytoskeleton-associated proteins is an important factor for cell structure and movement such as tubulin (Sadoul, Wang, Diagouraga, & Khochbin, 2011). Cortactin is acetylated by SIRT1 (Y. Zhang et al., 2009) and this dynamic acetylation plays a role in synapse structure and PSD 95 localization (Catarino, Ribeiro, Santos, & Carvalho, 2013). Our research confirmed the deacetylation function of the cytosolic SIRT1 and extends the SIRT1 deacetylation target to ion channels in the brain. Since BK channels are expressed in many neuron types, the deacetylation of BK channels could be an important contributor to synapse structure and function. In addition, BK channels are expressed in cells throughout the body, our data provide another novel mechanism through which SIRT1 can modulate cell



function, which may be used in cells throughout the body. While we did not investigate acetylation sites within the BK amino acid sequence in this study, several candidate sites exist, and the effects of local SIRT1 on acetylation and ubiquitination of these sites within the BK sequence will be investigated in future studies.

Since the DG is implicated in regulation of anxiety and stress behaviors (Kheirbek et al., 2013; Snyder, Soumier, Brewer, Pickel, & Cameron, 2011), the present study focused on the role of SIRT1 in modulation of cell excitability and synaptic inputs of granule cells of the DG. Interestingly, a recent study showed that inhibition of the principal neurons of the DG or CA3 can suppress anxiety (Engin et al., 2016). Consistent with this study, our electrophysiological and behavioral results demonstrated that SIRT1 activation can rapidly decrease glutamatergic excitatory synaptic transmission in the DG and has anxiolytic effects. These effects were detected within 10-20 minutes after pharmacological manipulation of SIRT1 activity, indicating they were independent of gene transcription and likely mediated by cytosolic SIRT1.

Our findings support and provide more details for the theory that SIRT1 links energy metabolism and mood disorder regulation (J. Song & Kim, 2016). SIRT1 activation is NAD<sup>+</sup>-dependent, and NAD<sup>+</sup> is a cofactor that is important in glycolysis and the

Kreb's cycle, key metabolic pathways important to ultimately produce ATP. Depletion of NAD<sup>+</sup> can inhibit glycolysis (Sheline, Behrens, & Choi, 2000), and thus consumption of NAD<sup>+</sup> by SIRT1 activity can modulate gluconeogenic and glycolytic pathways (Rodgers et al., 2005). Interestingly, our preliminary data show that cytosolic SIRT1 activity in DG is increased immediately after acute stress (data not shown), a period of high metabolic activity, which likely enables the important role of SIRT1 rapid effects in responding to acute stress. It is expected that increased SIRT1 activity induced by acute stress would decrease glutamatergic transmission in the DG and relieve anxiety behavior, functioning as an adaptive role after an acute stress. The present study, along with our previous research that showed increased nuclear SIRT1 activity after CVS (Ferland et al., 2013; Ferland & Schrader, 2011), indicate SIRT1 activity and cellular localization in the DG is dependent upon stress conditions, and importantly SIRT1 activity rapidly modulated mouse anxiety behaviors. Taken together, the SIRT1 cytosolic activity increase induced by the metabolic state change in a single stressor may initially contribute to changes in the synaptic inputs and intrinsic properties of DG granule cells which suppress stress-induced anxiety to respond effectively to an acute stressor, but loss of the ability of SIRT1 to affect the

physiological conditions of DG granule cells during chronic stress may contribute to the maladaptive processes that occur in response to repeated stressors.

Our results show that SIRT1/BK pathway is a candidate mechanism for adaptive processes that occur in response to acute stress. Within the brain, ATP is primarily consumed by electrical signaling processes, including synaptic transmission and action potential generation (Harris, Jolivet, & Attwell, 2012). Increased cytosolic SIRT1 activity as demonstrated in our study, likely results in enhanced NAD<sup>+</sup> consumption, and decreased sEPSC frequency in control mice. Since glutamatergic transmission is metabolically highly demanding, the reduction in sEPSC frequency may be an adaptive mechanism to compensate for increased NAD<sup>+</sup> consumption in control mice. However, prolonged stressor or repetitive stressors may cause long-term reductions in NAD<sup>+</sup> levels, thus preventing SIRT1 activation. Indeed, our preliminary data suggest reduced NAD<sup>+</sup> levels after chronic stress (data not shown). Reduced NAD<sup>+</sup> levels are also indicated in various pathological conditions, including physiological conditions such as aging (Canto, Menzies, & Auwerx, 2015) and further limits activity of cytosolic SIRT1 pathway. In this way, the adaptive loss of SIRT1/BK pathway and the concomitant loss of metabolic adaptation may contribute to the formation of depressive disorders under prolonged stress or repeated stressors.



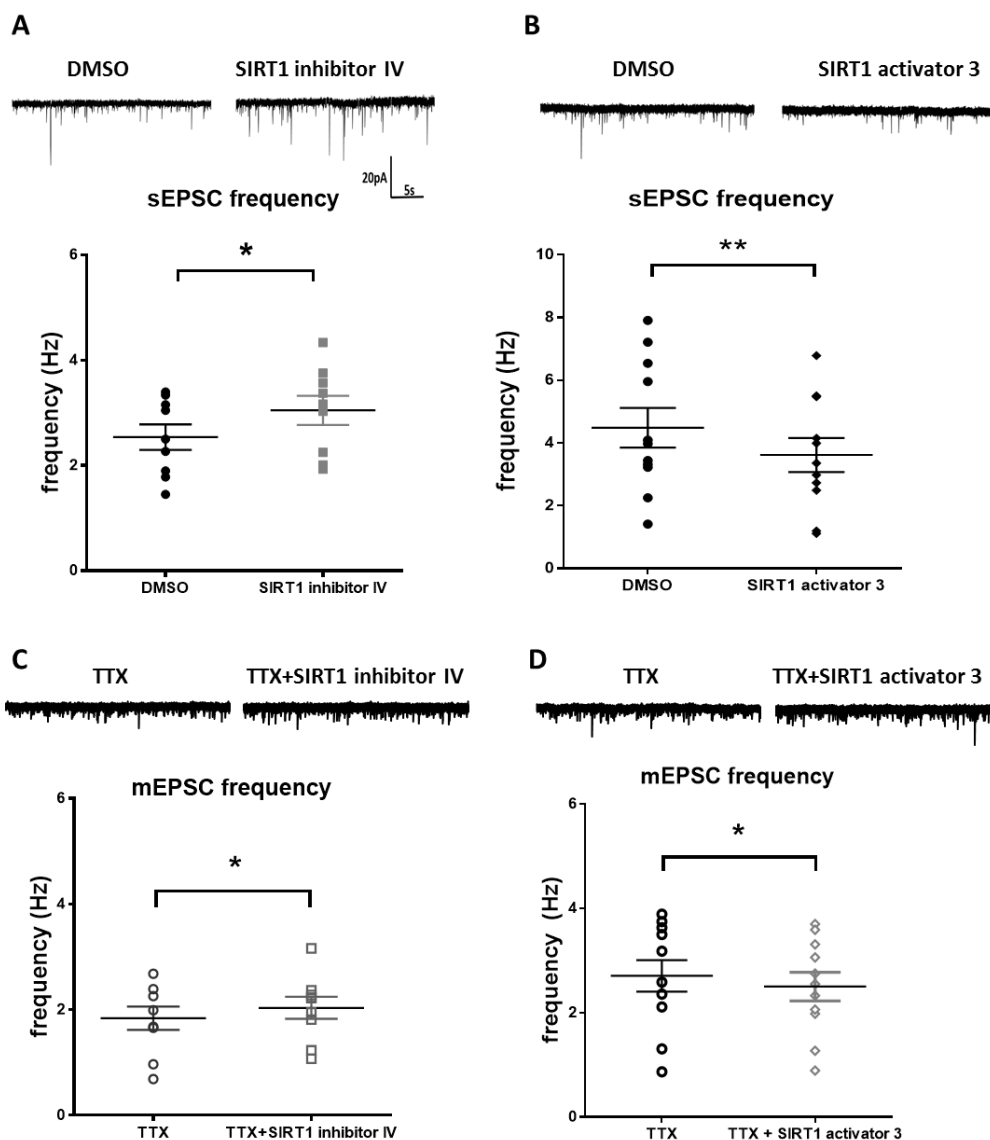


**Figure 1: Modulation of SIRT1 activity regulates excitatory synaptic transmission in DG from hippocampus slices of control mice.** A. SIRT1 inhibition with SIRT1 inhibitor IV (1 $\mu$ M) increased the frequency but not the amplitude of spontaneous excitatory postsynaptic currents (sEPSCs). Above: voltage-clamp recording of sEPSCs recorded at -70 mV from the same cell in control (DMSO) and SIRT1 inhibitor IV. Below: summary plot showing mean frequency from all cells in DMSO and SIRT1 inhibitor IV (n = 10). B. Activation of SIRT1 with SIRT1 activator 3 (50 $\mu$ M) reduced the frequency but not the amplitude of sEPSCs. Above: voltage-clamp recording of sEPSCs recorded at -70 mV. Below: summary plot showing frequency in DMSO and SIRT1 activator 3 (n = 11). C. SIRT1 inhibition (n = 9) increased the frequency but not the amplitude of miniature EPSCs (mEPSCs) compared to control (DMSO). D. SIRT1 activation (n = 11) reduced the frequency of mEPSCs. (\*, P<0.05, \*\*; P < 0.01; paired t-test; mean  $\pm$  SEM shown)

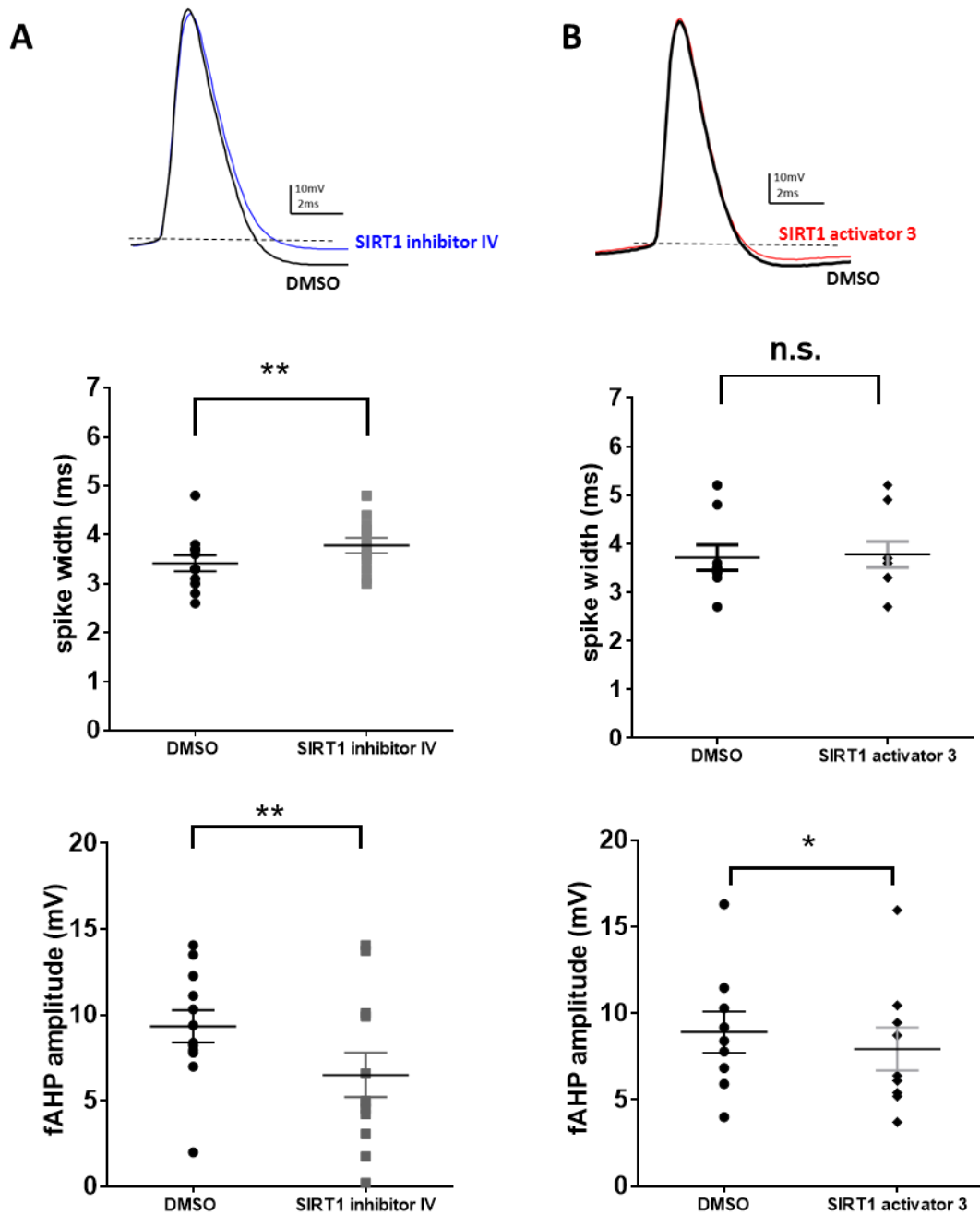


**Figure 2. SIRT1 manipulation increased spike width and decreased fAHP amplitude in the DG granule cells in slices from control mice.** A. SIRT1 inhibition increased spike width and decreased fAHP amplitude. Above: example of action potential recorded in control (black) and in SIRT1 inhibitor IV (blue). The dashed line indicates the threshold voltage which was used to determine the spike width and fAHP amplitude. Below: summary graph showing that SIRT1 inhibitor increased spike-width and decreased fAHP amplitude in dentate granule cells ( $n = 12$ ). B. SIRT1 activation had no effect on spike width but significantly decreased the fAHP amplitude. Above: example of action potential recorded in control (black) and SIRT1 activator (red). Below: SIRT1 activator

had no significant effect on spike width, but significantly decreased fAHP amplitude (n = 9). (\*,  $P < 0.05$ , \*\*;  $P < 0.01$ ; n.s., not significant; paired t-test; mean  $\pm$  SEM shown)

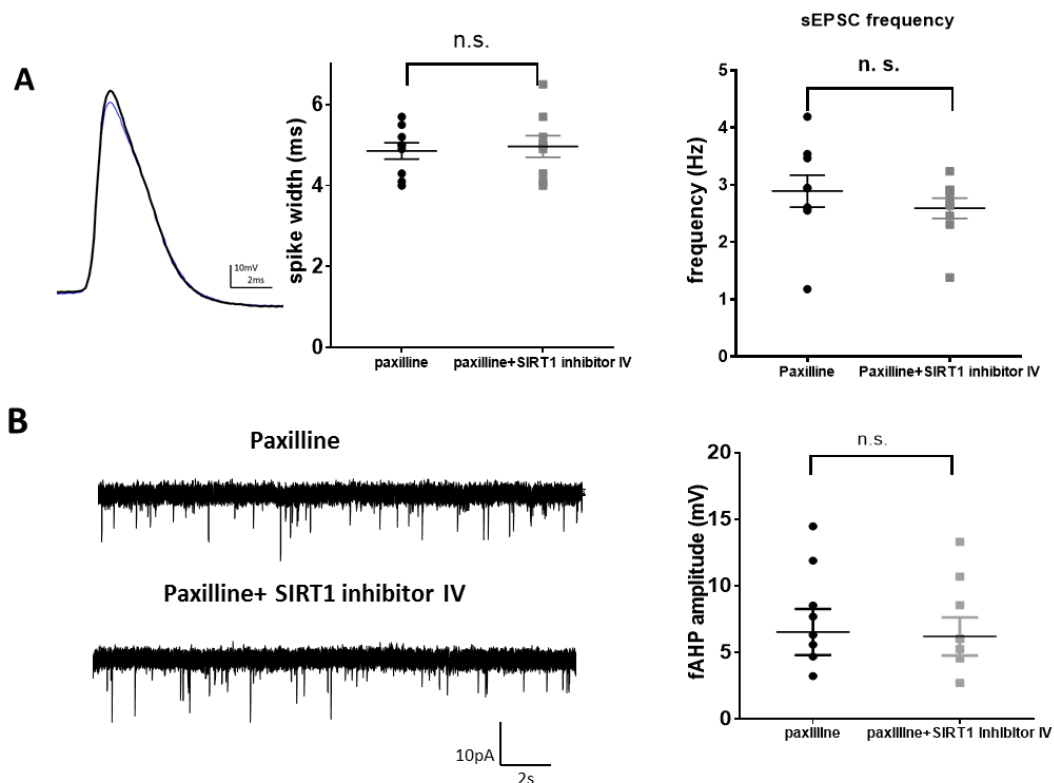


**Figure 3. Paxilline pre-incubation blocked the effects of SIRT1 inhibition on spike width and fAHP amplitude** A. Preincubation of slices with paxilline to block BK channels blocked the effects of SIRT1 inhibition of spike width and fAHP amplitude ( $n = 9$ ). Left: the overlapped spike trace before (black) and after (blue) application of SIRT1 inhibitor IV in cells pre-incubated with paxilline. B. Preincubation with paxilline blocked the effect of SIRT1 inhibition on sEPSC frequency ( $n = 9$ ). (n.s., not significant; paired t-test, mean  $\pm$  SEM shown).



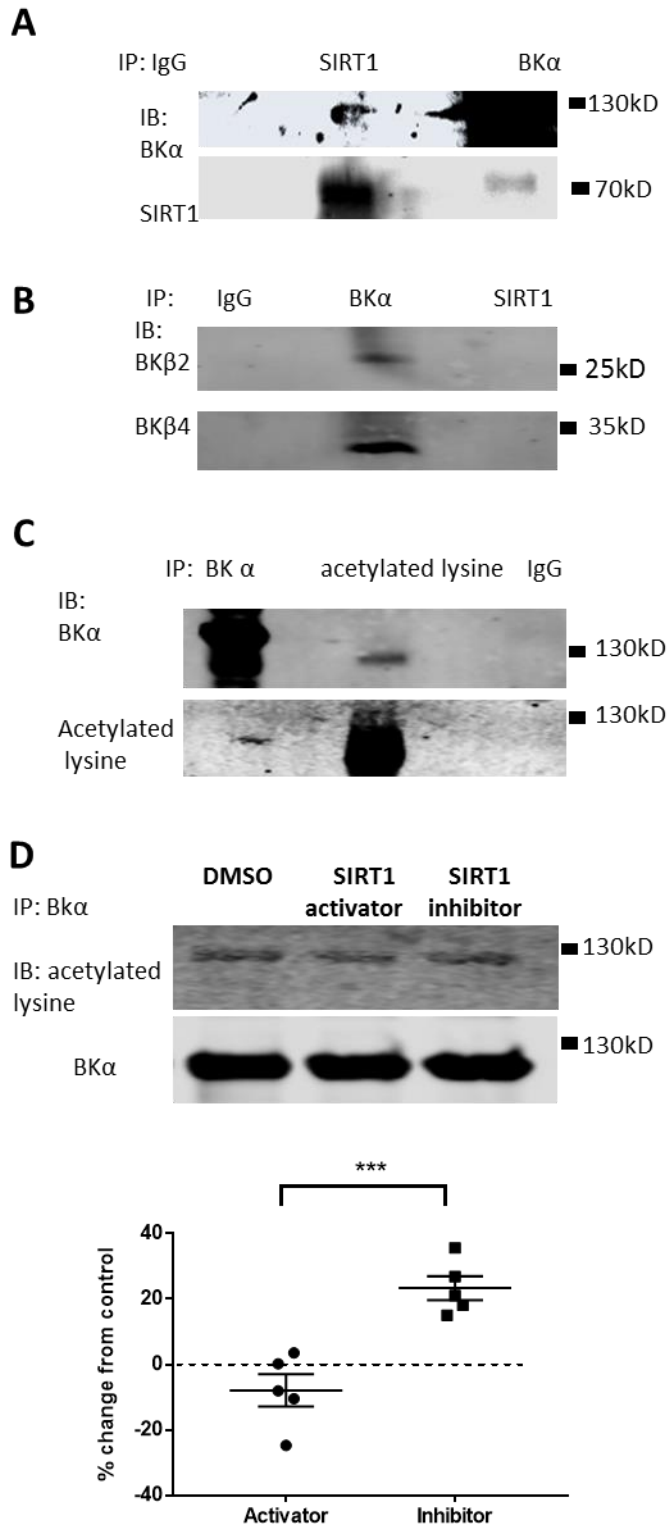


**Figure 4. The BK  $\alpha$  subunit interacts with SIRT1 and is a target of SIRT1.** A. Immunoprecipitation (IP) with SIRT1 and immunoblot with BK  $\alpha$  antibody and IP with BK  $\alpha$  and IB with SIRT1 shows that SIRT1 and BK  $\alpha$  interact. B. IP with BK  $\alpha$  subunit shows that BK  $\beta$  subunits interacted with the  $\alpha$  subunit but not with SIRT1. C. Co-IP with the BK $\alpha$  subunit and anti-acetylated lysine antibody shows that BK  $\alpha$  is acetylated.

D. Above: SIRT1 activation and inhibition in slices and subsequent IP with the BK subunit and immunoblot with the anti-acetylated lysine antibody demonstrated that the BK  $\alpha$  subunit is acetylated in hippocampus slices and the acetylation level is regulated by SIRT1 activity. Below: summary bar graph of BK  $\alpha$  acetylation showing the percent change from control (DMSO) in the SIRT1 activation and inhibition experiments. SIRT1 activity modulates BK  $\alpha$  acetylation (\*\*\*,  $p < 0.001$ , Student's t-test, mean  $\pm$  SEM shown).

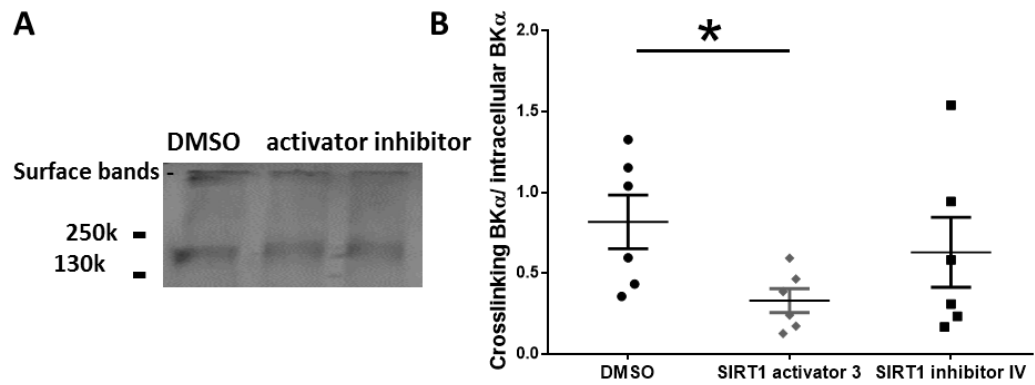


**Figure 5: SIRT1 manipulation affects BK $\alpha$  surface expression. BS3 crosslinking of surface proteins shows that SIRT1 activation affected membrane BK $\alpha$  distribution and enhances internalization. SIRT1 activation significantly decreased BK $\alpha$  surface expression (\*, Student's t-test, P = 0.02).**

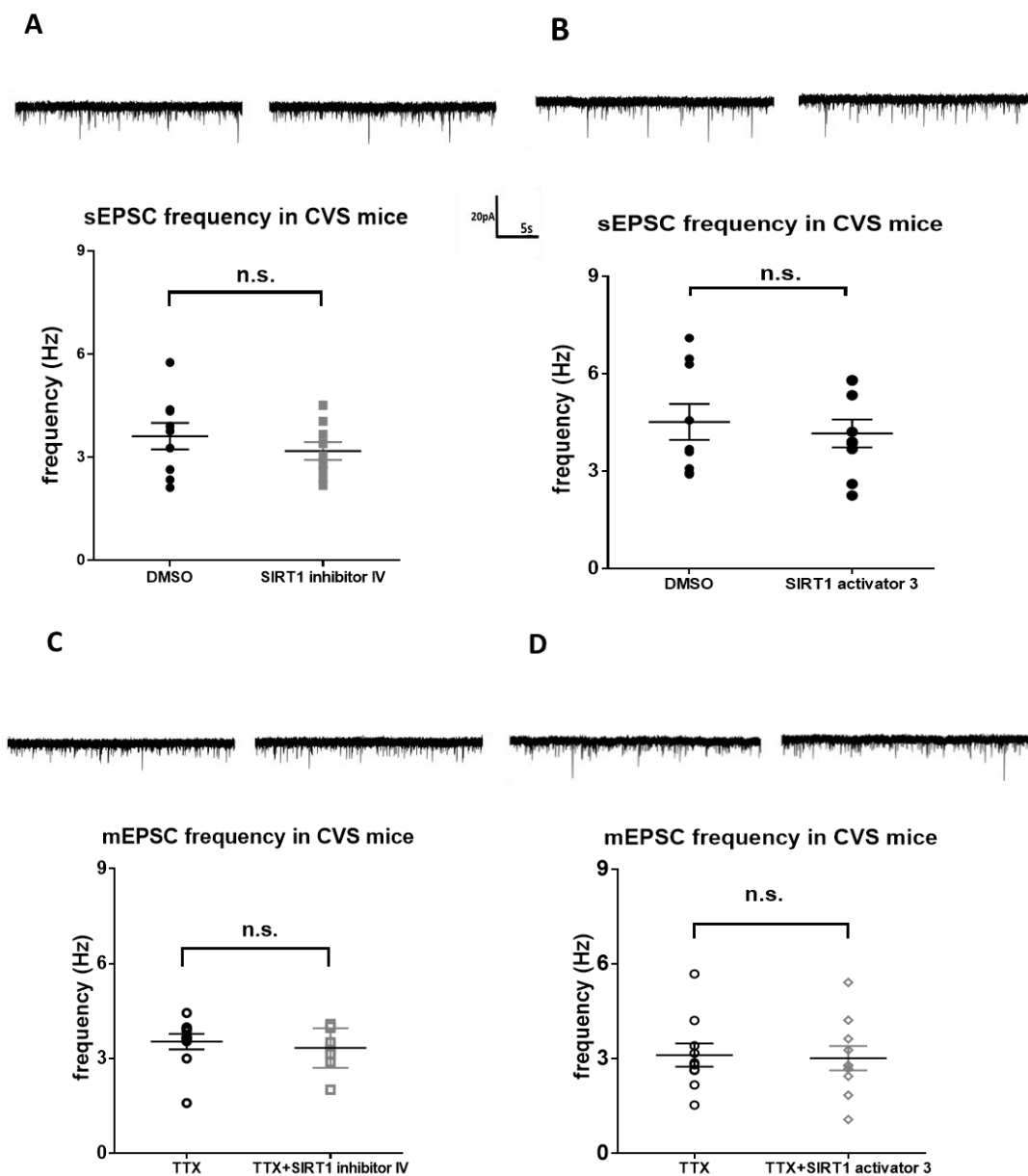


**Figure 6: Modulation of SIRT1 activity had no effect on excitatory synaptic transmission in DG from hippocampus slices of CVS-treated mice.** A. SIRT1 inhibition with SIRT1 inhibitor IV (1 $\mu$ M) had no effect on spontaneous excitatory postsynaptic currents (sEPSCs) in slices from CVS-treated mice. Above: voltage-clamp recording of sEPSCs recorded at -70 mV from the same cell in vehicle (DMSO) and SIRT1 inhibitor IV. Below: summary plot showing average sEPSC frequency from all cells in DMSO and SIRT1 inhibitor IV (n = 9). B. Activation of SIRT1 had no significant effect on the frequency of sEPSCs in slices from CVS-treated mice. Above: voltage-clamp recording of sEPSCs recorded at -70 mV. Below: summary plot showing frequency in DMSO and SIRT1 activator (n = 9). C. SIRT1 inhibition (n = 10) had no significant effect on the frequency of miniature EPSCs (mEPSCs) compared to vehicle (DMSO) in slices from

CVS-treated mice. D. SIRT1 activation (n = 10) reduced the frequency of mEPSCs in slices from CVS-treated mice. (n.s., not significant, paired t-test, mean  $\pm$  SEM shown)

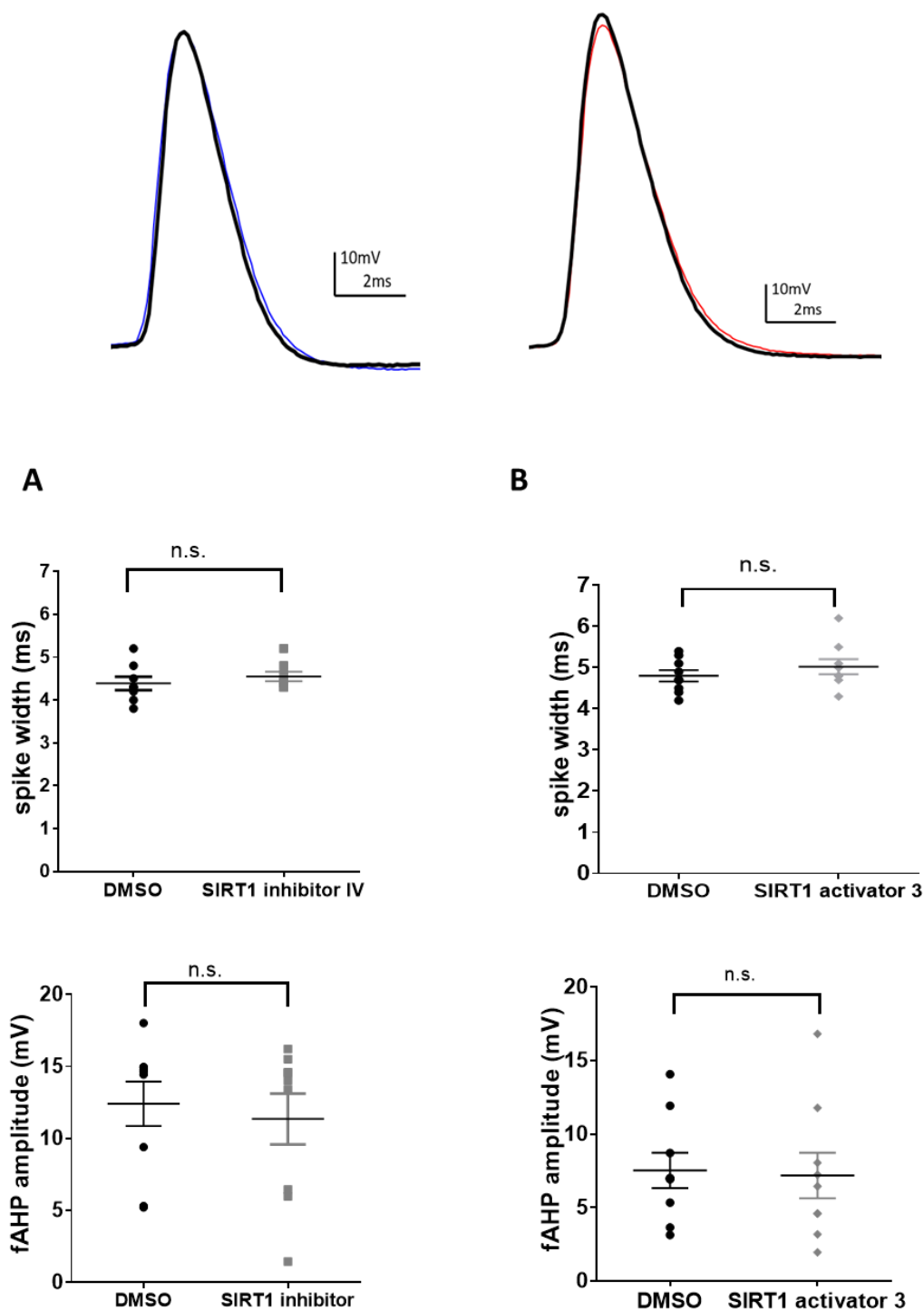


**Figure 7. SIRT1 manipulation had no effect on spike width and fAHP amplitude in the DG granule cells in slices from CVS-treated mice.** A. SIRT1 inhibition had no significant effect on spike width or fAHP amplitude. Above: example of action potential recorded in control (black) and in SIRT1 inhibitor (blue). Below: summary plot showing that SIRT1 inhibitor had no significant effect on spike width or fAHP amplitude ( $n = 9$ ) in slices from CVS-treated mice. B. SIRT1 activation had no effect on spike width or fAHP

amplitude. Above: example of action potential recorded in control (black) and SIRT1 activator (red). Below: summary plot showing that SIRT1 activation had no significant effect on spike width or fAHP amplitude in slices from CVS-treated mice (n = 9). (n.s., not significant, paired t-test, mean  $\pm$  SEM shown).

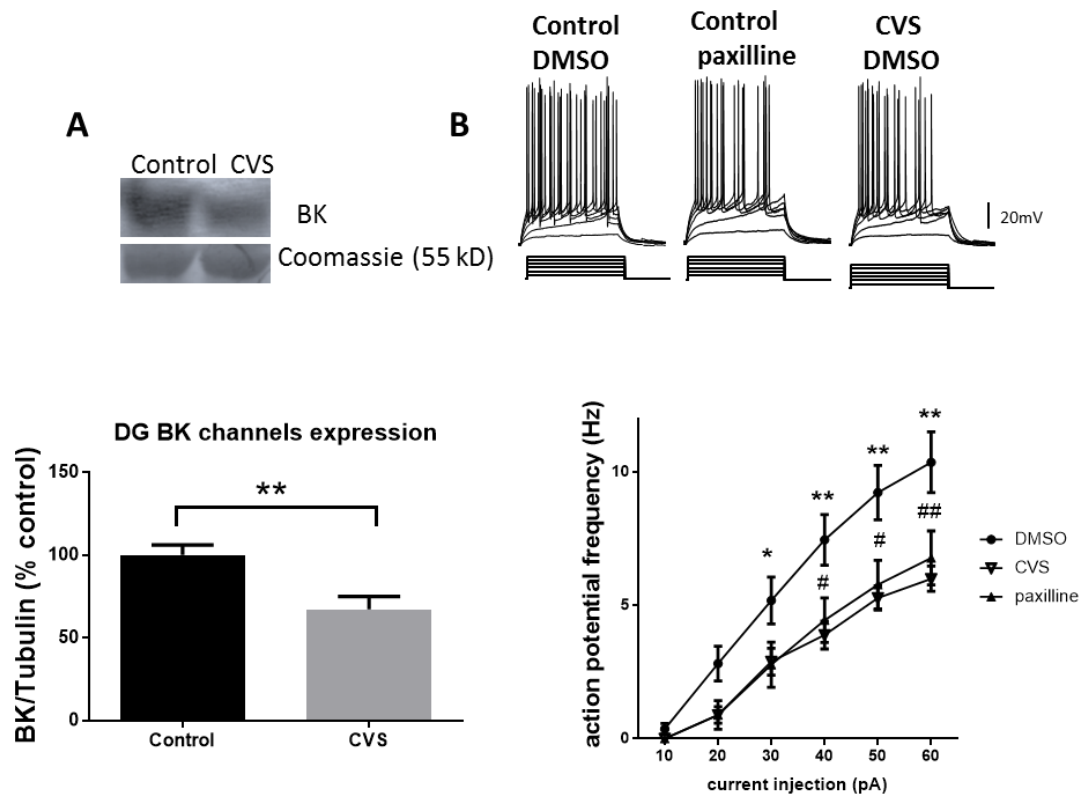


Figure 8. CVS treatment decreased membrane BK $\alpha$  expression and action potential frequency. A. Western blot showing that BK  $\alpha$  subunit expression was decreased in the dentate gyrus of CVS-treated rats compared to controls. B. Electrophysiological recordings show that paxilline decreased the frequency of action potentials evoked by a family of current injection ranging from 10pA to 60pA for 1 second in DG granule cells in slices from control animals, and that effect was similar to the frequency of action potentials recorded in granule cells from CVS-treated mice. (\* or #,  $p < 0.05$ ; \*\* or ##,  $p < 0.01$ ; \*\*\* or ###,  $p < 0.001$ ; \* shown post-hoc significance between DMSO and CVS treatment; # shown post-hoc significance between DMSO and paxilline treatment. Repeated measures ANOVA and post-hoc Bonferroni's test).



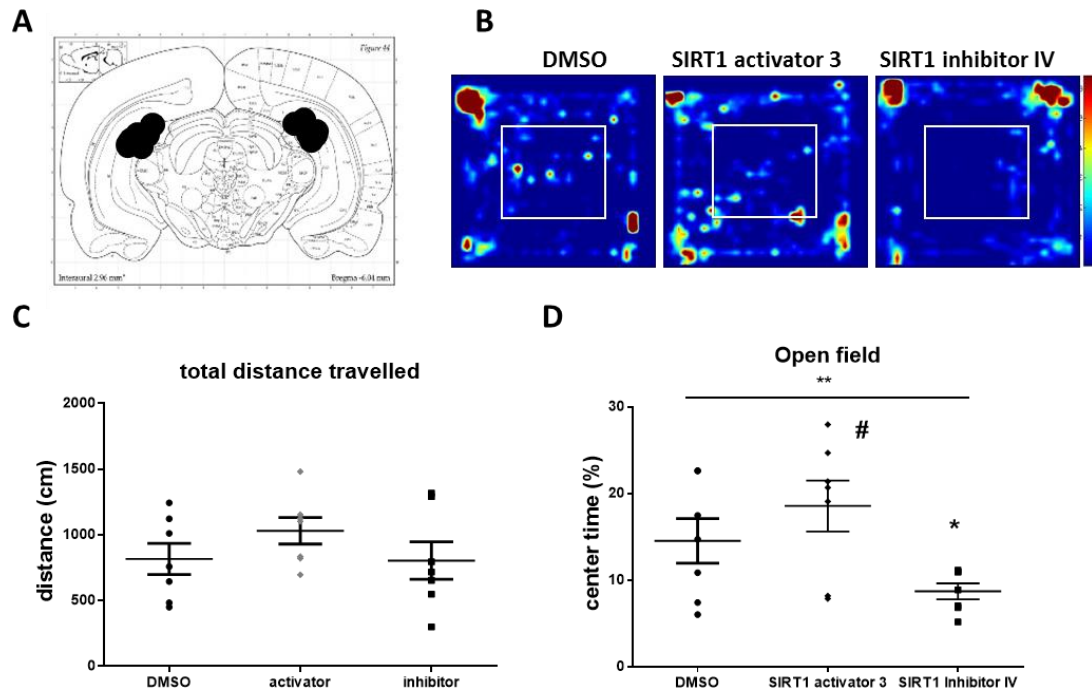
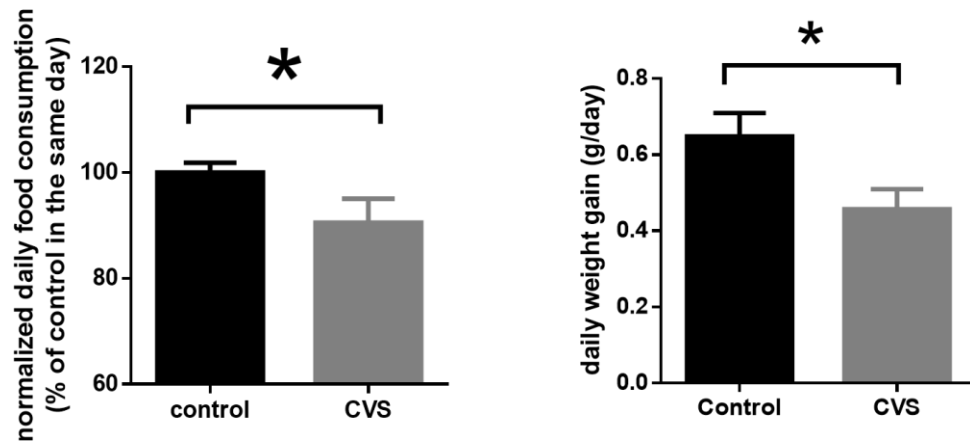
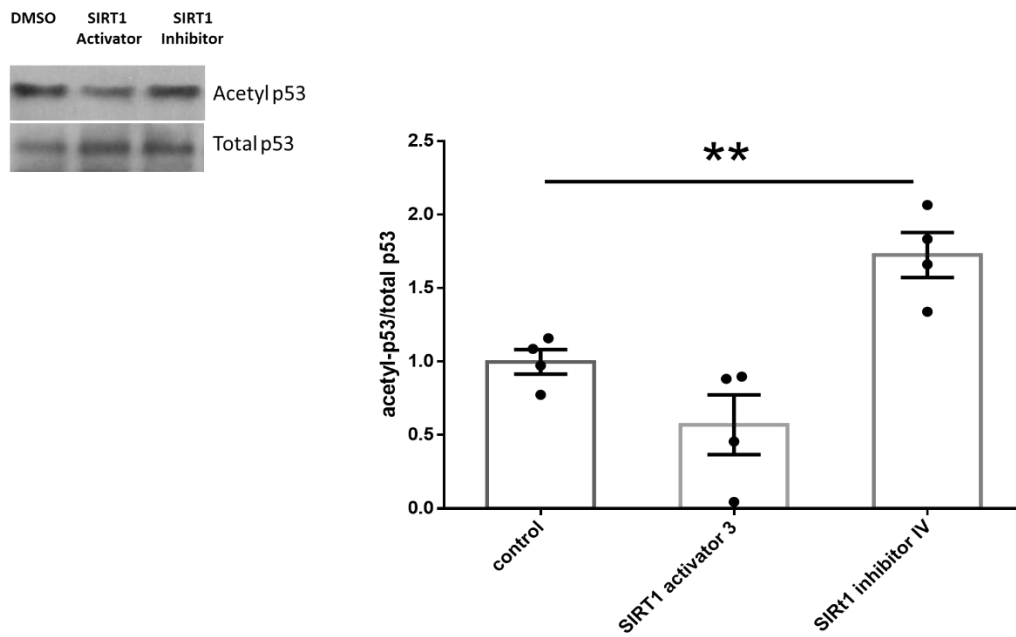


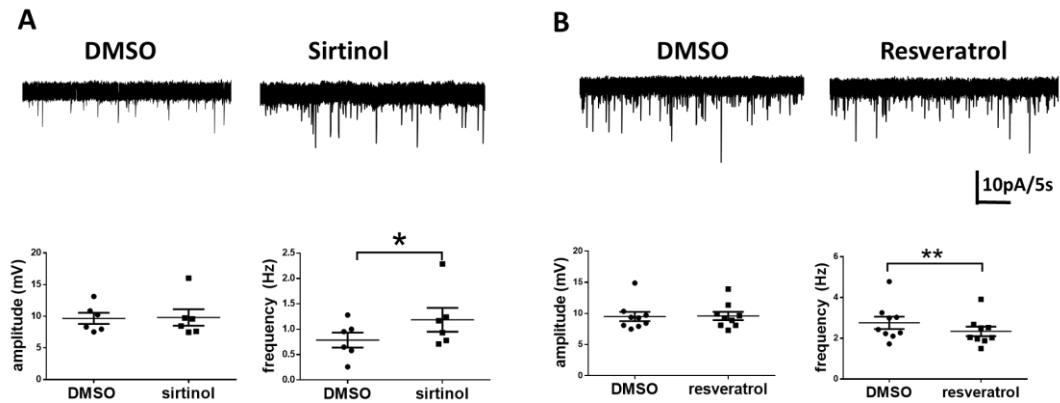
Figure 9. Direct infusion of SIRT1 inhibitor IV and SIRT1 activator 3 into the DG rapidly affected mice anxiety behavior in open field test. A. Injection points locating at Paxinos and Watson atlas demonstrate placement of infusions into the DG. B. Example heat map of time spent in the field from the same mouse when infused with saline with DMSO, SIRT1 activator or SIRT1 inhibitor. C. Summary plot of distance travelled in the open field. D. Summary plot of percent time spent exploring in the center of the field. The results indicated SIRT1 activity significantly affected the time spent in the center (one-way repeated measures ANOVA, \*\*,  $P<0.01$ ). SIRT1 activator 3 perfusion increased the time spent in the center (paired t-test, #,  $P=0.07$ ) and SIRT1 inhibitor IV perfusion significantly decreased the time spent in the center of the arena (paired t-test, \*,  $P<0.05$ ).



**Supplementary Figure 1. CVS-treated mice consumed significantly less food and gained significant less weight compared to control mice.** Food consumption (left) and weight gain (right) were monitored every day to determine the physiological conditions of the CVS-treated animals. CVS significantly reduced food consumption and weight gain, these results indicate that the the efficiency of our CVS protocols (\*,  $P < 0.05$ )



**Supplementary Figure 2. SIRT1 activator 3 and SIRT1 inhibitor IV modulated the acetylation level of p53.** We tested whether our SIRT1 activator IV and activator 3 could modulate protein acetylation level in our acute brain slices using the ratio between acetylated p53 and p53. One way ANOVA showed acetylation level of p53 is significantly regulated by SIRT1 drugs (one-way ANOVA,  $F_{(2,9)} = 14.26$ ,  $P < 0.01$ ).



**Supplementary Figure 3. Sirtinol and Resveratrol regulated sEPSC frequency in the dentate gyrus granule cells in the same way as SIRT1 inhibitor IV and SIRT1 activator 3, respectively.** A. Top: example sEPSC recording from the same cell before and after application of 30  $\mu$ M Sirtinol at a holding potential of -70mV. Sirtinol application significantly increased sEPSC frequency ( $t(5)=2.69$ ,  $P=0.04$ ) but no significant effect on sEPSC amplitude (paired t-test,  $t(5)=0.25$ ,  $P=0.81$ ). B. top traces are sEPSC recording from the same cell before and after application of 200  $\mu$ M resveratrol at a holding potential of -70mV. Resvetral application significantly decreased sEPSC frequency (paired t-test,  $t(8)=4.01$ ,  $P<0.01$ ) but no significant effect on sEPSC amplitude (paired t-test,  $t(8)=0.37$ ,  $P=0.72$ ).

		$V_m$ (mV)	$R_{input}$ (M $\Omega$ )	sEPSC amplitude (pA)	sEPSC decay time constant (ms)	mEPSC amplitude (pA)	mEPSC decay time constant (ms)	AP rise time (ms)
SIRT1 inhibitor IV (1 $\mu$ M)	control	-73.34 $\pm$ 0.87	589.67 $\pm$ 41.15	8.78 $\pm$ 0.58	4.47 $\pm$ 0.39	8.41 $\pm$ 0.59	5.35 $\pm$ 0.22	2.026 $\pm$ 0.358
	drug	-73.65 $\pm$ 0.84	548.67 $\pm$ 60.80	8.58 $\pm$ 0.51	4.68 $\pm$ 0.36	8.20 $\pm$ 0.41	4.96 $\pm$ 0.27	1.88 $\pm$ 0.225
SIRT1 activator 3 (50 $\mu$ M)	Control	-72.1 $\pm$ 2.00	498.36 $\pm$ 40.92	9.35 $\pm$ 0.51	4.13 $\pm$ 0.19	7.53 $\pm$ 0.28	4.15 $\pm$ 0.16	2.134 $\pm$ 0.249
	drug	-69.34 $\pm$ 2.76	513.09 $\pm$ 38.79	8.80 $\pm$ 0.61	4.15 $\pm$ 0.19	7.43 $\pm$ 0.28	4.37 $\pm$ 0.16	2.014 $\pm$ 0.219
CVS+ SIRT1 inhibitor IV (1 $\mu$ M)	CVS	-71.64 $\pm$ 2.43	487.33 $\pm$ 40.07	7.92 $\pm$ 0.33	4.48 $\pm$ 0.19	7.34 $\pm$ 0.25	4.08 $\pm$ 0.28	2.83 $\pm$ 0.24
	CVS+drug	-72.84 $\pm$ 3.31	496.45 $\pm$ 29.06	7.71 $\pm$ 0.34	4.55 $\pm$ 0.28	7.27 $\pm$ 0.28	4.12 $\pm$ 0.29	2.72 $\pm$ 0.22
CVS+ SIRT1 activator 3 (50 $\mu$ M)	CVS	-70.52 $\pm$ 2.40	554.14 $\pm$ 47.65	8.11 $\pm$ 0.45	4.18 $\pm$ 0.14	7.56 $\pm$ 0.26	4.09 $\pm$ 0.23	2.26 $\pm$ 0.21
	CVS+drug	-73.00 $\pm$ 2.34	569.52 $\pm$ 42.23	7.65 $\pm$ 0.36	4.15 $\pm$ 0.17	7.28 $\pm$ 0.30	4.05 $\pm$ 0.25	2.23 $\pm$ 1.96

**Table 1. Some properties of dentate gyrus granule cells recorded before and after drug application in control and CVS mice. No significance found;  $V_m$ : resting potentials;  $R_{input}$ : input resistance tested at the voltage of -65mV; AP: action potentials; mean $\pm$ SEM shown.**

## REFERENCES

- Cai et al., (2015). "Sparse whole-genome sequencing identifies two loci for major depressive disorder." Nature **523**(7562): 588-591.
- Abe-Higuchi, N., S. Uchida, H. Yamagata, F. Higuchi, T. Hobara, K. Hara, A. Kobayashi and Y. Watanabe (2016). "Hippocampal Sirtuin 1 Signaling Mediates Depression-like Behavior." Biol Psychiatry **80**(11): 815-826.
- Bai, W. and X. Zhang (2016). "Nucleus or cytoplasm? The mysterious case of SIRT1's subcellular localization." Cell Cycle **15**(24): 3337-3338.
- Boyault, C., K. Sadoul, M. Pabion and S. Khochbin (2007). "HDAC6, at the crossroads between cytoskeleton and cell signaling by acetylation and ubiquitination." Oncogene **26**(37): 5468-5476.
- Brenner, R., Q. H. Chen, A. Vilaythong, G. M. Toney, J. L. Noebels and R. W. Aldrich (2005). "BK channel beta4 subunit reduces dentate gyrus excitability and protects against temporal lobe seizures." Nat Neurosci **8**(12): 1752-1759.
- Butler, P. L., A. Staruschenko and P. M. Snyder (2015). "Acetylation stimulates the epithelial sodium channel by reducing its ubiquitination and degradation." J Biol Chem **290**(20): 12497-12503.
- Canto, C., K. J. Menzies and J. Auwerx (2015). "NAD(+) Metabolism and the Control of Energy Homeostasis: A Balancing Act between Mitochondria and the Nucleus." Cell Metab **22**(1): 31-53.
- Caron, C., C. Boyault and S. Khochbin (2005). "Regulatory cross-talk between lysine acetylation and ubiquitination: role in the control of protein stability." Bioessays **27**(4): 408-415.
- Catarino, T., L. Ribeiro, S. D. Santos and A. L. Carvalho (2013). "Regulation of synapse composition by protein acetylation: the role of acetylated cortactin." J Cell Sci **126**(Pt 1): 149-162.
- Engin, E., K. S. Smith, Y. Gao, D. Nagy, R. A. Foster, E. Tsvetkov, R. Keist, F. Crestani, J. M. Fritschy, V. Y. Bolshakov, M. Hajos, S. A. Heldt and U. Rudolph (2016). "Modulation of anxiety and fear via distinct intrahippocampal circuits." Elife **5**: e14120.
- Fabrizio, P., C. Gattazzo, L. Battistella, M. Wei, C. Cheng, K. McGrew and V. D. Longo (2005). "Sir2 blocks extreme life-span extension." Cell **123**(4): 655-667.
- Ferland, C. L., W. R. Hawley, R. E. Puckett, K. Wineberg, F. D. Lubin, G. P. Dohanich and L. A. Schrader (2013). "Sirtuin activity in dentate gyrus contributes to chronic stress-induced behavior and extracellular signal-regulated protein kinases 1 and 2 cascade changes in the hippocampus." Biol Psychiatry **74**(12): 927-935.

- Ferland, C. L. and L. A. Schrader (2011). "Regulation of histone acetylation in the hippocampus of chronically stressed rats: a potential role of sirtuins." Neuroscience **174**: 104-114.
- Haigis, M. C. and D. A. Sinclair (2010). "Mammalian sirtuins: biological insights and disease relevance." Annu Rev Pathol **5**: 253-295.
- Harris, J. J., R. Jolivet and D. Attwell (2012). "Synaptic energy use and supply." Neuron **75**(5): 762-777.
- Imai, S., C. M. Armstrong, M. Kaeberlein and L. Guarente (2000). "Transcriptional silencing and longevity protein Sir2 is an NAD-dependent histone deacetylase." Nature **403**(6771): 795-800.
- Imai, S. and L. Guarente (2010). "Ten years of NAD-dependent SIR2 family deacetylases: implications for metabolic diseases." Trends Pharmacol Sci **31**(5): 212-220.
- Jeong, J. K., M. H. Moon, B. C. Bae, Y. J. Lee, J. W. Seol, H. S. Kang, J. S. Kim, S. J. Kang and S. Y. Park (2012). "Autophagy induced by resveratrol prevents human prion protein-mediated neurotoxicity." Neurosci Res **73**(2): 99-105.
- Joels, M., H. Krugers and H. Karst (2008). "Stress-induced changes in hippocampal function." Prog Brain Res **167**: 3-15.
- Kaeberlein, M., M. McVey and L. Guarente (1999). "The SIR2/3/4 complex and SIR2 alone promote longevity in *Saccharomyces cerevisiae* by two different mechanisms." Genes Dev **13**(19): 2570-2580.
- Kakefuda, K., Y. Fujita, A. Oyagi, K. Hyakkoku, T. Kojima, K. Umemura, K. Tsuruma, M. Shimazawa, M. Ito, Y. Nozawa and H. Hara (2009). "Sirtuin 1 overexpression mice show a reference memory deficit, but not neuroprotection." Biochem Biophys Res Commun **387**(4): 784-788.
- Karst, H. and M. Joels (2003). "Effect of chronic stress on synaptic currents in rat hippocampal dentate gyrus neurons." J Neurophysiol **89**(1): 625-633.
- Kheirbek, M. A., L. J. Drew, N. S. Burghardt, D. O. Costantini, L. Tannenholz, S. E. Ahmari, H. Zeng, A. A. Fenton and R. Hen (2013). "Differential control of learning and anxiety along the dorsoventral axis of the dentate gyrus." Neuron **77**(5): 955-968.
- Kheirbek, M. A., K. C. Klemenhagen, A. Sahay and R. Hen (2012). "Neurogenesis and generalization: a new approach to stratify and treat anxiety disorders." Nat Neurosci **15**(12): 1613-1620.
- Kim, E. Y., L. D. Ridgway and S. E. Dryer (2007). "Interactions with filamin A stimulate surface expression of large-conductance Ca<sup>2+</sup>-activated K<sup>+</sup> channels in the absence of direct actin binding." Mol Pharmacol **72**(3): 622-630.
- Kim, S. J., Z. Ao, G. Warnock and C. H. McIntosh (2013). "Incretin-stimulated interaction

between beta-cell Kv1.5 and Kvbeta2 channel proteins involves acetylation/deacetylation by CBP/Sirt1." Biochem J **451**(2): 227-234.

Kishi, T., R. Yoshimura, T. Kitajima, T. Okochi, T. Okumura, T. Tsunoka, Y. Yamanouchi, Y. Kinoshita, K. Kawashima, Y. Fukuo, H. Naitoh, W. Umene-Nakano, T. Inada, J. Nakamura, N. Ozaki and N. Iwata (2010). "SIRT1 gene is associated with major depressive disorder in the Japanese population." J Affect Disord **126**(1-2): 167-173.

Leo, M. D., S. Bulley, J. P. Bannister, K. P. Kuruvilla, D. Narayanan and J. H. Jaggar (2015). "Angiotensin II stimulates internalization and degradation of arterial myocyte plasma membrane BK channels to induce vasoconstriction." Am J Physiol Cell Physiol **309**(6): C392-402.

Li, M., J. Luo, C. L. Brooks and W. Gu (2002). "Acetylation of p53 inhibits its ubiquitination by Mdm2." J Biol Chem **277**(52): 50607-50611.

Li, T., B. A. Diner, J. Chen and I. M. Cristea (2012). "Acetylation modulates cellular distribution and DNA sensing ability of interferon-inducible protein IFI16." Proc Natl Acad Sci U S A **109**(26): 10558-10563.

Li, Y., W. Xu, M. W. McBurney and V. D. Longo (2008). "Sirt1 inhibition reduces IGF-1/IRS-2/Ras/ERK1/2 signaling and protects neurons." Cell Metab **8**(1): 38-48.

Libert, S., K. Pointer, E. L. Bell, A. Das, D. E. Cohen, J. M. Asara, K. Kapur, S. Bergmann, M. Preisig, T. Otowa, K. S. Kendler, X. Chen, J. M. Hetteema, E. J. van den Oord, J. P. Rubio and L. Guarente (2011). "SIRT1 activates MAO-A in the brain to mediate anxiety and exploratory drive." Cell **147**(7): 1459-1472.

McDermott, C. M. and L. A. Schrader (2011). "Activation of kappa opioid receptors increases intrinsic excitability of dentate gyrus granule cells." J Physiol **589**(Pt 14): 3517-3532.

Nasca, C., B. Bigio, D. Zelli, F. Nicoletti and B. S. McEwen (2015). "Mind the gap: glucocorticoids modulate hippocampal glutamate tone underlying individual differences in stress susceptibility." Mol Psychiatry **20**(6): 755-763.

Nayagam, V. M., X. Wang, Y. C. Tan, A. Poulsen, K. C. Goh, T. Ng, H. Wang, H. Y. Song, B. Ni, M. Entzeroth and W. Stunkel (2006). "SIRT1 modulating compounds from high-throughput screening as anti-inflammatory and insulin-sensitizing agents." J Biomol Screen **11**(8): 959-967.

Petrik, D., B. Wang and R. Brenner (2011). "Modulation by the BK accessory beta4 subunit of phosphorylation-dependent changes in excitability of dentate gyrus granule neurons." Eur J Neurosci **34**(5): 695-704.

Porcu, M. and A. Chiarugi (2005). "The emerging therapeutic potential of sirtuin-interacting drugs: from cell death to lifespan extension." Trends Pharmacol Sci **26**(2):



94-103.

Rodgers, J. T., C. Lerin, W. Haas, S. P. Gygi, B. M. Spiegelman and P. Puigserver (2005). "Nutrient control of glucose homeostasis through a complex of PGC-1alpha and SIRT1." Nature **434**(7029): 113-118.

Rogina, B. and S. L. Helfand (2004). "Sir2 mediates longevity in the fly through a pathway related to calorie restriction." Proc Natl Acad Sci U S A **101**(45): 15998-16003.

Sadoul, K., J. Wang, B. Diagouraga and S. Khochbin (2011). "The tale of protein lysine acetylation in the cytoplasm." J Biomed Biotechnol **2011**: 970382.

Satoh, A., S. I. Imai and L. Guarente (2017). "The brain, sirtuins, and ageing." Nat Rev Neurosci **18**(6): 362-374.

Sheline, C. T., M. M. Behrens and D. W. Choi (2000). "Zinc-induced cortical neuronal death: contribution of energy failure attributable to loss of NAD(+) and inhibition of glycolysis." J Neurosci **20**(9): 3139-3146.

Snyder, J. S., A. Soumier, M. Brewer, J. Pickel and H. A. Cameron (2011). "Adult hippocampal neurogenesis buffers stress responses and depressive behaviour." Nature **476**(7361): 458-461.

Song, J. and J. Kim (2016). "Role of Sirtuins in Linking Metabolic Syndrome with Depression." Front Cell Neurosci **10**: 86.

Song, N. Y. and Y. J. Surh (2012). "Janus-faced role of SIRT1 in tumorigenesis." Ann N Y Acad Sci **1271**: 10-19.

Tang, B. L. (2009). "Sirt1's complex roles in neuroprotection." Cell Mol Neurobiol **29**(8): 1093-1103.

Tanno, M., J. Sakamoto, T. Miura, K. Shimamoto and Y. Horio (2007). "Nucleocytoplasmic shuttling of the NAD<sup>+</sup>-dependent histone deacetylase SIRT1." J Biol Chem **282**(9): 6823-6832.

Tissenbaum, H. A. and L. Guarente (2001). "Increased dosage of a sir-2 gene extends lifespan in *Caenorhabditis elegans*." Nature **410**(6825): 227-230.

Velazquez-Marrero, C., A. Burgos, J. O. Garcia, S. Palacio, H. G. Marrero, A. Bernardo, J. Perez-Laspiur, M. Rivera-Oliver, G. Seale and S. N. Treistman (2016). "Alcohol Regulates BK Surface Expression via Wnt/beta-Catenin Signaling." J Neurosci **36**(41): 10625-10639.

Wang, B., V. Bugay, L. Ling, H. H. Chuang, D. B. Jaffe and R. Brenner (2016). "Knockout of the BK beta4-subunit promotes a functional coupling of BK channels and ryanodine receptors that mediate a fAHP-induced increase in excitability." J Neurophysiol **116**(2): 456-465.

Wang, B., D. B. Jaffe and R. Brenner (2014). "Current understanding of iberiotoxin-

resistant BK channels in the nervous system." Front Physiol **5**: 382.

Zhang, Y., M. Zhang, H. Dong, S. Yong, X. Li, N. Olashaw, P. A. Kruk, J. Q. Cheng, W. Bai, J. Chen, S. V. Nicosia and X. Zhang (2009). "Deacetylation of cortactin by SIRT1 promotes cell migration." Oncogene **28**(3): 445-460.